(1)

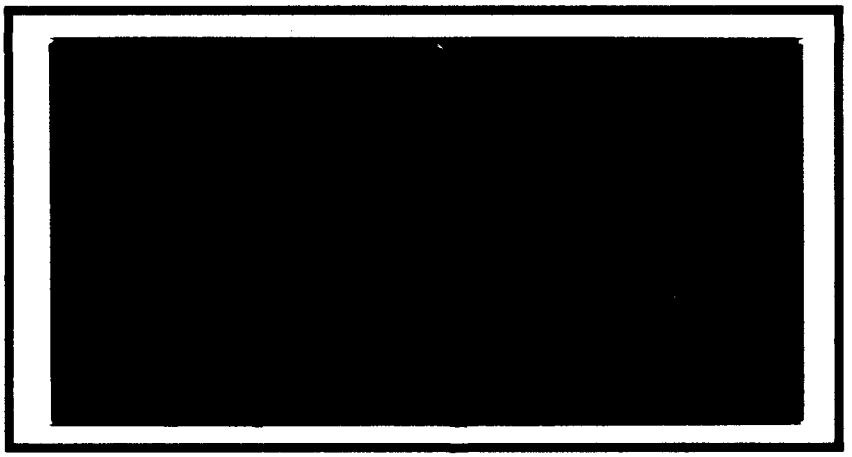

DEPARTMENT OF THE AIR FORCE

AIR UNIVERSITY

AIR FORCE INSTITUTE OF TECHNOLOGY

Wright-Patterson Air Force Base, Ohio

AFIT/GAE/ENY/90D-13

(1)

ROBUSTNESS OF H_2 AND H_∞ DESIGN TECHNIQUES IN THE DESIGN OF A GUIDED MISSILE CONTROLLER

THESIS

STEVEN R. KOLBOW
CAPTAIN, USAF

AFIT/GAE/ENY/90D-13

Approved for public release; distribution unlimited

AFIT/GAE/ENY/90D-13

ROBUSTNESS OF H_2 AND H_∞ DESIGN TECHNIQUES IN THE DESIGN OF A GUIDED MISSILE CONTROLLER

THESIS

Presented to the Faculty of the School of Engineering

of the Air Force Institute of Technology

Air University

In Partial Fulfillment of the

Requirements for the Degree of

Master of Science in Aeronautical Engineering

Steven R. Kolbow, B.S

Captain, USAF

December 1990

Preface

As a member of the class of GAE-90D I would like to dedicate this thesis to the memory of our departed classmate Capt Wayne Wilsdon.

I am grateful for the help I received during this study from the following individuals:

Capt Brett Ridgely . . . . . Thesis Advisor

Maj Curtis Mracek . . . . . Thesis Committee Member

Capt Randy Paschall . . . . . Thesis Committee Member

Dr Siva Banda . . . . . Study Sponsor

Capt Randy Riddle . . . . . Study Originator

Dr Brad Liebst . . . . . Pro-MatLab Assistance

Mr Jack Phillips . . . . . Vax System Assistance

Mr John Bowlus . . . . . Technical Assistance

Capt Andy Sparks . . . . . Technical Assistance

Capt Mary Manning . . . . . μ-Analysis Advice

Capt Sharon Heise . . . . . Technical Assistance

Mr Duane Schneider . . . . . Documentation Printing

Steven R Kolbow

Table of Contents

List of Figures

List of Tables

List of Symbols

A_c, B_c, C_c, D_c	controller state space matrices
A_n	acceleration normal to missile velocity
A_p, B_p, C_p, D_p	plant state space matrices
F	matrix adding unmodelled dynamics to output
G_c	controller transfer function
G_m	open loop missile transfer function
G_s	closed loop missile transfer function used in controller analysis
G_{sim}	closed loop missile transfer function used in missile simulation
H	matrix adapting H_2 and H_∞ controllers for use in simulation
h_M	missile altitude in meters
H_2	Hardy space with finite 2-norm
H_∞	Hardy space with finite ∞-norm
I	identity matrix
i	$\sqrt{-1}$
K_g	navigational constant used in simulation
M	transfer function used in μ-analysis
md	miss distance in meters
M_α	dimensional stability derivative
M_δ	dimensional stability derivative
N	matrix which removes η_3 and η_6 inputs
N_α	dimensional stability derivative
N_δ	dimensional stability derivative

P_M	an ordered pair indicating missile position downrange and crossrange in meters
PSCAL	scaling matrix used in μ-analysis
P_T	an ordered pair indicating target position downrange and crossrange in meters
r	vector of command signals
R	a matrix which isolates $\dot{\gamma}_M$ from the plant output
R_T	range from missile to target in meters
s	Laplace variable
SNOM	nominal plant used in μ-analysis
T	matrix representing the guidance command block in the missile
t	time in seconds
t_f	missile flyout time in seconds
t_s	simulation time step size in seconds
ud	high frequency unmodelled dynamics
u_p	plant input signal
v	vector of controlled variables which track reference signal
V_M	speed of missile in meters per second
V_T	speed of target in meters per second
w_p	plant external input
$W_{(\cdot)}$	weighting filter transfer function
x	downrange distance in meters; state vector
x_c	controller state vector
x_{int}	an intermediate value used in calculating miss distance
x_p	plant state vector

y	crossrange distance in meters; vector of command signals minus controlled variables
y_c	controller output vector
y_g	guidance block output vector
y_{int}	an intermediate value used in calculating miss distance
y_p	plant output vector
z	vector of command signals minus controlled variables and control inputs
α	missile angle of attack in degrees
δ	missile fin deflection in degrees
Δ	μ-analysis variation matrix
ϕ	true boresight error
ϕ_e	boresight error signal
ϕ_T	bearing to target from inertial reference in degrees
γ_M	missile heading in degrees
γ_T	target heading in degrees
η	sensor noises
λ_M	line of sight angle from missile velocity vector to target in degrees
λ_T	line of sight angle from negative target velocity vector to missile in degrees
μ	structured singular value
θ_m	missile body heading from inertial reference
θ_s	antenna angle relative to missile body
ω	antenna servomotor input; frequency
ζ	plant disturbances
$\lvert\cdot\rvert$	magnitude
$\lVert\cdot\rVert_2$	2-norm

$\|\cdot\|_\infty$	∞-norm
$\dot{(\cdot)}$	first time derivative
$(\cdot)_c$	controller variable
$(\cdot)_{com}$	commanded value
$(\cdot)_g$	guidance block variable
$(\cdot)_p$	plant variable
$\left[\begin{array}{c\|c} A & B \\ \hline C & D \end{array}\right]$	transfer function in state space form = $C(sI-A)^{-1}B+D$

Abstract

This work follows Capt. Riddle's 1989 thesis, which compared conventional, H_2, and H_∞ controlled guided missiles in simulated flyouts against an airborne target. The simulation results did not clearly demonstrate the H_2 and H_∞ controller advantages. In this study the missile model and simulation were refined. In addition to simulation runs, performance, noise attenuation, and μ robustness analyses were conducted. Results showed areas where improvement was needed in the H_2 and H_∞ controllers used in the study. An H_2 and H_∞ controller redesign is recommended using the μ synthesis design technique. Additional simulation runs are also recommended to examine whether the improved controllers reduce miss distances.

ROBUSTNESS OF H_2 AND H_∞ DESIGN TECHNIQUES IN THE DESIGN OF A GUIDED MISSILE CONTROLLER

I Introduction

1.1 Motivation

The objective of this effort is to show the advantages of H_2 and H_∞ controllers through their application in a surface-to-air missile simulation.

Capt Riddle began this project with his 1989 thesis, "Design of a Robust Controller for an Unstable Nonminimum Phase Guided Missile" [1]. He constructed a missile model and simulation, formulated a design technique for H_2 and H_∞ controllers, designed an H_2, H_∞, and conventional controller, and measured their performance with miss distance results. The results showed no advantage in using the H_2 and H_∞ controllers over the conventional controller.

Building upon Capt Riddle's work, the approach here is to show the advantages of H_2 and H_∞ controllers in three ways: 1) increase simulation fidelity, 2) examine limits of missile performance, and 3) develop a detailed analysis procedure for evaluating the controllers.

This study shows that the H_2 controller designed by Capt Riddle offers a robustness advantage, but could be improved to achieve quicker time response and noise rejection characteristics. The H_∞ controller designed by Capt Riddle was found to be a faulty design. Unlike the intent of H_∞ optimization to provide good robustness characteristics, this controller was unable to stabilize the missile when high frequency unmodelled dynamics were

added. The missile flyout simulations corresponded well with the controller analysis predictions.

The analysis and simulation developed in this study provide a very good means of evaluating advanced controllers. The study shows that the H_2 and H_∞ controllers used by Capt Riddle were not optimally designed.

1.2 Overview

To assist the reader, a brief mapping of the document contents is presented here. Chapters 2, 3, 4 and part of 7 summarize work done by Capt Riddle. Chapters 5 through 10 describe the progress made during this study.

1.2.1 Missile System Description

Chapter 2 describes the surface-to-air missile model developed by Capt Riddle. It includes the high frequency unmodelled dynamics which were added in this study.

1.2.2 Simulation Description

Chapter 3 describes the missile flyout simulation. It includes a development of the missile simulation transfer function, G_{sim}, and the nonlinear calculations performed by the simulation.

1.2.3 Guidance Law

Since the guidance law plays an important role in target miss distances, Chapter 4 is devoted to a description of the guidance command block used by the missile.

1.2.4 Refining the Model and Simulation

Three areas of missile model and simulation improvement are investigated in Chapter 5: 1) reducing simulation time step size, 2) adding high frequency unmodelled dynamics, and 3) examining plant parameter variations.

1.2.5 Controller Analysis

It is difficult to measure the controllers relative capabilities based on target miss distances so a detailed controller analysis was undertaken in Chapter 6. Performance, noise attenuation, and robustness characteristics of each controller are examined.

1.2.6 H_2 and H_∞ Controller Design

The controller analysis identifies areas where improvements can be made to the H_2 and H_∞ controllers. Chapter 7 describes the process used to design the controllers and the initial values for weighting filters chosen for controller redesign.

1.2.7 Simulation Runs

Chapter 8 describes a set of simulation runs which were made with the refinements described in Chapter 5. The runs are limited to one engagement scenario to reduce scenario-dependent miss distance variations.

1.2.8 Conclusions and Recommendations

Chapter 9 summarizes what was learned from this study and gives recommendations for follow-on work.

1.2.9 Missile Transfer Functions To State Space

An important part of the missile model development is the process of converting single-input single-output transfer functions into state space form and combining them to create a state space model. The same processes are important in the developement of large transfer functions in state space form used throughout the study. To aid follow-on efforts and to confirm correctness of the model used, the developement of the missile model is presented in Appendix A.

1.2.10 Description of Code Created for Study

Again with the intent of aiding follow-on efforts, a description of the features of the computer coding developed for this study is presented in Appendix B.

II Missile System Description

The missile used in this study is the same generic tail-control missile used by Capt Riddle except for the addition high frequency unmodeled dynamics. Details of the origin and development of the missile model can be found in Capt Riddle's thesis. This chapter is a summary of the model. Some of the characteristics of the nominal missile are given in Table 2.1.

Table 2.1 Some Nominal Missile Characteristics

Guidance	Radar
Control	Tail Fin
Speed	Mach 3.5
Mass	127 kg
Center of Gravity	2.63 m from nose
Inertia (pitch & yaw)	271.3 kg-m^2

Relationships of important variables are shown in Figure 2.1.

The closed loop missile system can be represented as shown in Figure 2.2. Its components will be described in detail starting with the nominal plant, the addition of the high frequency unmodelled dynamics, the guidance command block, and finally the controller. A simplified closed loop missile block diagram is shown in Figure 2.3.

2.1 Nominal Plant

The assumption is made that the missile has finished boosting and is in a 16 to 20 degree climb. Its climb rate is 328 m/s (1000 ft/s) starting from 4921 meters (15,000 ft) altitude. The missile model is two dimensional

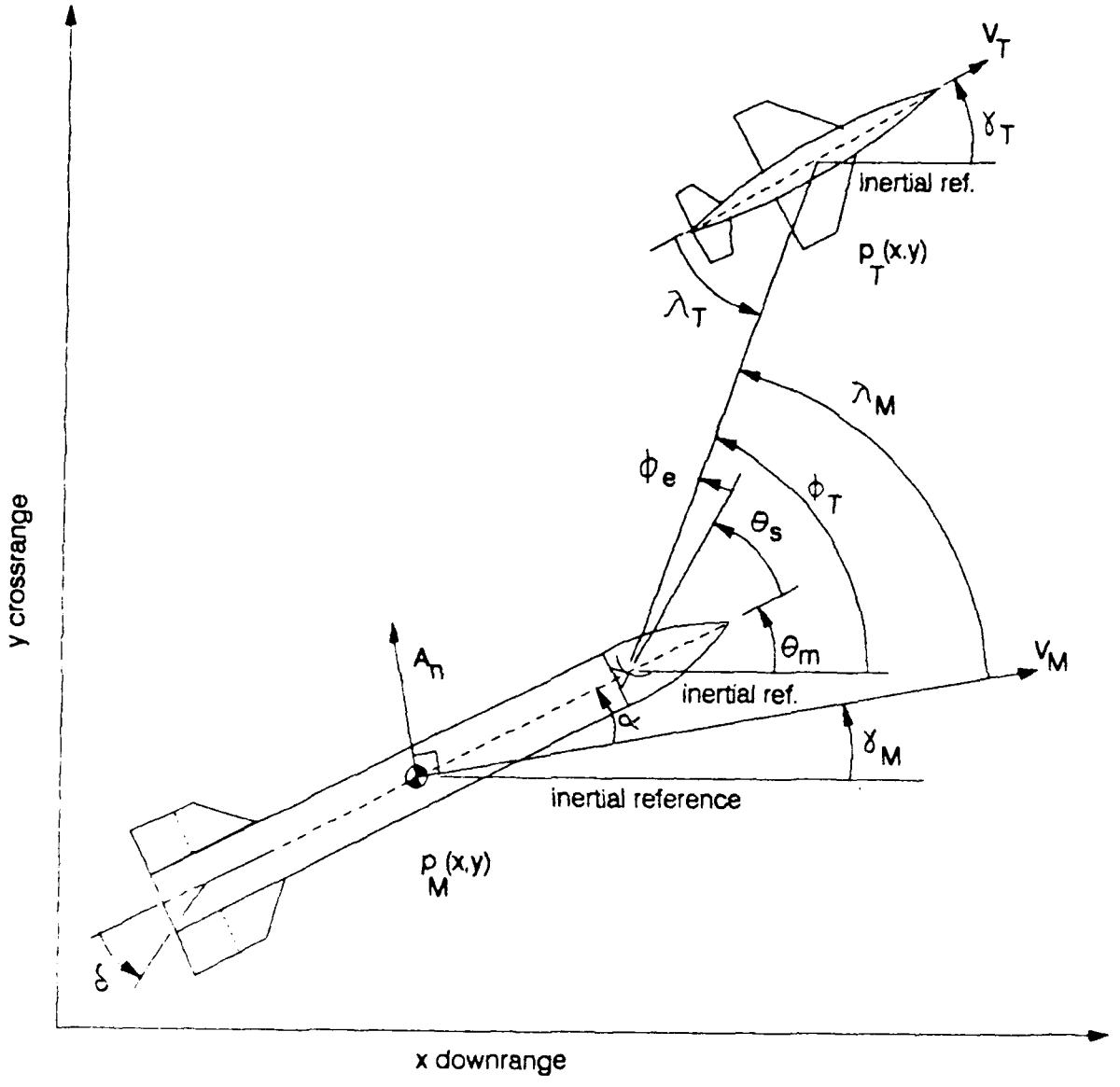

Figure 2.1 Coordinate System

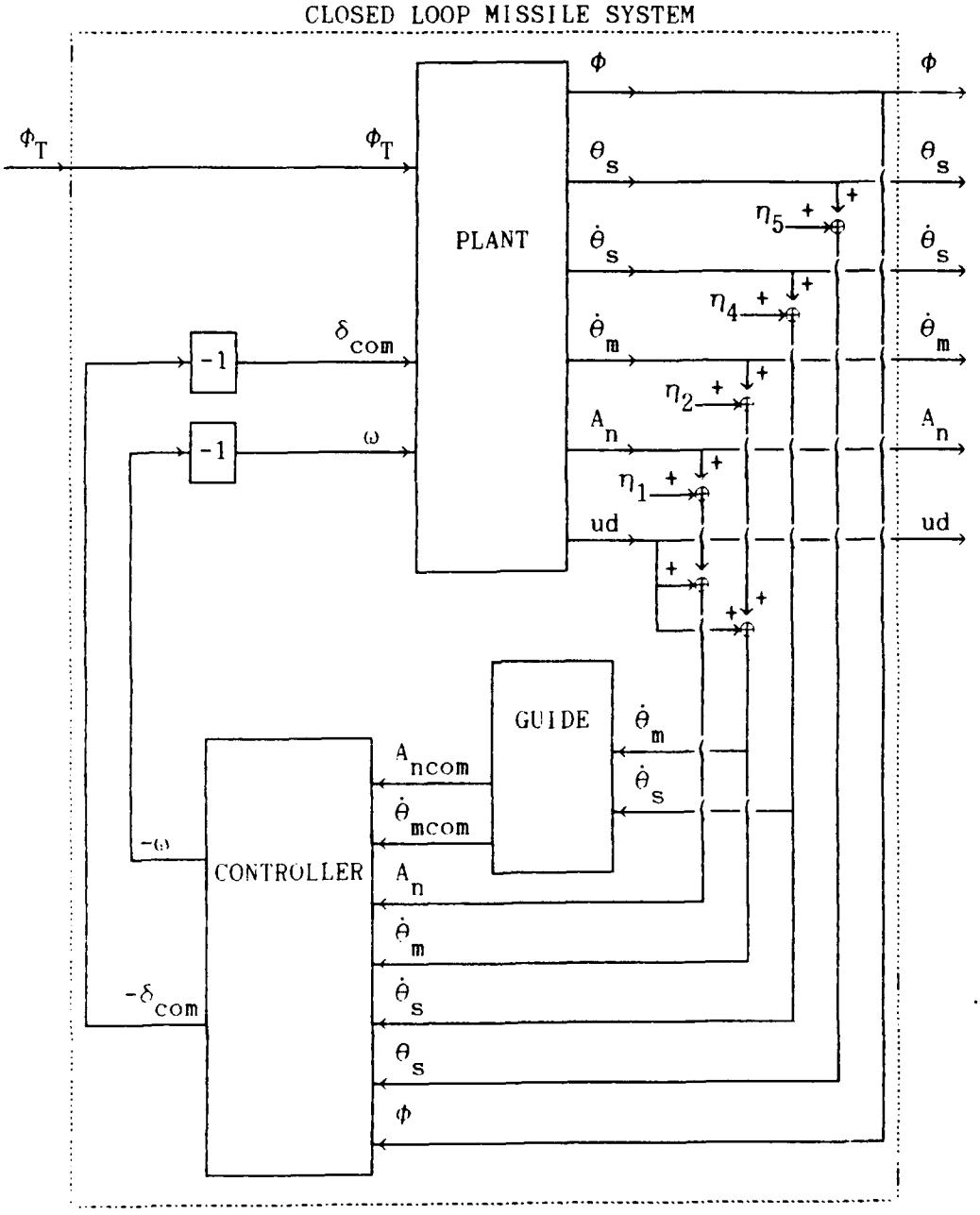

Figure 2.2 Closed Loop Missile Block Diagram

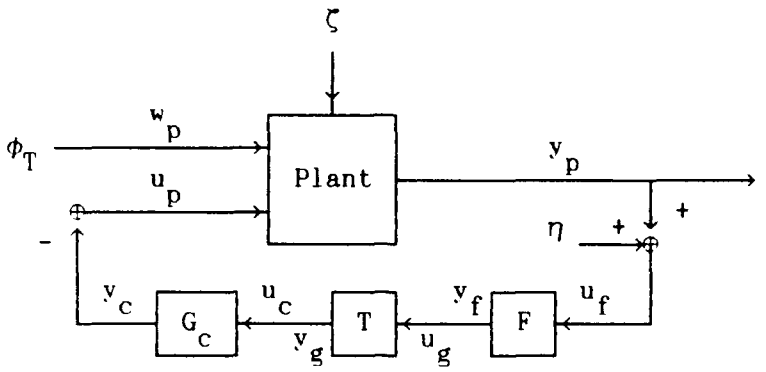

Figure 2.3 Simplified Closed Loop Missile Block Diagram

in the horizontal plane; however, dynamic pressure, weight, moment of inertia and center of gravity are varied as if the missile was in a sustained propulsion climb. Dimensional stability derivatives of the missile resulting from these variations are given by the following equations and shown in Figures 2.4 through 2.10. These equations are polynomials which approximate tabulated values. They are accurate in the range of 0 to 8 seconds of missile flyout time.

$$N_\alpha(t) = 1.871 + 0.202t - 0.0262t^2 + 0.0008t^3 \text{ (g's/deg)} \quad (2.1)$$

$$N_\delta(t) = 1.016 + 0.076t - 0.0161t^2 - 0.0004t^3 \text{ (g's/deg)} \quad (2.2)$$

$$M_\alpha(t) = 0.0144 - 0.3109t - 0.0111t^2 + 0.0085t^3 \text{ (deg/s}^2\text{/deg)} \quad (2.3)$$

$$M_\delta(t) = -2.78 - 0.230t + 0.044t^2 - 0.001t^3 \text{ (deg/s}^2\text{/deg)} \quad (2.4)$$

$$V_M(t) = 1000 + 80t - 8t^2 \text{ (m/s)} \quad (2.5)$$

$$h_M(t) = 4921 + 328t \text{ (m)} \quad (2.6)$$

The nominal flight conditions and dimensional stability derivatives used in the controller design are given in Table 2.2. A block diagram of the resulting nominal plant can be seen in Figure 2.11.

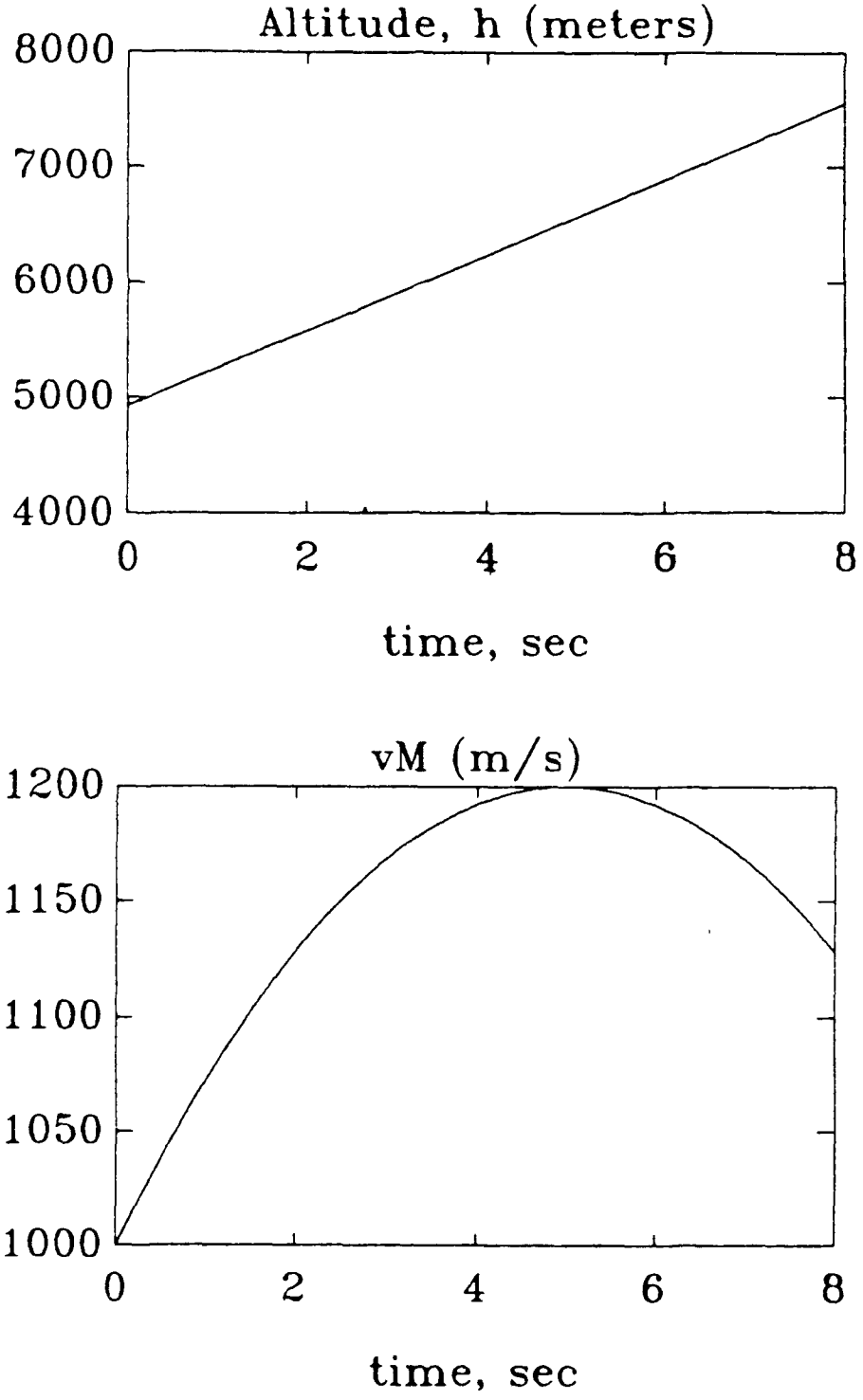

Figure 2.4 Missile Altitude and Velocity Variation

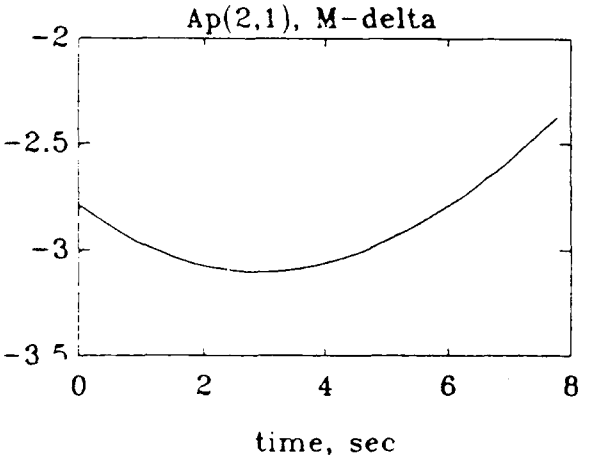

Figure 2.5 M_{δ} Variation

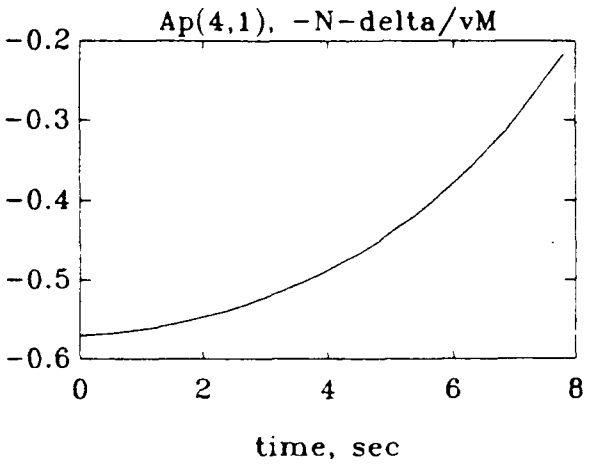

Figure 2.6 $-M_{\alpha}$ Variation

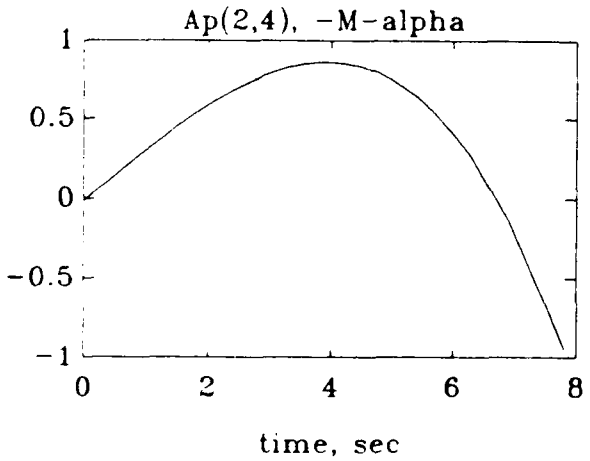

Figure 2.7 $-N_{\delta}/V_{M}$ Variation

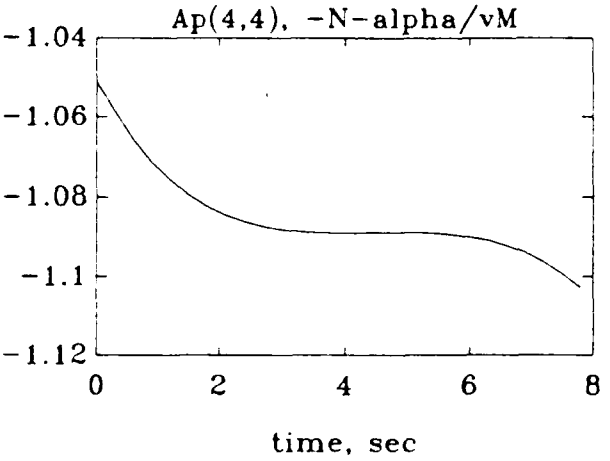

Figure 2.8 $-N_{\alpha}/V_{M}$ Variation

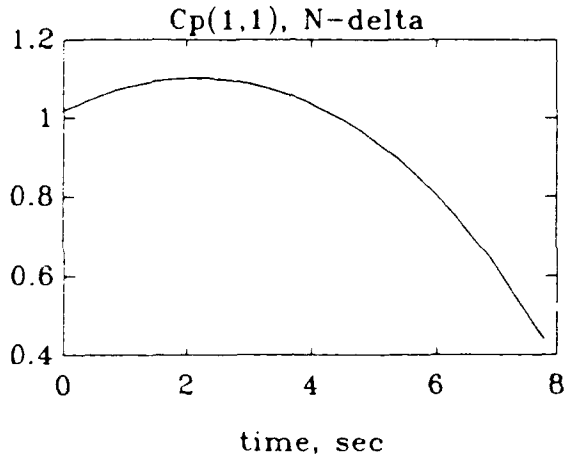

Figure 2.9 N_{δ} Variation

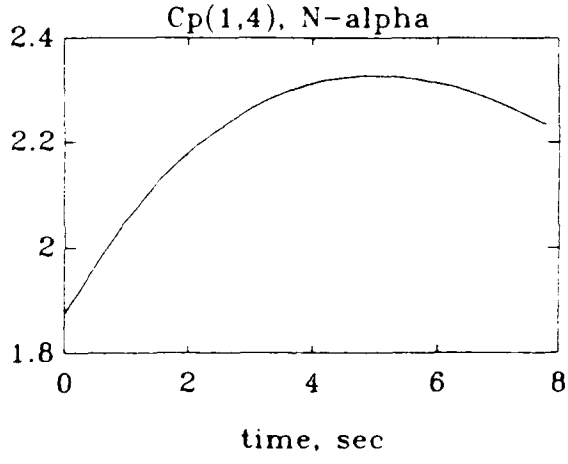

Figure 2.10 N_{α} Variation

Table 2.2 Nominal Missile Parameters

Altitude	6096 m (20,000 ft)
Mach	3.5
V_M	1100 m/s
N_α	2.0 g's/deg
N_δ	1.0 g's/deg
M_α	-0.91 deg/s^2/deg
M_δ	-2.74 deg/s^2/deg
$\lvert\dot{R}_T\rvert$	1500 m/s
R_T	1000 m
K_g	3.3

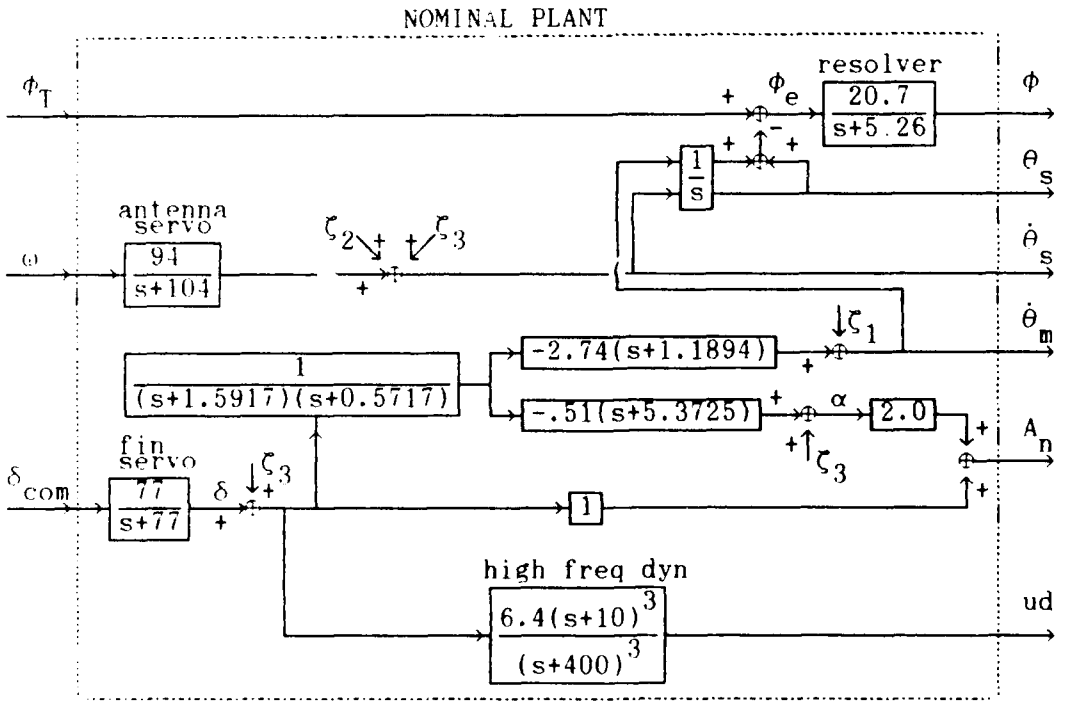

Figure 2.11 Missile Model Block Diagram

The resulting state space representation is shown in Equations (2.7) through (2.14).

$$\dot{x}_p = A_p\, x_p + B_{p11}\, u_p + B_{p12}\, w_p + B_{p2}\, \zeta \tag{2.7}$$

$$y_p = C_p\, x_p + D_{p11}\, u_p + D_{p12}\, w_p + D_{p2}\, \zeta + \eta \tag{2.8}$$

where

$$x_p = \begin{bmatrix} \delta \text{ (deg)} \\ \dot{\theta}_m \text{ (deg/sec)} \\ \theta_m \text{ (deg)} \\ \alpha \text{ (deg)} \\ \phi \text{ (deg)} \\ \dot{\theta}_s \text{ (deg/sec)} \\ \theta_s \text{ (deg)} \\ x_{ud1} \\ x_{ud2} \\ x_{ud3} \end{bmatrix} \tag{2.9}$$

$$u_p = \begin{bmatrix} \delta_{com} \text{ (deg)} \\ \omega \text{ (deg/sec)} \end{bmatrix} \tag{2.10}$$

$$w_p = \begin{bmatrix} \phi_T \text{ (deg)} \end{bmatrix} \tag{2.11}$$

$$y_p = \begin{bmatrix} A_n \text{ (g's)} \\ \dot{\theta}_m \text{ (deg/sec)} \\ \phi \text{ (deg)} \\ \dot{\theta}_s \text{ (deg/sec)} \\ \theta_s \text{ (deg)} \\ \text{ud (deg/sec \& g's)} \end{bmatrix} \tag{2.12}$$

The values shown for ζ and η are the range of values used in the simulation.

$$\zeta = \begin{bmatrix} \pm\ (0 - 0.03) & \text{turbulence (deg/sec)} \\ \pm\ (0 - 3000)/R_T & \text{target glint (deg/sec)} \\ \pm\ (0 - 0.5) & \text{power supply noise (deg/sec \& deg)} \end{bmatrix} \tag{2.13}$$

$$\eta = \begin{bmatrix} \pm\ (0 - 1.0) & \text{accelerometer noise (g's)} \\ \pm\ (0 - 0.5) & \text{body rate gyro noise (deg/sec)} \\ 0 & \text{no measurement noise} \\ \pm\ (0 - 1.0) & \text{rate gyro noise (deg/sec)} \\ \pm\ (0 - 0.5) & \text{potentiometer noise (deg)} \\ 0 & \text{nothing added to high frequency dynamics} \end{bmatrix} \tag{2.14}$$

The state space values for the plant are given in Equations (2.15) through (2.18). Details on converting the missile transfer functions to state space form can be found in Appendix A. The nominal values used for the plant during controller design can be seen in Equations (2.19) and (2.20).

$$A_p = \begin{bmatrix} \text{fin actuator pole} & 0 & 0 & 0 & 0 & 0 & 0 & 0 & 0 & 0 \\ M_\delta & 0 & 0 & -M_\alpha & 0 & 0 & 0 & 0 & 0 & 0 \\ 0 & 1 & 0 & 1 & 0 & 1 & 0 & 1 & 0 & 1 \\ -N_\delta/V_M & 1 & 0 & -N_\alpha/V_M & 0 & 0 & 0 & 0 & 0 & 0 \\ 0 & 0 & \text{-target resolver gain} & 0 & \text{target resolver pole} & 0 & \text{-target resolver gain} & 0 & 0 & 0 \\ 0 & 0 & 0 & 0 & 0 & \text{antenna servo pole} & 0 & 0 & 0 & 0 \\ 0 & 0 & 0 & 0 & 0 & 1 & 0 & 0 & 0 & 0 \\ \text{high freq dyn gain} & 0 & 0 & 0 & 0 & 0 & 0 & \text{high freq dyn pole} & \text{high freq dyn pole -zero} & \text{high freq dyn pole -zero} \\ \text{high freq dyn gain} & 0 & 0 & 0 & 0 & 0 & 0 & 0 & \text{high freq dyn pole} & \text{high freq dyn pole -zero} \\ \text{high freq dyn gain} & 0 & 0 & 0 & 0 & 0 & 0 & 0 & 0 & \text{high freq dyn pole} \end{bmatrix} \quad (2.15)$$

$$\begin{bmatrix} B_{p11} & B_{p12} & B_{p2} \end{bmatrix} = \left[\begin{array}{cc:c:ccc} \begin{matrix}\text{fin}\\ \text{actuator}\\ \text{gain}\end{matrix} & 0 & 0 & 0 & 0 & 1 \\ 0 & 0 & 0 & 1 & 0 & 0 \\ 0 & 0 & 0 & 0 & 0 & 0 \\ 0 & 0 & 0 & 1 & 0 & 0 \\ 0 & 0 & \begin{matrix}\text{target}\\ \text{resolver}\\ \text{gain}\end{matrix} & 0 & 0 & 1 \\ 0 & \begin{matrix}\text{antenna}\\ \text{servo}\\ \text{gain}\end{matrix} & 0 & 0 & 1 & 1 \\ 0 & 0 & 0 & 0 & 0 & 0 \\ 0 & 0 & 0 & 0 & 0 & 0 \\ 0 & 0 & 0 & 0 & 0 & 0 \\ 0 & 0 & 0 & 0 & 0 & 0 \end{array}\right] \qquad (2.16)$$

$$C_p = \begin{bmatrix} 1 & 0 & 0 & 2 & 0 & 0 & 0 & 0 & 0 & 0 \\ 0 & 1 & 0 & 0 & 0 & 0 & 0 & 0 & 0 & 0 \\ 0 & 0 & 0 & 0 & 1 & 0 & 0 & 0 & 0 & 0 \\ 0 & 0 & 0 & 0 & 0 & 1 & 0 & 0 & 0 & 0 \\ 0 & 0 & 0 & 0 & 0 & 0 & 1 & 0 & 0 & 0 \\ \begin{matrix}\text{high}\\ \text{freq dyn}\\ \text{gain}\end{matrix} & 0 & 0 & 0 & 0 & 0 & 0 & \begin{matrix}\text{high}\\ \text{freq}\\ \text{dyn}\\ \text{pole}\\ \text{-zero}\end{matrix} & \begin{matrix}\text{high}\\ \text{freq}\\ \text{dyn}\\ \text{pole}\\ \text{-zero}\end{matrix} & \begin{matrix}\text{high}\\ \text{freq}\\ \text{dyn}\\ \text{pole}\\ \text{-zero}\end{matrix} \end{bmatrix} \qquad (2.17)$$

$$\begin{bmatrix} D_{p11} & D_{p12} & D_{p2} \end{bmatrix} = \left[\begin{array}{cc:c:ccc} 0 & 0 & 0 & 0 & 0 & 0 \\ 0 & 0 & 0 & 0 & 0 & 0 \\ 0 & 0 & 0 & 0 & 0 & 0 \\ 0 & 0 & 0 & 0 & 0 & 0 \\ 0 & 0 & 0 & 0 & 0 & 0 \\ 0 & 0 & 0 & 0 & 0 & 0 \end{array}\right] \qquad (2.18)$$

$$G_p = \left[\begin{array}{c|ccc} A_p & B_{p11} & B_{p12} & B_{p2} \\ \hline C_p & D_{p11} & D_{p12} & D_{p2} \end{array}\right] \tag{2.19}$$

$$G_p = \left[\begin{array}{cccccccccc:ccccccc}
-77 & 0 & 0 & 0 & 0 & 0 & 0 & 0 & 0 & 0 & 77 & 0 & 0 & 0 & 0 & 1 \\
-2.74 & 0 & 0 & 0.91 & 0 & 0 & 0 & 0 & 0 & 0 & 0 & 0 & 0 & 1 & 0 & 0 \\
0 & 1 & 0 & 0 & 0 & 0 & 0 & 0 & 0 & 0 & 0 & 0 & 0 & 0 & 0 & 0 \\
-0.51 & 1 & 0 & -1.02 & 0 & 0 & 0 & 0 & 0 & 0 & 0 & 0 & 0 & 1 & 0 & 0 \\
0 & 0 & -20.7 & 0 & -5.26 & 0 & -20.7 & 0 & 0 & 0 & 0 & 0 & 20.7 & 0 & 0 & 1 \\
0 & 0 & 0 & 0 & 0 & -104 & 0 & 0 & 0 & 0 & 0 & 94 & 0 & 0 & 1 & 1 \\
0 & 0 & 0 & 0 & 0 & 1 & 0 & 0 & 0 & 0 & 0 & 0 & 0 & 0 & 0 & 0 \\
6.4 & 0 & 0 & 0 & 0 & 0 & 0 & -400 & -390 & -390 & 0 & 0 & 0 & 0 & 0 & 0 \\
6.4 & 0 & 0 & 0 & 0 & 0 & 0 & 0 & -400 & -390 & 0 & 0 & 0 & 0 & 0 & 0 \\
6.4 & 0 & 0 & 0 & 0 & 0 & 0 & 0 & 0 & -400 & 0 & 0 & 0 & 0 & 0 & 0 \\ \hdashline
1 & 0 & 0 & 2 & 0 & 0 & 0 & 0 & 0 & 0 & 0 & 0 & 0 & 0 & 0 & 0 \\
0 & 1 & 0 & 0 & 0 & 0 & 0 & 0 & 0 & 0 & 0 & 0 & 0 & 0 & 0 & 0 \\
0 & 0 & 0 & 0 & 1 & 0 & 0 & 0 & 0 & 0 & 0 & 0 & 0 & 0 & 0 & 0 \\
0 & 0 & 0 & 0 & 0 & 1 & 0 & 0 & 0 & 0 & 0 & 0 & 0 & 0 & 0 & 0 \\
0 & 0 & 0 & 0 & 0 & 0 & 1 & 0 & 0 & 0 & 0 & 0 & 0 & 0 & 0 & 0 \\
6.4 & 0 & 0 & 0 & 0 & 0 & 0 & -390 & -390 & -390 & 0 & 0 & 0 & 0 & 0 & 0
\end{array}\right] \tag{2.20}$$

2.2 Adding The High Frequency Unmodelled Dynamics

The unmodeled high frequency dynamics is added to $\dot{\theta}_m$ and A_n by multplying y_p by a matrix called F which is given in Equation (2.21).

$$F = \begin{bmatrix} 1 & 0 & 0 & 0 & 0 & 1 \\ 0 & 1 & 0 & 0 & 0 & 1 \\ 0 & 0 & 1 & 0 & 0 & 0 \\ 0 & 0 & 0 & 1 & 0 & 0 \\ 0 & 0 & 0 & 0 & 1 & 0 \end{bmatrix} \tag{2.21}$$

2.3 Guidance Command Block

The guidance command block can be seen in Figure 2.12. Either A_{ncom} or $\dot{\theta}_{mcom}$ can be used. More details on the proportional navigation used are in

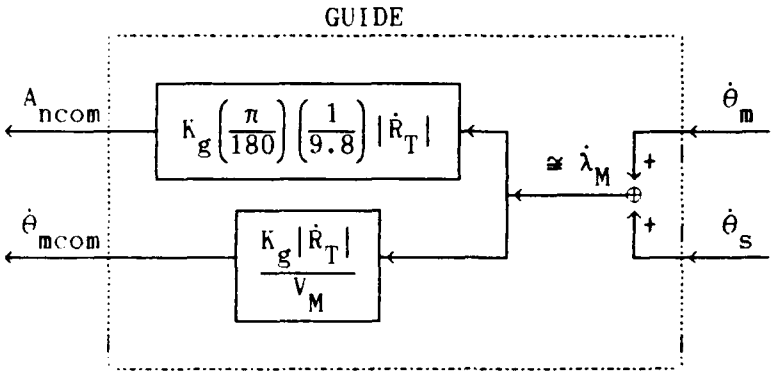

Figure 2.12 Guidance Command Block Diagram

Chapter 5. The guidance command block will be represented by a matrix called T as shown in Equations (2.22) through (2.24).

$$\begin{bmatrix} y_p \\ y_g \end{bmatrix} = T\ y_p \tag{2.22}$$

where

$$y_g = A_{ncom} \text{ or } \dot{\theta}_{mcom} \tag{2.23}$$

$$T = \begin{bmatrix} 1 & 0 & 0 & 0 & 0 \\ 0 & 1 & 0 & 0 & 0 \\ 0 & 0 & 1 & 0 & 0 \\ 0 & 0 & 0 & 1 & 0 \\ 0 & 0 & 0 & 0 & 1 \\ 0 & K_g|\dot{R}_T|/561.5 & 0 & K_g|\dot{R}_T|/561.5 & 0 \end{bmatrix} \tag{2.24}$$

The 561.5 in Equation (2.24) would be replaced by 1100 if $\dot{\theta}_{mcom}$ was desired.

2.4 Controller

Capt Riddle's conventional controller can be seen in Figure 2.13.

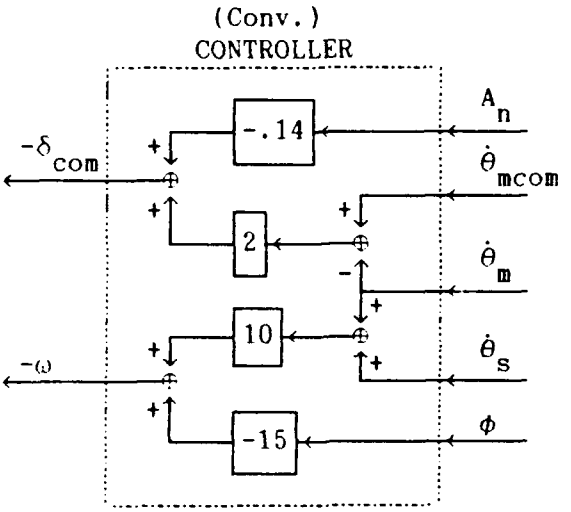

Figure 2.13 Conventional Controller Block Diagram

This controller is designed for use with negative feedback. Equations (2.25) through (2.28) show how the controller transfer function will be represented.

$$\dot{x}_c = A_c x_c + B_c u_c \tag{2.25}$$

$$y_c = C_c x_c + D_c u_c \tag{2.26}$$

Dynamic Controller

$$G_c = \left[\begin{array}{c|c} A_c & B_c \\ \hline C_c & D_c \end{array}\right] \tag{2.27}$$

Static Controller

$$G_c = D_c \tag{2.28}$$

III Simulation Description

A diagram of the simulation process can be seen in Figure 3.1. Each block of the diagram will be described in detail.

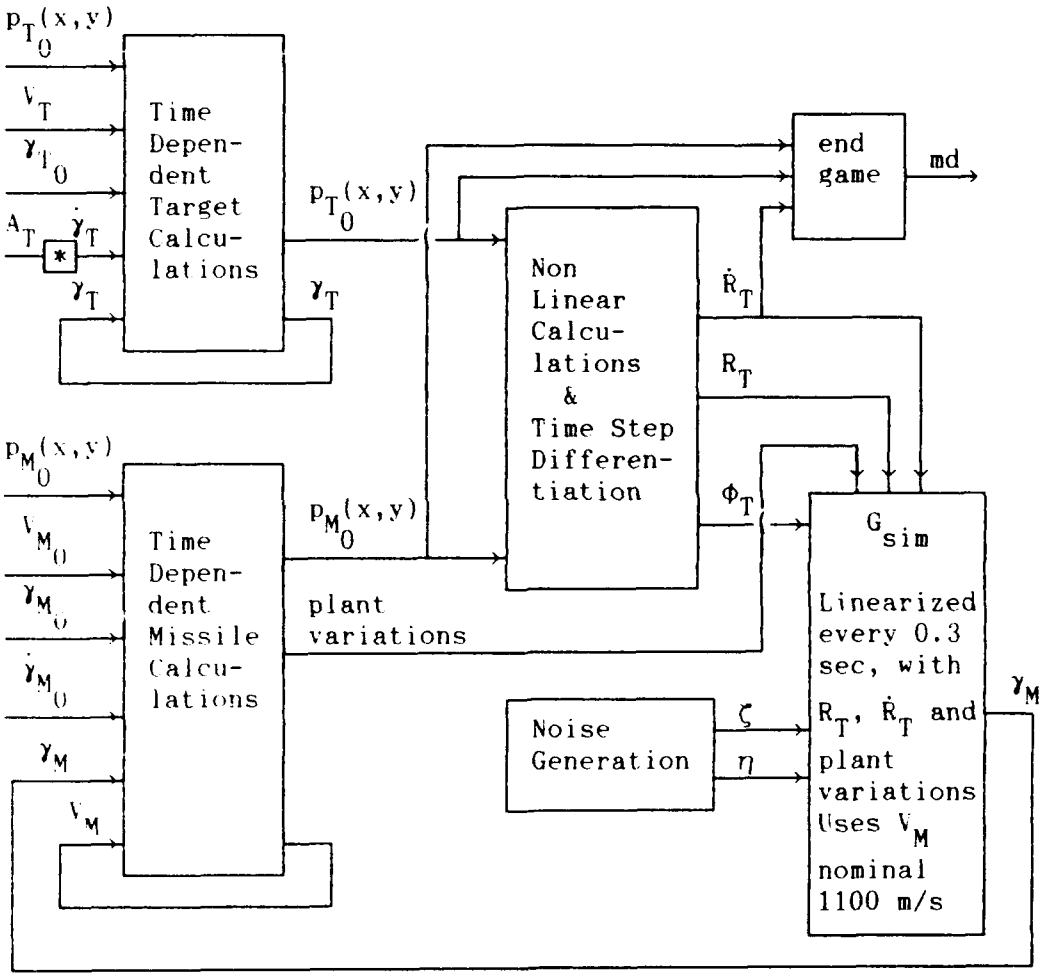

* Computation shown by Equation (3.8)

Figure 3.1 Diagram of Simulation Process

Initial conditions used in the missile simulation are shown in Table 3.1.

Table 3.1 Simulation Initial Conditions

Variable	Value Used In Study
$p_{T_0}(x,y)$	[5000, 5000] meters
V_T	470 m/s
A_T	-8.4 g's
$\dot{\gamma}_T$	-10 deg/s
γ_{T_0}	0 deg
$p_{M_0}(x,y)$	[0, 0] meters
V_{M_0}	1000 m/s
$\dot{\gamma}_{M_0}$	0 deg/s
γ_{M_0}	45 deg
ϕ_{T_0}	45 deg
$\dot{\phi}_{T_0}$	0 deg/s
R_{T_0}	7071 meters
$\dot{R}_{T_0}$	-746 m/s
λ_{M_0}	0 deg
λ_{T_0}	45 deg
x_{p_0}	0
x_{c_0}	0
ζ_0	0
η_0	0

3.1 Linearized Scenario System

The linearized scenario system, G_{sim} used in the missile simulation can be seen in Figure 3.2.

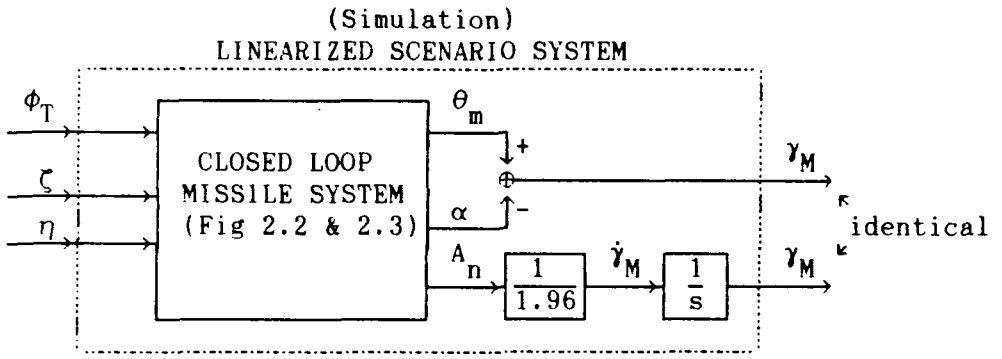

Figure 3.2 Linearized Scenario System for Simulation

Two ways to obtain γ_M are shown. Both yield the same values. Obtaining γ_M from A_n was used in the simulation. Capt Riddle used $(\theta_m - \alpha)$ to obtain γ_M in his simulation.

The closed loop missile system state space representation used in the missile simulation is shown in Equations (3.1) and (3.2).

$$\begin{bmatrix} \dot{x}_p \\ \dot{x}_c \end{bmatrix} = \begin{bmatrix} A_p & 0 \\ 0 & A_p \end{bmatrix} \begin{bmatrix} x_p \\ x_c \end{bmatrix} + \begin{bmatrix} B_{p11} & B_{p12} & B_{p2} & 0 \\ 0 & 0 & 0 & B_c \end{bmatrix} \begin{bmatrix} u_p \\ w_p \\ \zeta \\ u_c \end{bmatrix} \tag{3.1}$$

$$\begin{bmatrix} y_p \\ y_c \end{bmatrix} = \begin{bmatrix} C_p & 0 \\ 0 & C_c \end{bmatrix} \begin{bmatrix} x_p \\ x_c \end{bmatrix} + \begin{bmatrix} D_{p11} & D_{p12} & D_{p2} & 0 \\ 0 & 0 & 0 & D_c \end{bmatrix} \begin{bmatrix} u_p \\ w_p \\ \zeta \\ u_c \end{bmatrix} + \begin{bmatrix} \eta \\ 0 \end{bmatrix} \tag{3.2}$$

Removing u_p and u_c through substitution using $u_p = -y_p$ and $u_c = T\ F\ y_p$ results in Equations (3.3) and (3.4).

$$\begin{bmatrix} \dot{x}_p \\ \dot{x}_c \end{bmatrix} = \begin{bmatrix} \left(A_p - B_{p11} D_c TFC_p\right) & -B_{p11} C_c \\ B_c TFC_p & A_c \end{bmatrix} \begin{bmatrix} x_p \\ x_c \end{bmatrix} + \begin{bmatrix} B_{p12} - B_{p11} D_c TFD_{p12} \end{bmatrix} w_p$$

$$+ \begin{bmatrix} \left(B_{p2} - B_{p11} D_c TFD_{p2}\right) \\ B_c TFD_{p2} \end{bmatrix} \zeta + \begin{bmatrix} \left(B_{p2} - B_{p11} D_c TF\right) \\ B_c TF \end{bmatrix} \eta \qquad (3.3)$$

$$y_p = \begin{bmatrix} C_p & 0 \end{bmatrix} \begin{bmatrix} x_p \\ x_c \end{bmatrix} + \begin{bmatrix} D_{p12} & D_{p2} & I \end{bmatrix} \begin{bmatrix} w_p \\ \zeta \\ \eta \end{bmatrix} \qquad (3.4)$$

Now substituting $\dot{y}_M = R\, y_p$ where R = [.51 0 0 0 0 0] and integrating to get y_M results in G_{sim} as shown in Equations (3.5) through (3.7).

$$\gamma_M = G_{sim} \begin{bmatrix} w_p \\ \zeta \\ \eta \end{bmatrix} \qquad (3.7)$$

$$\text{the states of } G_{sim} = \begin{bmatrix} x_p \\ x_c \\ \gamma_M \end{bmatrix} \qquad (3.8)$$

$$G_{sim} =$$

$$\left[\begin{array}{ccc|ccc} \left(A_p - B_{p11} D_c TFC_p\right) & -B_{p11} C_c & 0 & \left(B_{p12} - B_{p11} D_c TFD_{p12}\right) & \left(B_{p2} - B_{P11} D_c TFD_{p2}\right) & \left(B_{p2} - B_{p11} D_c TF\right) \\ B_c TFC_p & A_c & 0 & B_c TFD_{p12} & B_c TFD_{p2} & B_c TF \\ RC_p & 0 & 0 & RD_{p12} & RD_{p2} & R \\ \hline 0 & 0 & 1 & 0 & 0 & 0 \end{array}\right] \tag{3.7}$$

3.2 Time Dependent Target Calculations

Time dependent target calculations consist of the following. The target's turn rate ($\dot{\gamma}_T$) is calculated for a given target speed and g's of acceleration. For a constant altitude, turn rate $\dot{\gamma}_T$ is given by Equation (3.8).

$$\dot{\gamma}_T = \left(\frac{A_T}{|A_T|}\right)\left(\frac{180}{\pi}\right)\left(\frac{9.8}{V_T}\right)\sqrt{\left(A_T^{\,2} - 1\right)} \tag{3.8}$$

The target heading is calculated at each time step through Equation (3.9).

$$\gamma_T = \gamma_T + \dot{\gamma}_T\left(t_s\right) \tag{3.9}$$

The target's position is calculated using Equation (3.10).

$$P_T(x,y) = \left[\left(p_T(x) + V_T\left(t_s\right)\cos\left(\gamma_T\right)\right), \left(p_T(y) + V_T\left(t_s\right)\sin\left(\gamma_T\right)\right)\right] \tag{3.10}$$

3.3 Time Dependent Missile Calculations

The time dependent missile calculations consist of the following. The

plant variations and missile velocity variation which were described in Chapter 2 are updated every 0.3 seconds of flyout time in the missile simulation. The heading of the missile (γ_T) is obtained from G_{sim}. Missile position is calculated each time step, similar to target position with Equation (3.11).

$$P_M(x,y) = \left[\left(p_M(x) + V_M(t_s)\cos(\gamma_M)\right), \left(p_M(y) + V_M(t_s)\sin(\gamma_M)\right)\right] \quad (3.11)$$

3.4 Nonlinear Calculations and Time Step Differentiation

Nonlinear calculations and time step differentiation consist of the following. Angle from the missile to the target with respect to an inertial reference (ϕ_T) is calculated from missile and target positions with Equation (3.12).

$$\phi_T = \arctan\left\{\left\{p_T(y) - p_M(y)\right\}/\left\{p_T(x) - p_M(x)\right\}\right\} \quad (3.12)$$

Range from missile to target (R_T) is calculated from missile and target positions with Equation (3.13).

$$R_T = \sqrt{\left(p_T(x) - p_M(x)\right)^2 + \left(p_T(y) - p_M(y)\right)^2} \quad (3.13)$$

Range rate ($\dot{R}_T$) is obtained through time step differentiation (first order backwards difference estimation) as shown in Equation (3.14).

$$\dot{R}_T = \left(R_T(i) - R_T(i-1)\right)/t_s \quad (3.14)$$

3.5 Noise Generation

The derivation of the equations used for noise generation can be found in [Ref 1]. The ζ and η noise generation are calculated each time step with Equations (3.15) through (3.23).

Turbulence:

$$\zeta_1 = .015\left(\sin(t_f) + \sin(10 + t_f) + .1 \times \text{rand}(1)\right) \tag{3.15}$$

Target Glint:

$$\zeta_2 = 1500/R_T\left(\sin\left(t_f + \frac{\pi}{\text{rand}(1)}\right) + \sin\left(10 \times t_f + \frac{\pi}{\text{rand}(1)}\right) + .1 \times \text{rand}(1)\right) \tag{3.16}$$

Power Supply Noise:

$$\zeta_3 = .25\left(\sin\left(200 \times t_f + \frac{\pi}{\text{rand}(1)}\right) + \sin\left(2000 \times 10 \times t_f + \frac{\pi}{\text{rand}(1)}\right) + .1 \times \text{rand}(1)\right) \tag{3.17}$$

Accelerometer Noise:

$$\eta_1 = .5\left(\sin\left(40 \times t_f + \frac{\pi}{\text{rand}(1)}\right) \sin\left(400 \times t_f + \frac{\pi}{\text{rand}(1)}\right) + .1 \times \text{rand}(1)\right) \tag{3.18}$$

Body Rate Gyro Noise:

$$\eta_2 = .25\left(\sin\left(10 \times t_f + \frac{\pi}{\text{rand}(1)}\right) + \sin\left(100 \times t_f + \frac{\pi}{\text{rand}(1)}\right) + .1 \times \text{rand}(1)\right) \tag{3.19}$$

No Measurement Noise:

$$\eta_3 = 0 \tag{3.20}$$

Antenna Rate Gyro Noise:

$$\eta_4 = .5\left(\sin\left(10 \times t_f + \frac{\pi}{\text{rand}(1)}\right) + \sin\left(100 \times t_f + \frac{\pi}{\text{rand}(1)}\right) + .1 \times \text{rand}(1)\right) \tag{3.21}$$

Antenna Potentiometer Noise:

$$\eta_5 = .25\left(\sin\left(t_f + \frac{\pi}{\text{rand}(1)}\right) + \sin\left(10 \times t_f + \frac{\pi}{\text{rand}(1)}\right) + .1 \times \text{rand}(1)\right) \tag{3.22}$$

Nothing Added to High Frequency Dynamics:

$$\eta_6 = 0 \tag{3.23}$$

The rand(1) function generates a random distribution of values between one and minus one. A typical noise generated by these equations during a simulation run can be seen in Figures 3.3 and 3.4.

3.6 End Game

Once range rate is no longer negative, the missile is going away from the target, so end game calculations are made. Calculation of the distance of closest approach, or miss distance, is as follows. Find the x and y components of the range from missile to target at the last time step where $\dot{R}_T \leq 0$.

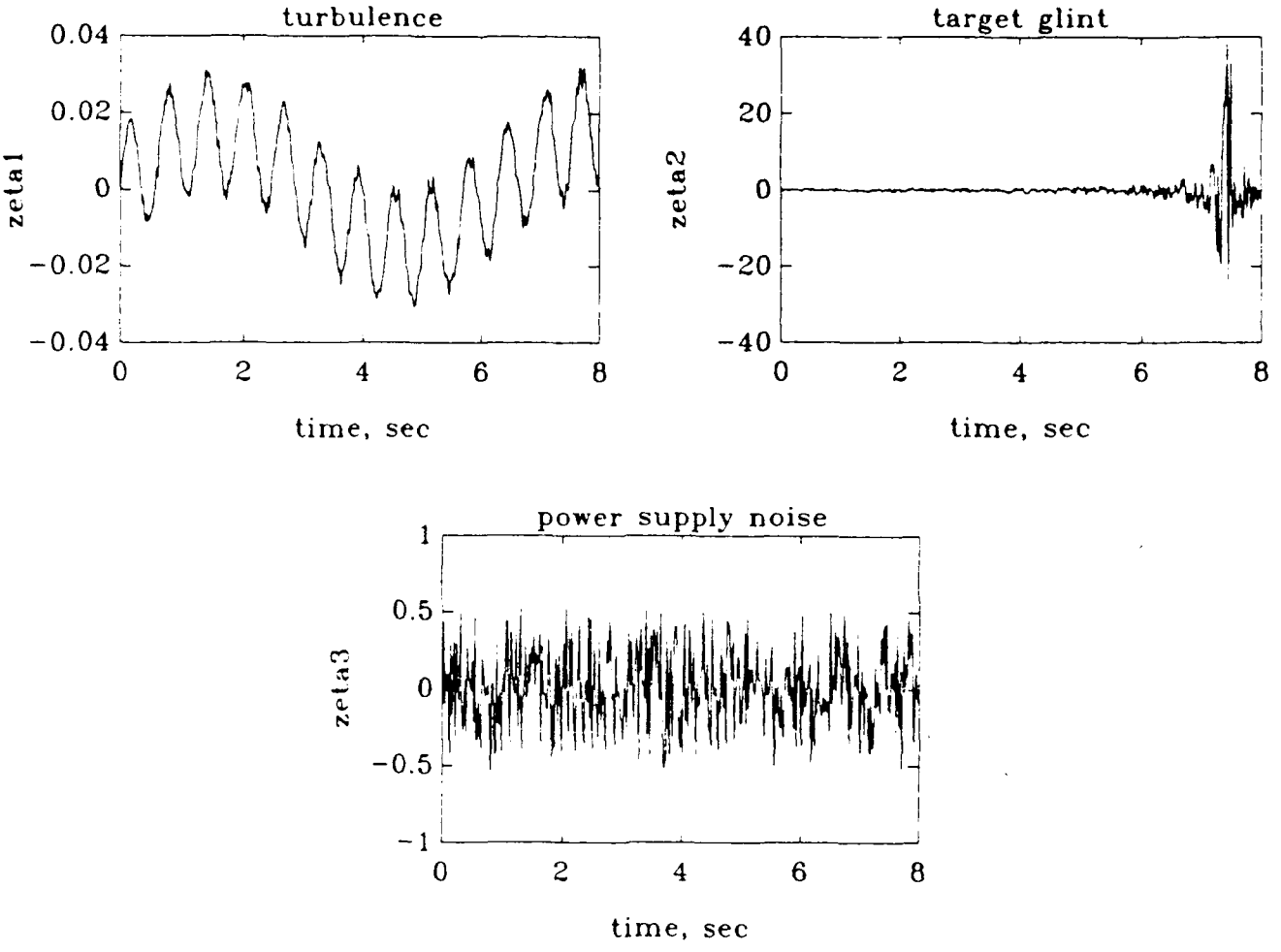

Figure 3.3 ζ Noise Inputs Used in Simulation

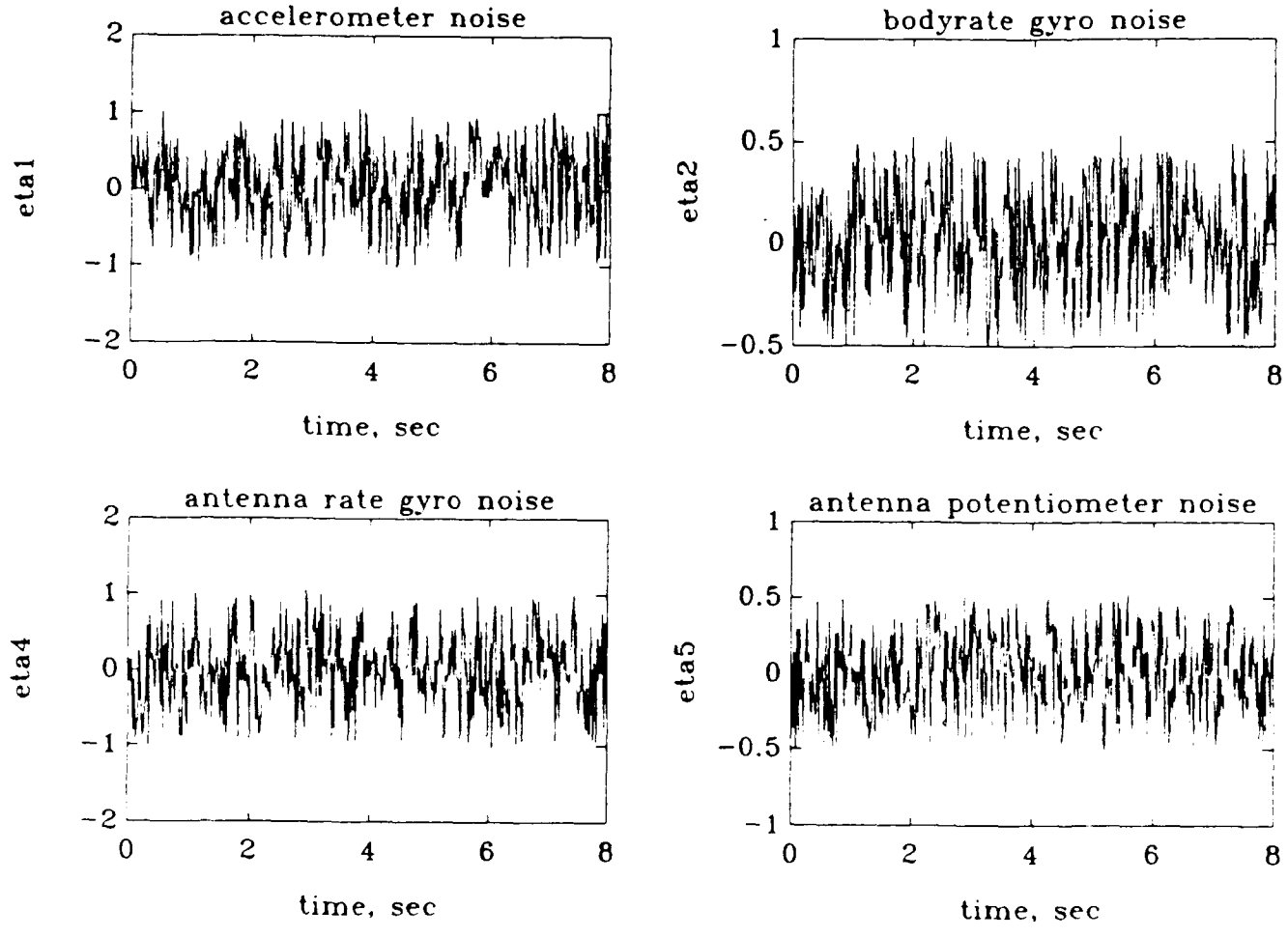

Figure 3.4 η Noise Inputs Used in Simulation

$$x_1 = p_T(x) - p_M(x) \tag{3.24}$$

$$y_1 = p_T(y) - p_M(y) \tag{3.25}$$

At the first time step where $\dot{R}_T > 0$, define

$$x_2 = p_T(x) - p_M(x) \tag{3.26}$$

$$y_2 = p_T(y) - p_M(y) \tag{3.27}$$

Write the x and y range components in terms of t and component closure rate, so that

$$x = x_1 + t(dx/dt) \tag{3.28}$$

$$y = y_1 + t(dy/dt) \tag{3.29}$$

Set $y = 0$ and solve for t/dt.

$$t/dt = -y_1/dt \tag{3.30}$$

Substitute into Equation 3.28 to find the x intercept (x_{int}).

$$x_{int} = x_1 - y_1(dx/dy) \tag{3.31}$$

Using the same process find y_{int}.

$$y_{int} = y_1 - x_1(dy/dx) \tag{3.32}$$

The relationship between x_{int}, y_{int}, and miss distance (md) is shown in Figure 3.5.

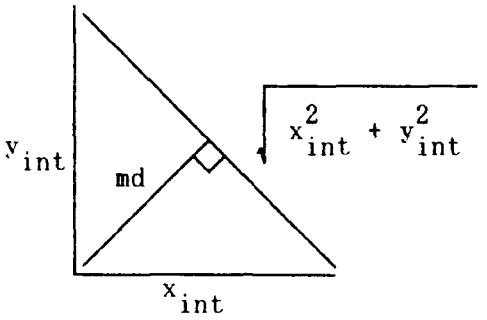

Figure 3.5 Relationships to Miss Distance

Using this relationship the area of the triangle in Figure 3.5 is equal to:

$$\text{Area} = .5 \times x_{int} \times y_{int} \tag{3.33}$$

$$\text{Area} = .5 \times md \times \sqrt{x_{int}^2 + y_{int}^2} \tag{3.34}$$

Combine Equations (3.33) and (3.34) to solve for md.

$$md = \left(y_{int} \times x_{int}\right) \Big/ \sqrt{x_{int}^2 + y_{int}^2} \tag{3.35}$$

IV The Guidance Law

Proportional navigation was used as the guidance law. Changing the value of the navigational constant in the guidance law plays a key role in miss distance results. Breuer [2:2-173] gives the equation for proportional navigation commands as

$$A_B = \varepsilon \, |\dot{R}_T| \, \dot{\lambda}_T \, (\pi/180) \quad m/s^2 \tag{4.1}$$

where A_B is the acceleration of the missile perpendicular to the vector from the missile to the target and ε is the navigational constant used by Breuer. The A_B acceleration will maintain a constant angle between the target and the missile (λ_T) by maintaining $\dot{\lambda}_T$ at zero. The value chosen for ε is related to how tightly the missile will turn to achieve a new desired heading.

An acceleration normal to the missile velocity vector would have the following component of acceleration in the A_B direction

$$A_B = A_n \cos(\lambda_M)(9.8) \quad m/s^2 \tag{4.2}$$

Substituting into Equation (4.1) and solving for A_n yields

$$A_n = \varepsilon/\cos(\lambda_m) \, |\dot{R}_T| \, \dot{\lambda}_T \, (\pi/180)/9.8 \quad g's \tag{4.3}$$

From Figure 2.1 it can be seen that

$$\lambda_T = \phi_T - \gamma_T \quad \text{deg} \tag{4.4}$$

Therefore

$$\dot{\lambda}_T = \dot{\phi}_T - \dot{\gamma}_T \quad \text{deg/s} \tag{4.5}$$

Substituting this result into Equation (4.3) yeilds

$$A_n = \varepsilon/\cos(\lambda_M)\ |\dot{R}_T|\ (\dot{\phi}_T - \dot{\gamma}_T)\ (\pi/180)/9.8 \quad \text{g's} \tag{4.6}$$

The variables of Equation (4.6) must now be transformed into quantities which the missile can measure. Acceleration normal to the missile velocity vector can be approximated by accelerometer readings normal to the missile body axis for small missile angles of attack. In this model it is assumed that the accelerometer readings from the missile are the same as the acceleration normal to the missile velocity vector, or

$$A_n \approx A_{nm} \tag{4.7}$$

During perfect target tracking

$$\theta_m + \theta_s = \phi_T \tag{4.8}$$

so if the seeker is tracking well $\dot{\phi}_T$ can be approximated with $\dot{\theta}_m$ and $\dot{\theta}_s$, which are measureable with rate gyros.

$$\dot{\theta}_m + \dot{\theta}_s \approx \dot{\phi}_T \tag{4.9}$$

The term λ_M is the lead angle which you want to give the target. This angle will depend on the type of targets you are engaging. It can be incorporated into the navigational constant called K_g.

$$K_g = \epsilon/\cos(\lambda_M) \tag{4.10}$$

Closure rate, $|\dot{R}_T|$, is measured by the seeker radar. This missile is unable to measure the target turn rate so target turn rate will be approximated by 0.

$$\dot{\gamma}_T \approx 0 \tag{4.11}$$

Substituting Equations (4.9) through (4.11) into Equation (4.6) yeilds the form of the guidance commands used in the simulation.

$$\begin{aligned} A_{ncom} &= K_g \, |\dot{R}_T| \, (\dot{\theta}_m + \dot{\theta}_s) \, (\pi/180)/9.8 \quad g's \\ &= K_g \, |\dot{R}_T| \, (\dot{\theta}_m + \dot{\theta}_s) \, /561.5 \quad g's \end{aligned} \tag{4.12}$$

This can also be put into the form of a missile heading command using the relationship

$$9.8\left(\frac{180}{\pi}\right)\left(A_n \, / \, V_M\right) = \dot{\gamma}_M = (\dot{\theta}_m - \dot{\alpha}) \quad deg/s \tag{4.13}$$

Combining Equations (4.12) and (4.13) using the nominal value for V_M of 1100

m/s and again saying angle of attack of the missile and its rate are small yields

$$\dot{\theta}_{mcom} = K_g \, |\dot{R}_T| \, (\dot{\theta}_m + \dot{\theta}_s) \, / \, 1100 \quad \text{deg/s} \tag{4.14}$$

This is the guidance command used by Capt Riddle.

A navigational constant, K_g, equal to 3.3 was used for this study. The guidance law was tested by running the simulation with no missile dynamics; that is, a 1100 m/s point moving in space at a 0.02 second simulation time step. Target miss distances were only a few centimeters caused by the time steping. To add realism the simulation limits guidance gain updates to once every 0.3 second and commands straight ahead flight near end game when $R_T/|\dot{R}_T| <= 0.6$. With these limitations the simulation with no missile dynamics still came within 2 meters of the target for the engagement chosen for this study, Figure 4.1. This gave confidence that the miss distance which resulted would be due almost entirely to the response lag caused by the missile and seeker dynamics and not due to the limitations of the guidance command block.

When the simulation was run with a point mass responding with a 0.9 second lag to the guidance commands miss distances corresponded surprisingly well with those resulting from the simulation run with full missile and seeker dynamics, Figure 4.2. The relationship between guidance command execution lag and resulting miss distance for the chosen engagement can be seen in Figure 4.3. How the navigational constant, K_g, effects miss distances for a no execution lag flyout in the same engagement is also shown in Figure 4.3.

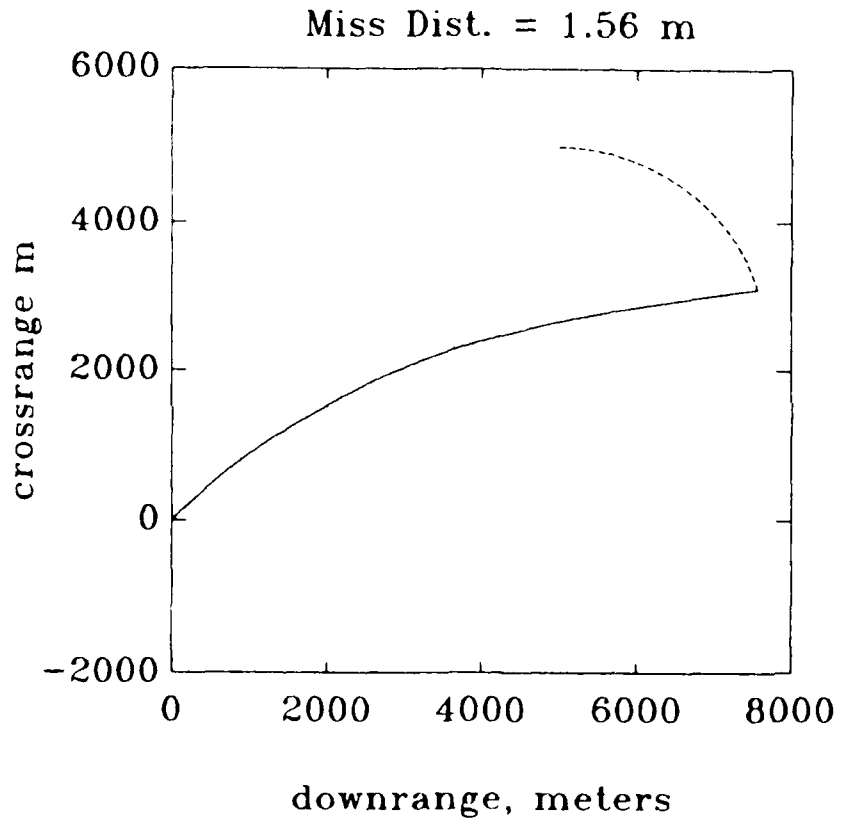

Run number 1
Time Step (sec) = 2.0000e-02
Flyout Time (sec) = 7.28
Target velocity (m/s) = 470
Target turn rate (deg/s) = -9.964
Navigation Constant = 3.3
Comptype = guide
Lag (sec) = 0

Figure 4.1 Run 1, Ideal Missile with No Execution Lag

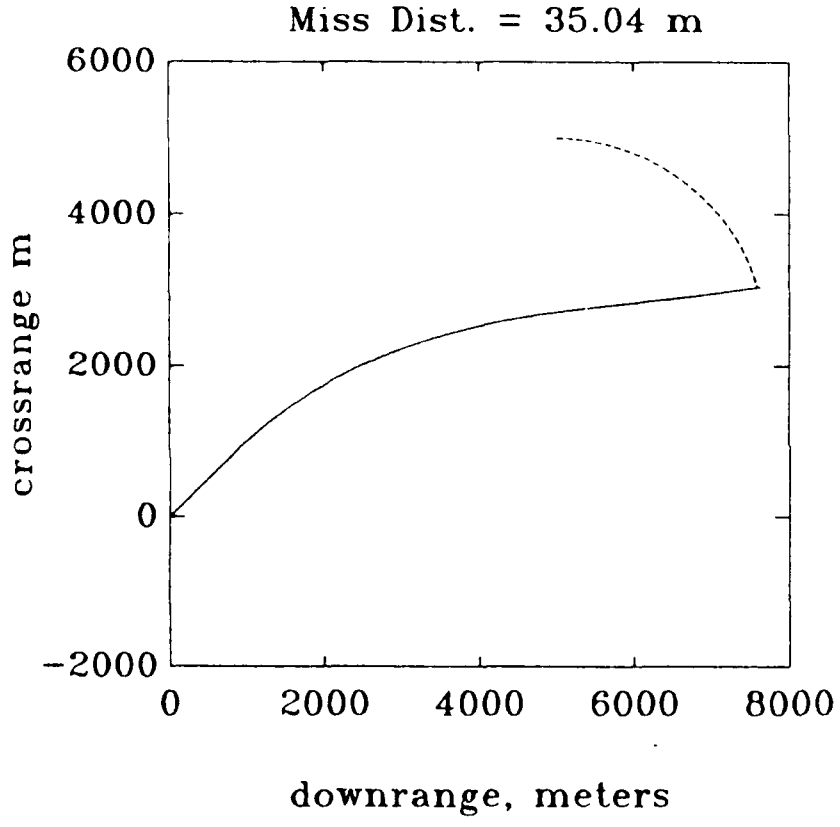

Run number 2
Time Step (sec) = 2.0000e-02
Flyout Time (sec) = 7.38
Target velocity (m/s) = 470
Target turn rate (deg/s) = -9.964
Navigation Constant = 3.3
Comptype = guide
Lag (sec) = 0.9

Figure 4.2 Run 2, Ideal Missile with 0.9 Second Execution Lag

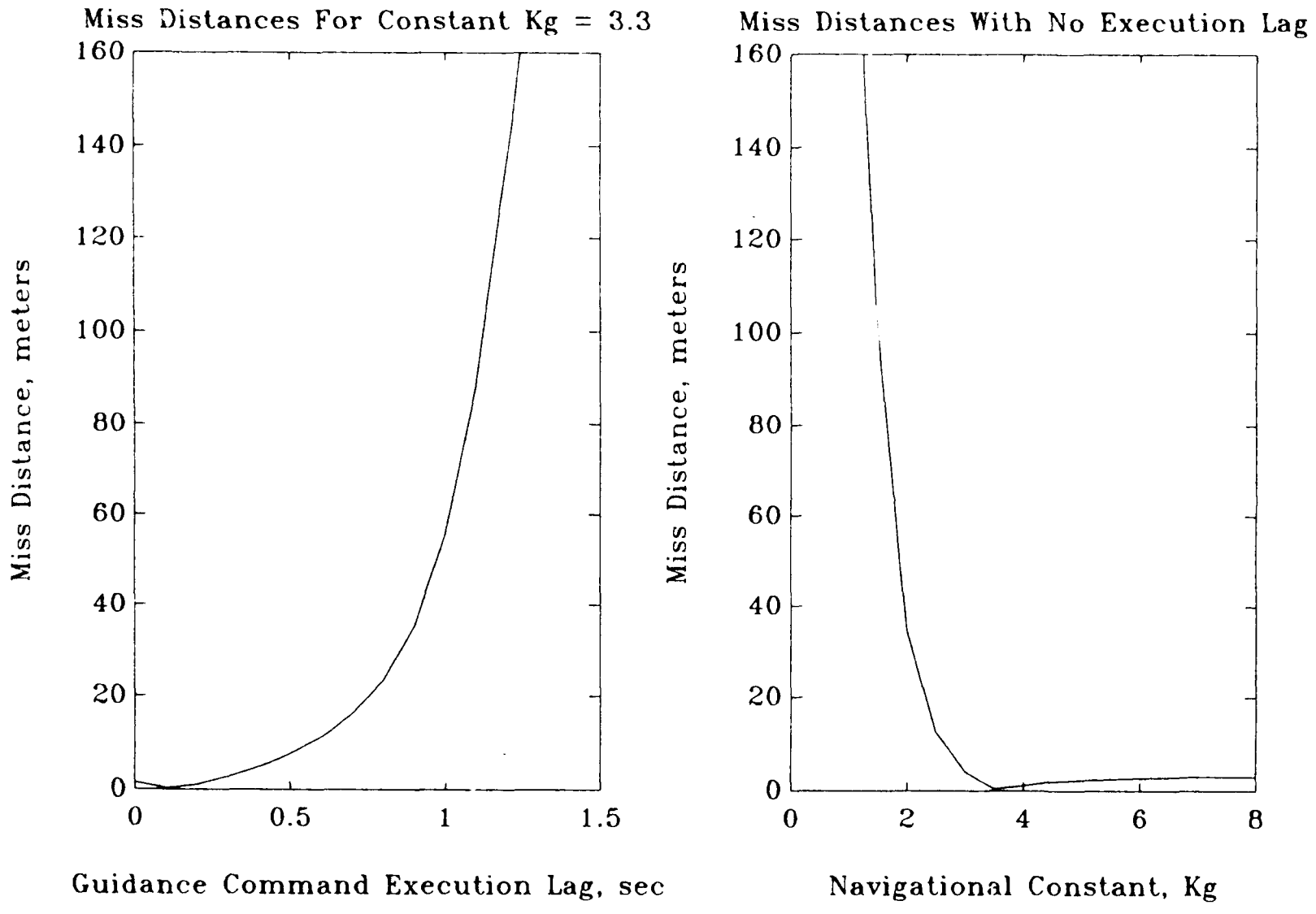

Figure 4.3 Execution Lag and Navigational Constant Effects

When running the simulations with full missile dynamics it was found that for a given engagement a value of the navigational constant could be chosen to increase the missile turn rate just enough to offset the guidance command execution lag at the point of end game, resulting in near zero miss distance. That was equivalent to flying a timed pattern to point in space where the target would be when the missile arrived. It is entirely scenario dependent and not something which could be could practically applied but it does point out that using miss distance for a measure of merit in judging competeing controller performance can sometimes be misleading. That is why other techniques to evaluate controller performance were used along with miss distance.

V Refining the Model and Simulation

Three areas of model and simulation refinment were investigated. Simulations were run with a smaller time step, the missile parameter variations were checked, and high frequency unmodeled dynamics were added to the missile model.

Capt Riddle ran his simulations with a 0.02 second time step. To increase the fidelity of the simulation a selection of Capt Riddle's runs were made with a 0.02 and a 0.001 second time step. Runs were made with and without noise and parameter variations. The results showed there was no significant difference in flyout and miss distance results. Average miss distances were within a meter of each other for the two time steps.

Capt Riddle's simulation runs with the nominal missile performed worse than with the missile run with parameter variations. Though this seems unnatural it proved to be resonable. The δ_{com} to A_n and δ_{com} to $\dot{\theta}_m$ transfer functions are shown with Equations (5.1) and (5.2) and in Table 5.1. The nominal system, which is roughly the system at 4 seconds of flyout, has the nonminimum phase zero and the unstable pole closest together making it the most difficult control problem to solve. Thus, even though this is the

$$\frac{A_n}{\delta_{com}} = \left[\begin{array}{ccc:c} -77 & 0 & 0 & 77 \\ M_\delta & 0 & -M_\alpha & 0 \\ -N_\delta/V_M & 1 & -N_\alpha/V_M & 0 \\ \hdashline 1 & 0 & 2 & 0 \end{array}\right] \qquad (5.1)$$

$$\frac{\dot{\theta}_m}{\delta_{com}} = \left[\begin{array}{ccc:c} -77 & 0 & 0 & 77 \\ M_\delta & 0 & -M_\alpha & 0 \\ -N_\delta/V_M & i & -N_\alpha/V_M & 0 \\ \hdashline 0 & 1 & 0 & 0 \end{array}\right] \qquad (5.2)$$

Table 5.1 δ_{com} to A_n and δ_{com} to $\dot{\theta}_m$ Transfer Functions

Fly Out Time (sec)	Transfer Functions δ_{com} to A_n	Transfer Functions δ_{com} to $\dot{\theta}_m$
0	$\frac{77(s+2.3103)(s-2.4003)}{(s+77)(s+1.0361)(s+0.0139)}$	$\frac{77(-2.78)(s+1.047)}{(s+77)(s+1.0361)(s+0.0139)}$
4	$\frac{77(s+2.699)(s-2.5872)}{(s+77)(s+1.6209)(s-0.5323)}$	$\frac{77(-3.06)(s+1.2263)}{(s+77)(s+1.6209)(s-0.5323)}$
8	$\frac{77(s+2.2543)(s-1.5363)}{\Delta}$	$\frac{77(-2.316)(s+1.0073)}{\Delta}$
	where $\Delta = (s+77)(s+0.5525+0.92927i)(s+0.5525-0.92927i)$	
nominal system	$\frac{77(s+2.5278)(s-2.5278)}{(s+77)(s+1.5917)(s-0.5712)}$	$\frac{77(-2.74)(s+1.1894)}{(s+77)(s+1.5917)(s-0.5712)}$

controller design point, it is not unreasonable that variations which are easier to control performed better. During this investigation it was found that Capt Riddle's Taylor series approximations for $-N_\delta/V_M$ and $-N_\alpha/V_M$ were not very good so Taylor series approximations were replaced with the actual division in the simulation and the analysis.

High frequency unmodeled dynamics were added to the simulation and the

missile for analysis purposes. They are not included for controller design. Through their addition it was hoped that the H_2 and H_∞ controllers robustness advantages could be seen. Based on a plot of measured data, Reichert, in reference [3:2371-2372], adds high frequency unmodeled missile dynamics to A_n using

$$\frac{ud}{\delta} = \frac{100(s+10)^3}{(s+1000)^3} \tag{5.3}$$

This was adapted for this study's missile model. The high frequency unmodeled dynamics were added to A_n and $\dot{\theta}_m$ as

$$\frac{ud}{\delta} = \frac{6.4(s+10)^3}{(s+400)^3} \tag{5.4}$$

Equation (5.4) adequately characterized the measured data and the smaller pole value, -400 versus -1000, makes the $(sI-A)^{-1}$ matrix inversion computationally easier. The state space form transfer function used is shown in Equation (5.5).

$$\frac{ud}{\delta} = \left[\begin{array}{ccc:c} -400 & 0 & 0 & -390 \\ -390 & -400 & 0 & -390 \\ -390 & -390 & -400 & -390 \\ \hdashline 6.4 & 6.4 & 6.4 & 6.4 \end{array}\right] \tag{5.5}$$

Appendix A shows how this was integrated into the plant state space matrices. Chapter 8 shows the effects the high frequency unmodeled dynamics had on the simulations.

VI Controller Analysis

Because Capt Riddle's simulation miss distance results did not clearly differentiate desirability of the three controllers, other analysis techniques to supplement miss distances were deemed necessary. The controllers were evaluated by evaluating the closed loop missile in three areas: performance, noise attenuation, and robustness.

6.1 Performance Analysis

The missile's ability to carry out commanded inputs with minimal lag was evaluated by taking the guidance command block derived in Chapter 6

$$A_{ncom} = K_g \, |\dot{R}_T| \, \dot{\phi}_T \, / \, 561.5 \quad g's \tag{6.1}$$

converting A_{ncom} to turn rate

$$\dot{\gamma}_M = K_g \, |\dot{R}_T| \, \dot{\phi}_T \, / \, 1100 \quad deg/s \tag{6.2}$$

and inputing a step command for $\dot{\phi}_T$ using the nominal values for $|\dot{R}_T|$, V_M and K_g shown in Table 6.1.

Table 6.1 Nominal Values Used in Performance Evaluation

$\dot{\phi}_T$ = 10 deg/s
$\|\dot{R}_T\|$ = 1500 m/s
K_g = 3.3
V_M = 1100 m/s

The value of 10 deg/s for $\dot{\phi}_T$ was chosen after running some simulated engagements to find the upper limit which $\dot{\phi}_T$ reached outside of the endgame. The result is a commanded acceleration normal to the missile velocity vector of 88 g's or a turn rate of 45 deg/s. The $\dot{\phi}_T$ to $\dot{\gamma}_M$ transfer function was found for the nominal missile system. The $\dot{\gamma}_M$ time response was examined for a $\dot{\phi}_T$ step input of 10 deg/s. This was compared to the commanded turn rate of 45 deg/s as a measure of controller performance. Singular value plots for this transfer function were also examined.

To find the $\dot{\phi}_T$ to $\dot{\gamma}_M$ transfer function, first calculate the closed loop transfer function for the nominal missile, G_m. Figure 6.1 shows the block diagram and Equation (6.3) shows the transfer function in state space form of G_m.

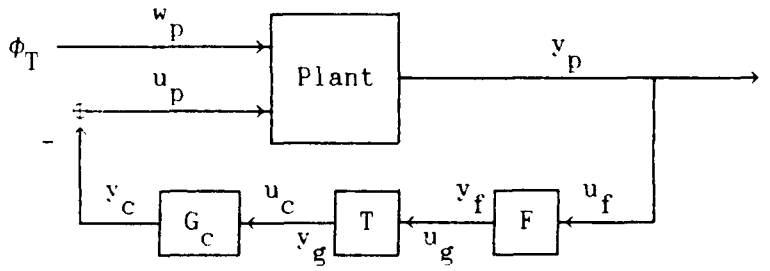

Figure 6.1 Simplified Closed Loop Missile Block Diagram

$$G_m = \left[\begin{array}{cc|c} (A_p - B_{p11} D_c TFC_p) & -B_{p11} C_c & B_{p12} \\ B_c TFC_p & A_c & 0 \\ \hline C_p & 0 & 0 \end{array}\right] \qquad (6.3)$$

Next, an integrator is put in front of the input and R = [.51 0 0 0 0 0]

is multiplied by the output to obtain the transfer function for $\dot{\phi}_T$ to $\dot{\gamma}_M$, G_s. The block diagram for G_s is shown in Figure 6.2 and its state space transfer function is shown in Equation (6.4).

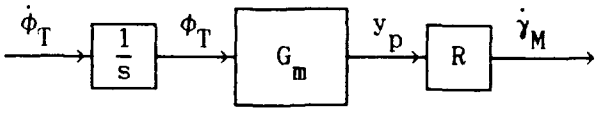

Figure 6.2 G_s System Block Diagram

$$G_s = \left[\begin{array}{ccc:c} (A_p - B_{p11} D_c TFC_p) & -B_{p11} C_c & B_{p12} & 0 \\ B_c TFC_p & A_c & 0 & 0 \\ 0 & 0 & 0 & 1 \\ \hdashline RC_p & 0 & 0 & 0 \end{array}\right] \qquad (6.4)$$

The results of this analysis is shown in Figures 6.3 through 6.6. It is done with and without the unmodeled dynamics added.

The closed loop missile time responses with the the H_2 and H_∞ controllers are better damped than the conventional controller but without a reduction in lag time. The only difference in time responses when the high frequency unmodeled dynamics are added is that the H_∞ controlled missile goes unstable. This is contrary to H_∞ optimization theory indicating that this is an improperly formulated H_∞ controller.

The closed loop missile singular value plots should have a flat gain of 4.5 (13 dB) at low frequencies with a gain drop off at high frequencies. The singular value plots of the closed loop missile with the H_2 and H_∞

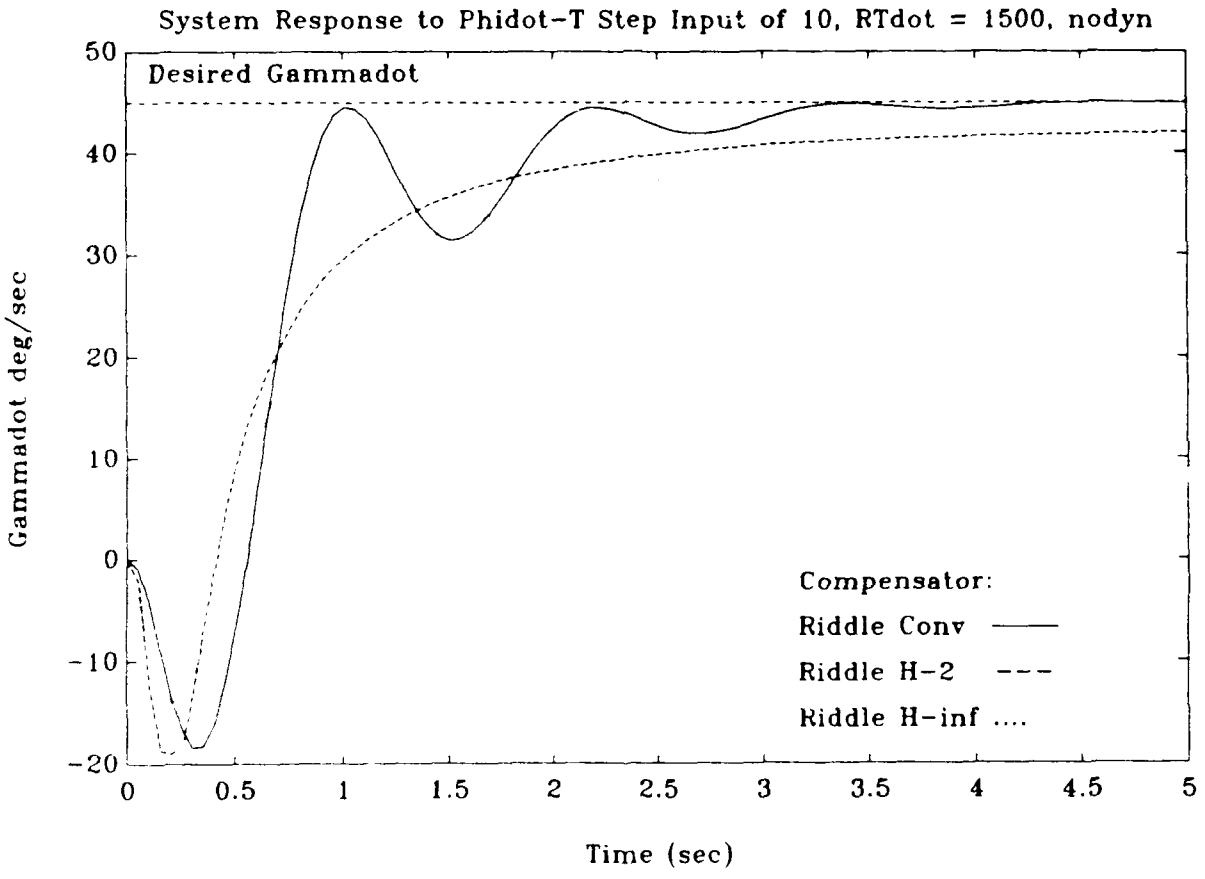

Figure 6.3 Missile Turn Rate Time Responses without Unmodelled Dynamics

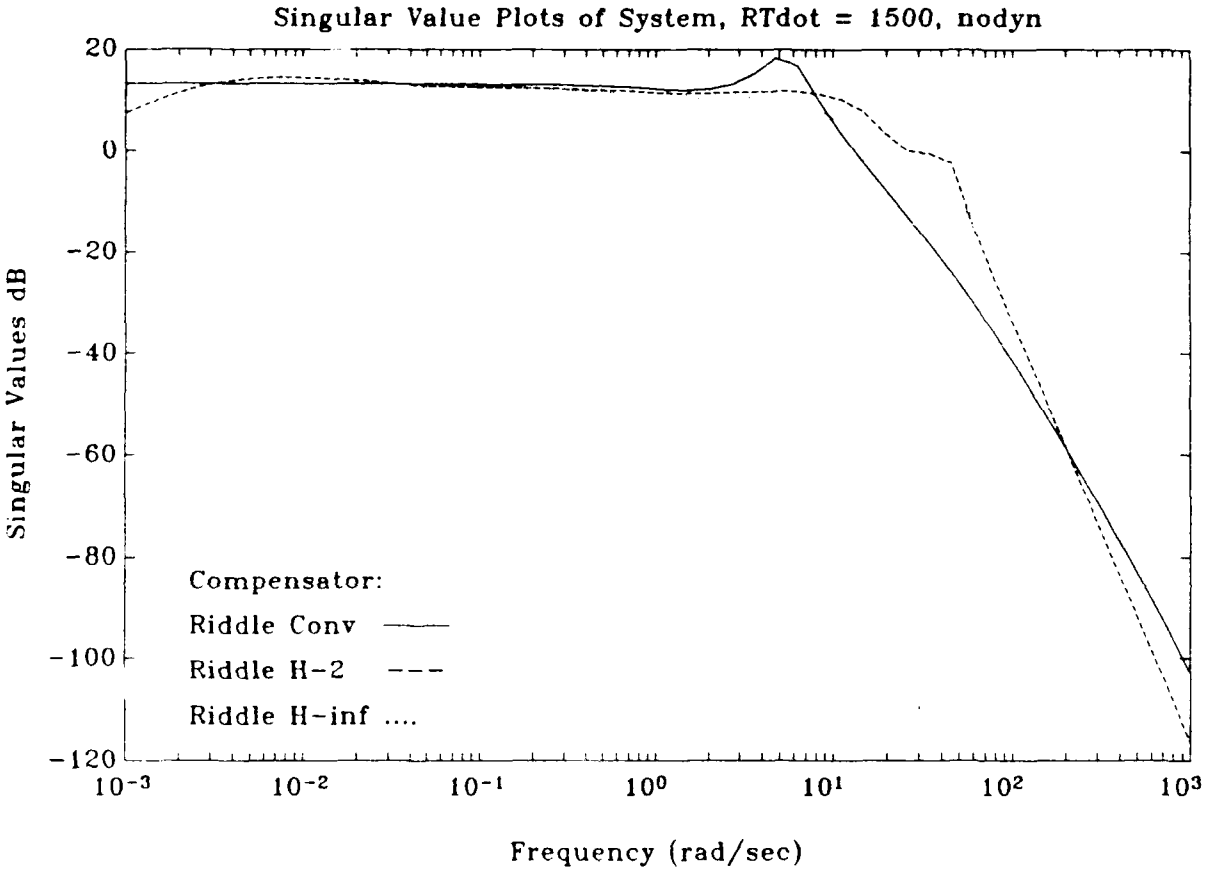

Figure 6.4 G_s Singular Value Plots without Unmodelled Dynamics

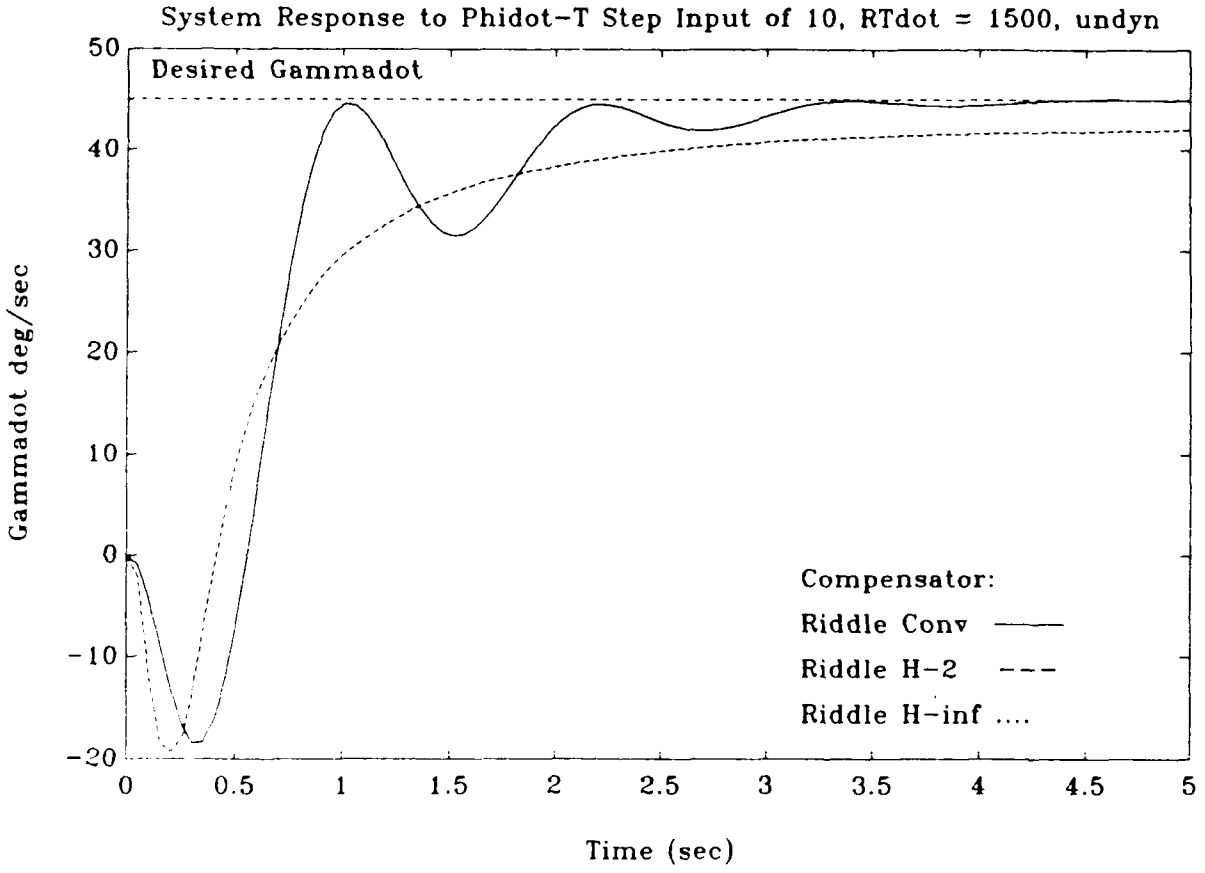

Figure 6.5 Missile Turn Rate Time Responses with Unmodelled Dynamics

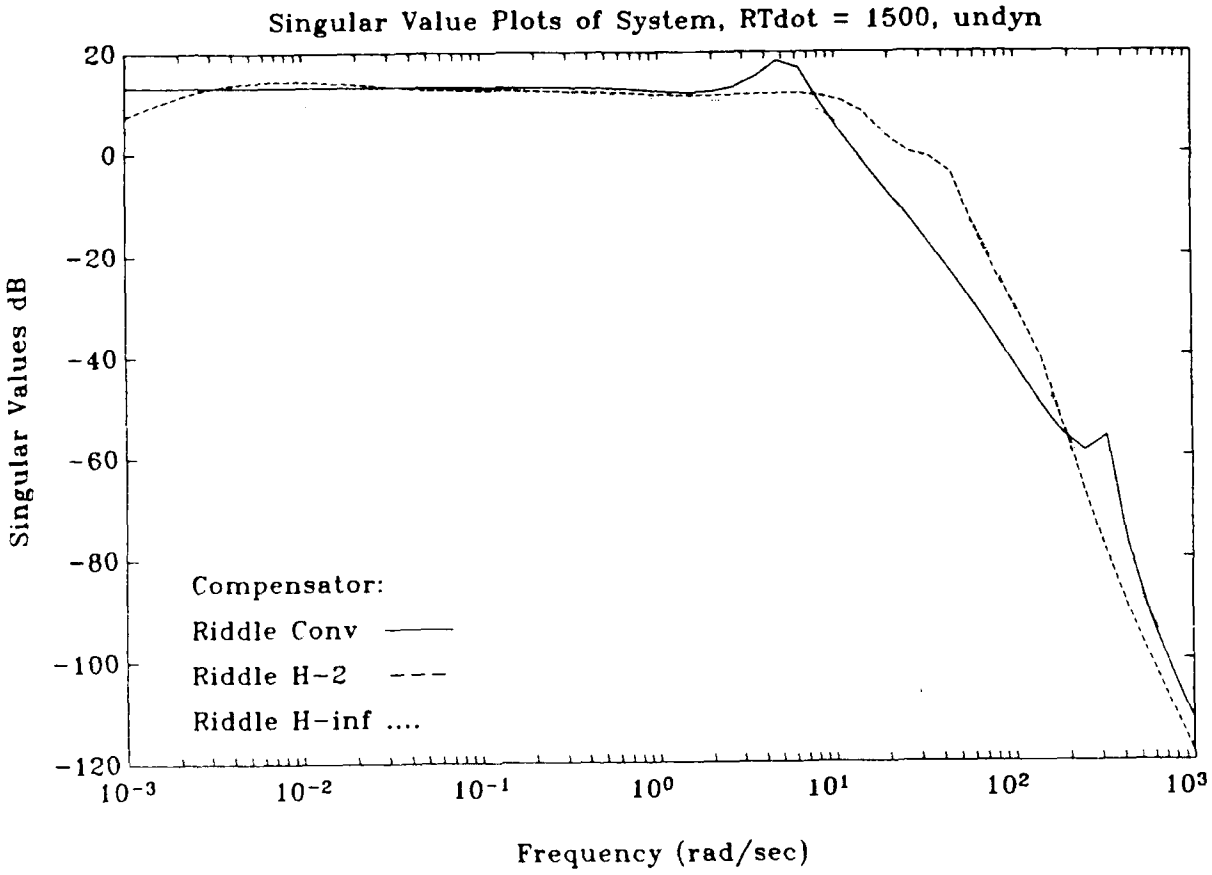

Figure 6.6 G_s Singular Value Plots with Unmodelled Dynamics

controllers are better than those with the conventional controller at high frequencies but are lacking in gain at the lower frequencies. This indicates the need for some filter shifting during the H_2 and H_∞ controller design process. Adding high frequency unmodelled dynamics only slightly effected the singular value plots at high frequencies.

6.2 Noise Attenuation Analysis

For this analysis the same nominal system is used as in the performance analysis except this time the η to $\dot{\gamma}_M$ and ζ to $\dot{\gamma}_M$ transfer functions are found. Singular value plots of the transfer functions are analyzed to see how well noise inputs are attenuated. Again cases with and without high frequency unmodeled dynmics are examined.

The block diagram for the η to $\dot{\gamma}$ transfer function is shown in Figure 6.7.

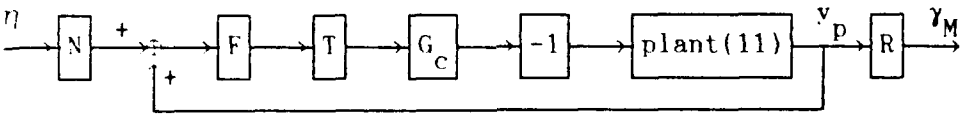

Figure 6.7 η to $\dot{\gamma}_M$ Block Diagram, G_η

N is a matrix which removes η_3 and η_6 inputs since there are none in the simulation. N is given in Equation (6.5).

$$N = \begin{bmatrix} 1 & 0 & 0 & 0 \\ 0 & 1 & 0 & 0 \\ 0 & 0 & 0 & 0 \\ 0 & 0 & 1 & 0 \\ 0 & 0 & 0 & 1 \\ 0 & 0 & 0 & 0 \end{bmatrix} \tag{6.5}$$

The state space transfer function for η to $\dot{\gamma}_M$ is shown in Equation (6.6).

$$G_\eta = \left[\begin{array}{cc|c} (A_p - B_{p11} D_c TFC_p) & -B_{p11} C_c & -B_{p11} D_c TFN \\ B_c TFC_p & A_c & B_c TFN \\ \hline RC_p & 0 & 0 \end{array}\right] \qquad (6.6)$$

The block diagram for the ζ to $\dot{\gamma}_M$ transfer function is shown in Figure 6.8.

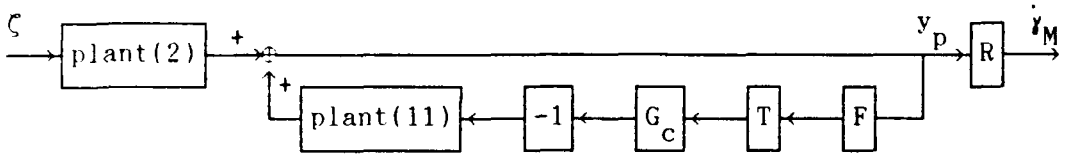

Figure 6.8 ζ to $\dot{\gamma}_M$ Block Diagram, G_ζ

The state space transfer function for ζ to $\dot{\gamma}_M$ is shown in Equation (6.7).

$$G_\zeta = \left[\begin{array}{ccc|c} A_p & 0 & 0 & B_{p2} \\ -B_{p11} D_c TFC_p & (A_p - B_{p11} D_c TFC_p) & -B_{p11} C_c & -B_{p11} D_c TFD_{p2} \\ B_c TFC_p & B_c TFC_p & A_c & B_c TFD_{p2} \\ \hline RC_p & RC_p & 0 & RD_{p2} \end{array}\right] \qquad (6.7)$$

The noise analysis results are shown in Figures 6.9 through 6.12. Again 13 dB would be zero attenuation. In general both the η and ζ attenuation are

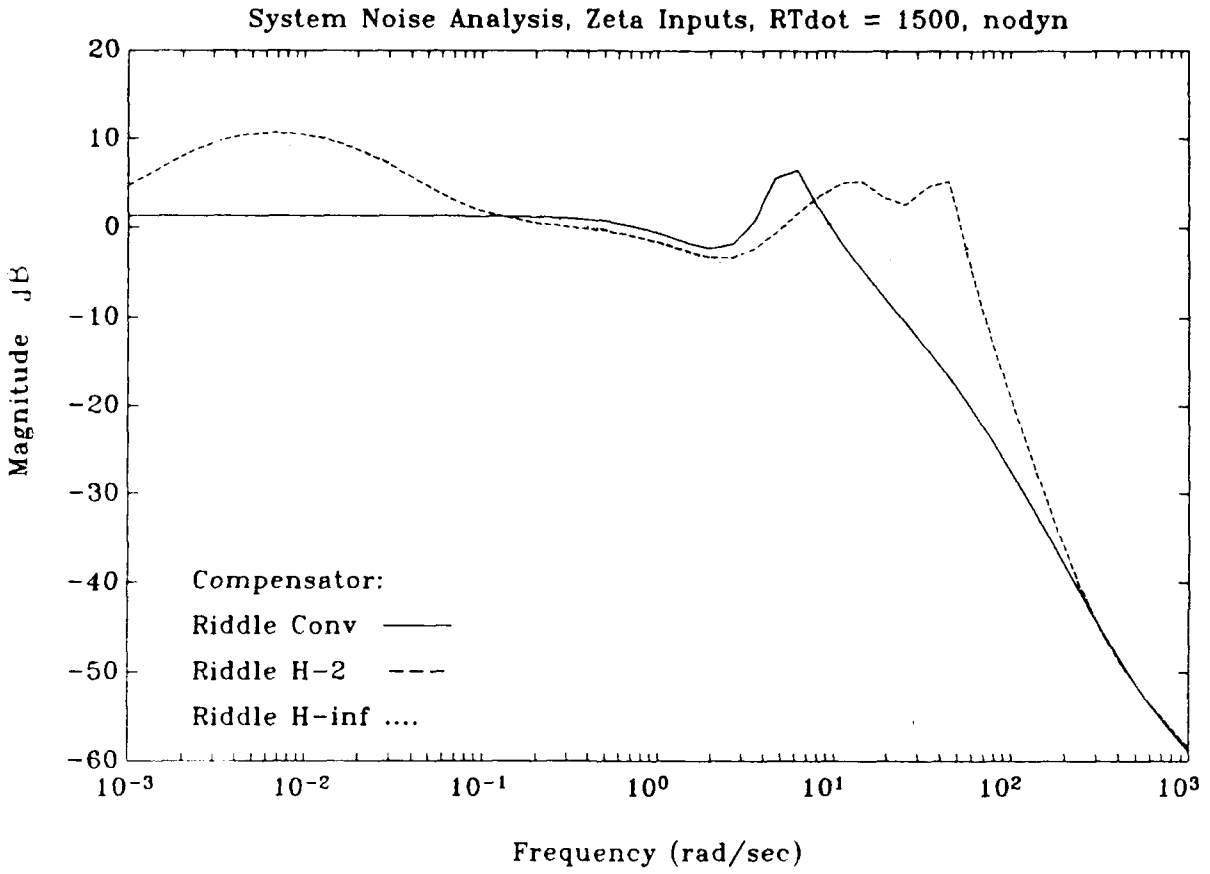

Figure 6.9 G_ζ Singular Value Plots without Unmodelled Dynamics

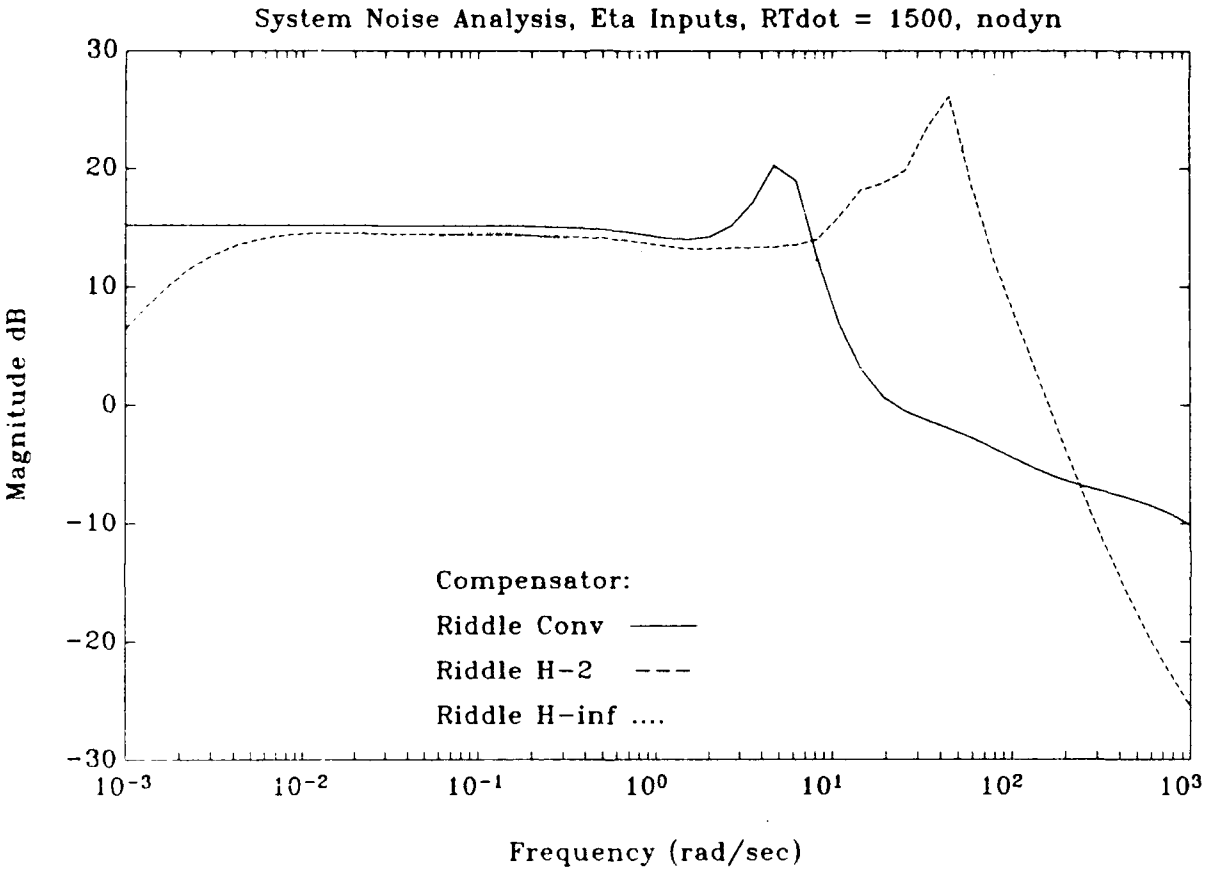

Figure 6.10 G_{η} Singular Value Plots without Unmodelled Dynamics

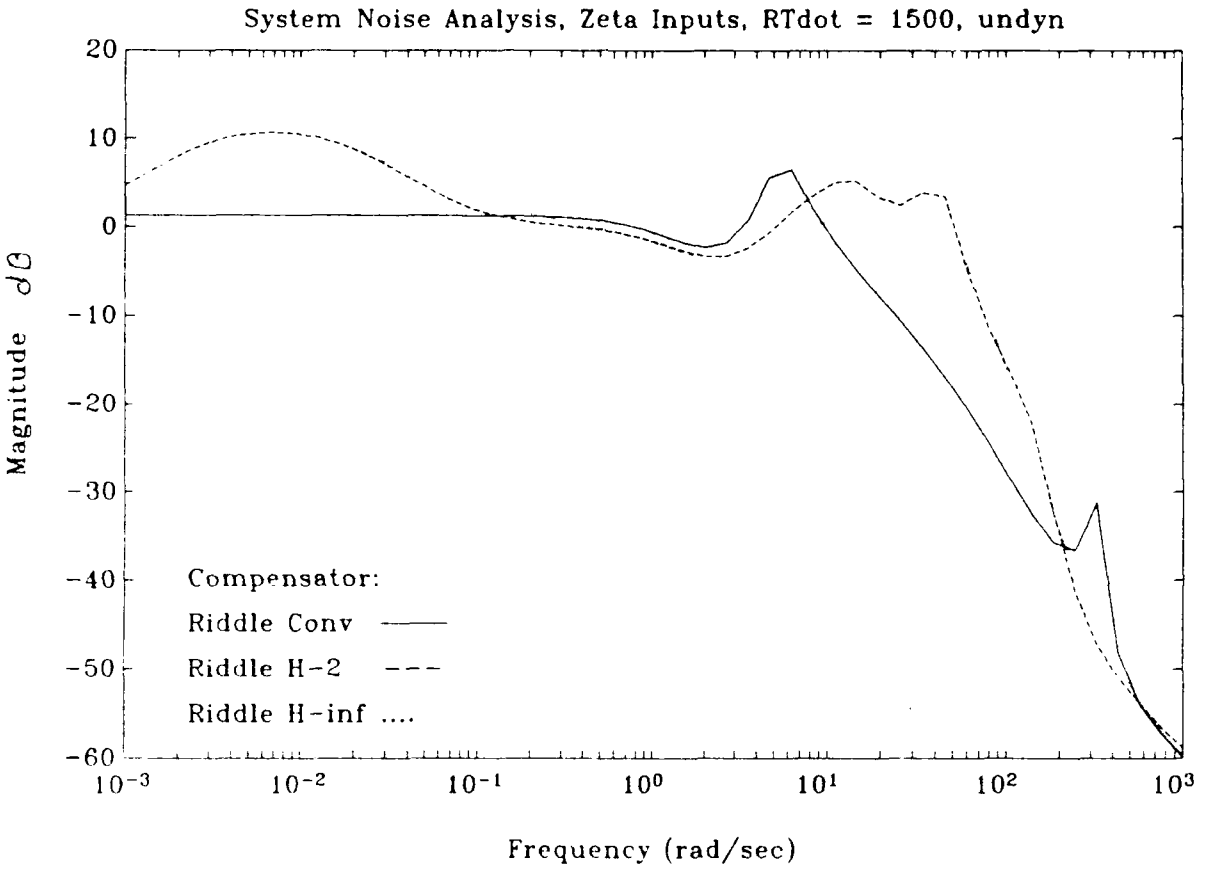

Figure 6.11 G_ζ Singular Value Plots with Unmodelled Dynamics

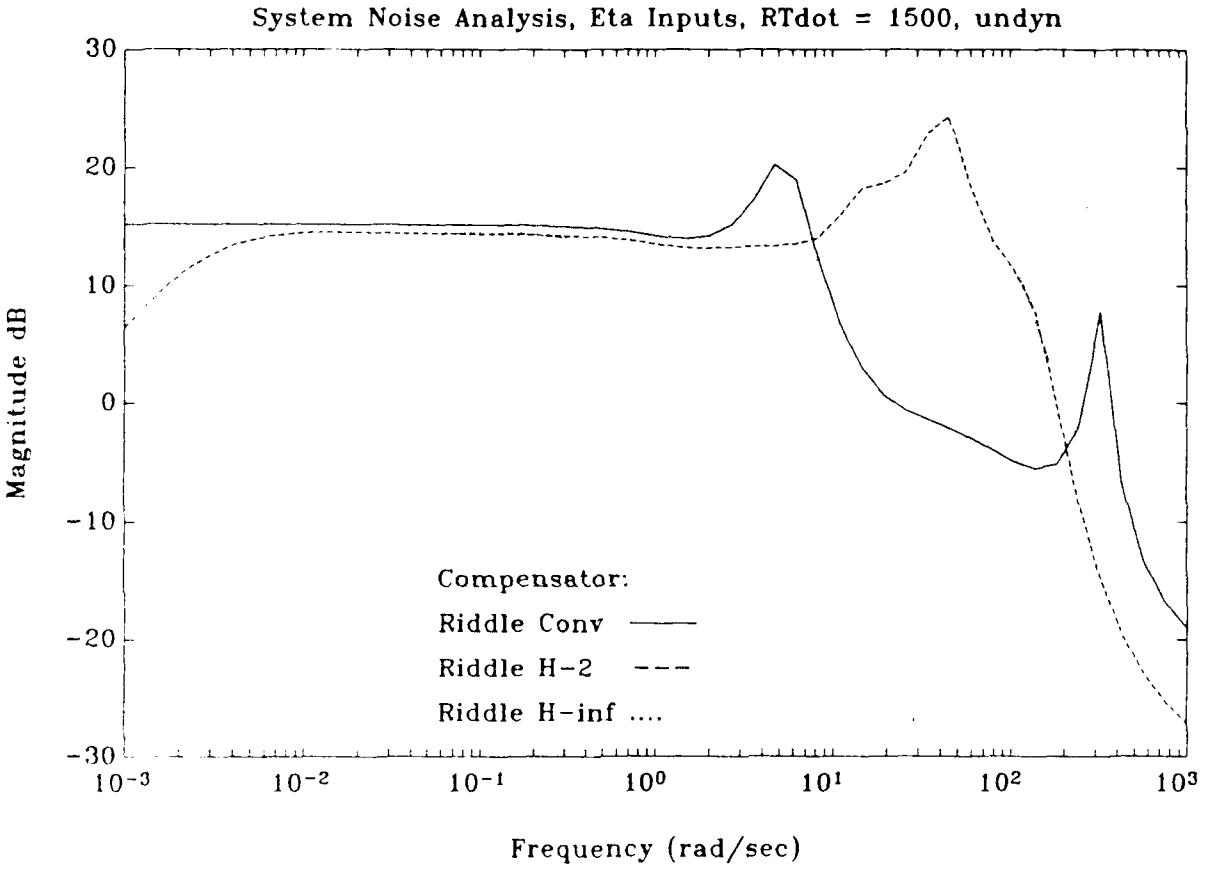

Figure 6.12 G_{η} Singular Value Plots with Unmodelled Dynamics

better with the conventional controller than with the H_2 and H_∞ controllers indicating a need to change the filters used during H_2 and H_∞ design.

6.3 μ Robustness Analysis

The μ robustness analysis was performed as described in reference [4]. The code from this reference is also used. The first step in the μ analysis is to construct an M matrix. The form of the M matrix is shown in Figures 6.13 and 6.14.

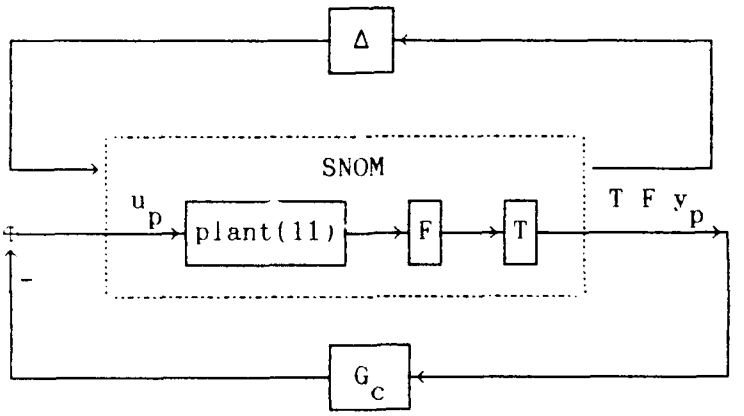

Figure 6.13 Formation of M Transfer Function for μ-Analysis

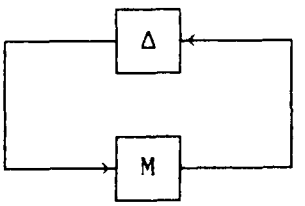

Figure 6.14 M Transfer Function for μ-Analysis

A nominal system is chosen with state space values set at the midpoint of the range of their variations. The nominal system is shown in Equation (6.8).

$$SNOM = \left[\begin{array}{c|c} A_p & B_{p11} \\ \hline TFC_p & D_{p11} \end{array}\right] \quad \begin{array}{l}\text{with state space values} \\ \text{selected at the midpoint} \\ \text{of their range}\end{array} \qquad (6.8)$$

Then a scale value is chosen to indicate the extent of the variation. Plant variations considered are those due to aerodynamic changes with altitude and missile weight changes as described in Chapter 2. Variations in the guidance law gain are also considered. The guidance law is allowed to vary by changing $|\dot{R}_T|$ from 0 to 2000 m/s. Again a nominal value at the midpoint of the range is chosen with scaling inputs indicating the extent of the variation. The scaling information is contained in a matrix called PSCAL shown in Table 6.2.

Table 6.2 Plant Scaling Matrix Used in μ Analysis

PSCAL = SNOM

index	row	column	scale	center value	notes
1	2	1	0.4	-2.70	M_δ
1	2	4	-1.0	-0.15	$-M_\alpha$
1	4	1	0.1885	-0.382	$-N_\delta/V_M$
1	4	4	-0.0272	-1.0778	$-N_\alpha/V_M$
1	11	1	0.35	0.75	N_δ
1	11	4	0.2	2.10	N_α
2	16	2	3.0	3.0	guidance gain on $\dot{\theta}_m$
2	16	6	3.0	3.0	guidance gain on $\dot{\theta}_s$

If A_{ncom} is used instead of $\dot{\theta}_{mcom}$ the 3.0 scaling for the guidance law must be changed to 5.88, since Equation (4.12) is used instead of Equation (4.14). The sign of the scale value indicates its slope with respect to the other varying parameters. The aerodynamic changes are considered to be a function of the same parameters, therefore they have the same index, one. Likewise all the guidance law variations also have the same index, two. This information was input into the mrform.m and mureal.m functions described in reference [4] to obtain the μ robustness analysis results seen in Figures 6.15 and 6.16. The functions don't give the exact μ solution but an upper limit of its value. The true value of μ could be as much as 20% lower.

All the controllers maintain a value of μ_{real} below one for the case without high frequency unmodelled dynamics, indicating the closed-loop systems are stable. When high frequency unmodelled dynamics are added, only the system with the H_2 controller remains stable for high frequency inputs. The performance of the H_∞ controller is worse than expected again indicating an error was made during the formulation of the H_∞ controller design.

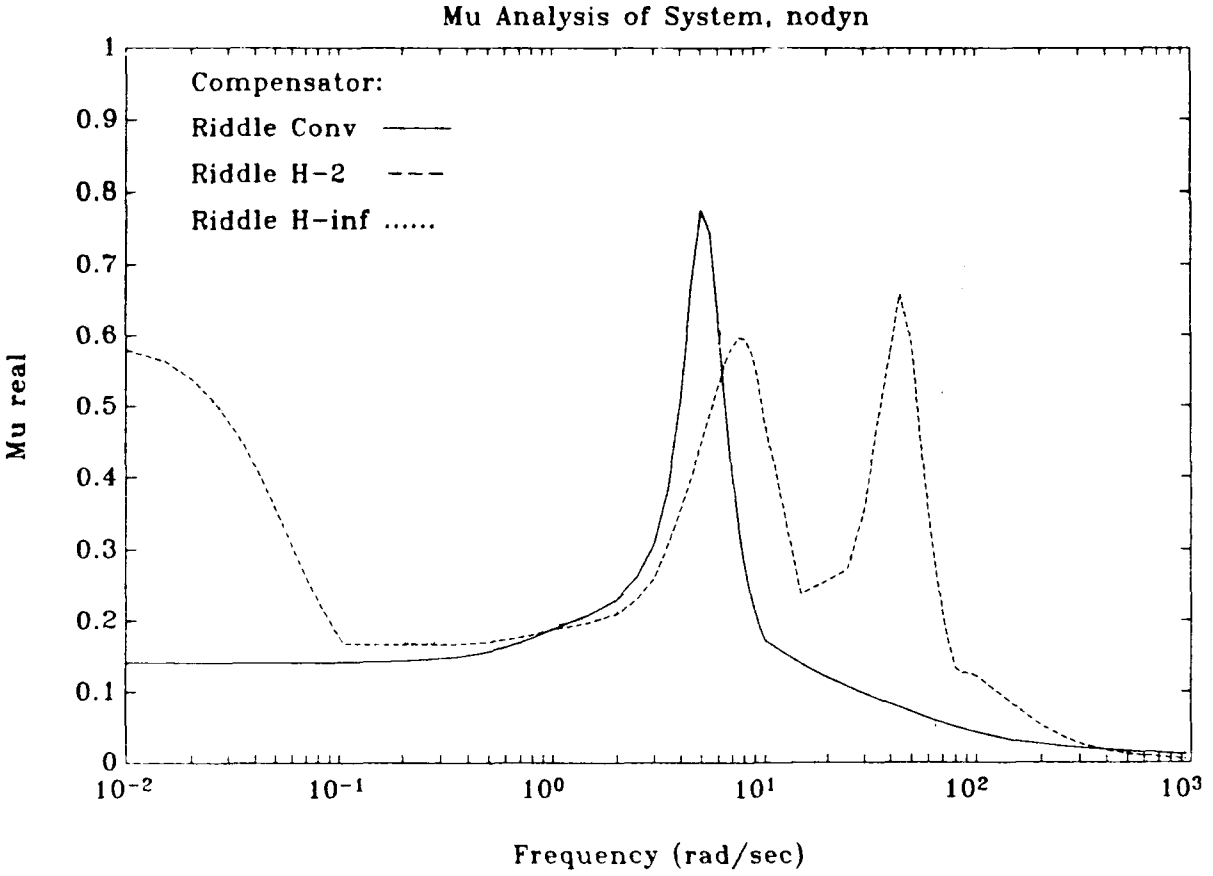

Figure 6.15 μ-Analysis of System without Unmodelled Dynamics

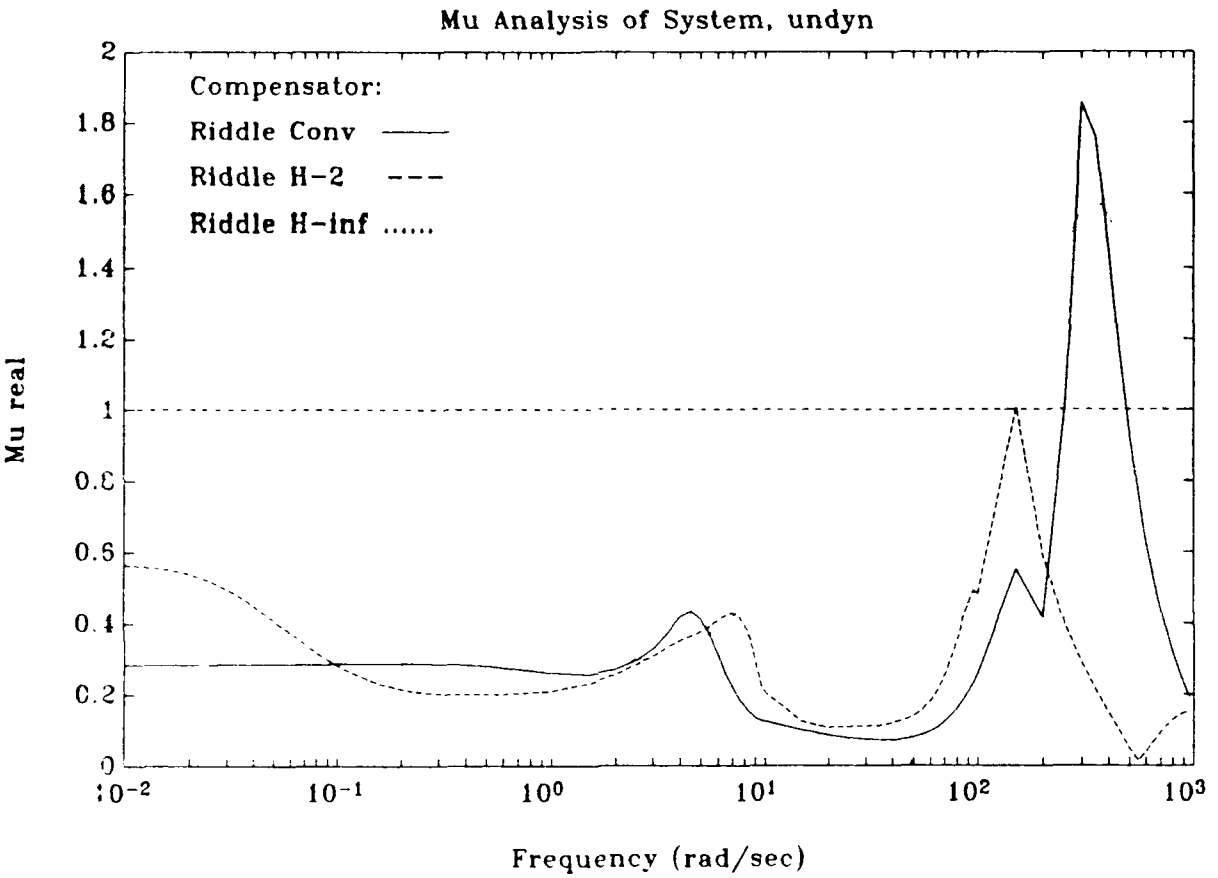

Figure 6.16 μ-Analysis of System with Unmodelled Dynamics

VII H_2 and H_∞ Controller Design

Due to lack of time an improved controller design was not completed. However, a brief background of the design process used will be described in this chapter.

The appeal of H_2 and H_∞ controller designs is that they minimize disturbance effects, w, on outputs, z. This is shown in block diagram form in Figure 7.1.

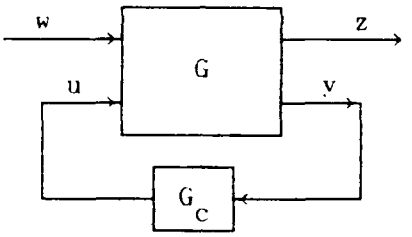

Figure 7.1 Plant Block Diagram for H_2 and H_∞ Construction

The variable definitions as applied to the problem in this study are given in Table 7.1.

The H_2 design objective is to minimize the 2-norm shown in Equation (7.1).

$$\|G_{zw}\|_2 := \left(\frac{1}{2\pi}\int_{-\infty}^{+\infty} \text{trace}\left(G_{zw}(j\omega)^* G_{zw}(j\omega)\right) d\omega\right)^{1/2} \qquad (7.1)$$

The 2-norm is related to the area under a singular value plot. H_2 optimization is good for minimizing the effect of random noise type disturbances.

Table 7.1 Variable Definitions for H_2 and H_∞ Designs

external inputs

$$w = \begin{bmatrix} r \\ \phi_T \\ \zeta \\ \eta \end{bmatrix}$$

outputs to be minimized

$$z = \begin{bmatrix} r - v \\ \rho\, u_p \end{bmatrix}$$

commanded inputs

$$r = \begin{bmatrix} A_{ncom} \\ \dot{\theta}_{mcom} \\ \phi_{com} \\ \dot{\theta}_{scom} \\ \theta_{scom} \end{bmatrix}$$

plant outputs $v = F\, y_p$

$$v = \begin{bmatrix} A_n \\ \dot{\theta}_m \\ \phi \\ \dot{\theta}_s \\ \theta_s \end{bmatrix}$$

controller output or plant input

$$u = \begin{bmatrix} \delta_{com} \\ \omega \end{bmatrix}$$

controller input

$$y = \begin{bmatrix} r - v \end{bmatrix}$$

The H_∞ design objective is to mininmize the ∞-norm shown in Equation (7.2).

$$\|G_{zw}\|_\infty := \sup_\omega \sigma_{max}\left(G_{zw}(j\omega)\right) \qquad (7.2)$$

The ∞-norm is the peak value of a singular value plot. H_∞ optimization is best for minimizing the effect of bounded energy disturbances and for stability robustness.

For multiple-input/multiple-output designs weighting filters are used

to tailor the relative importance and frequency ranges of different inputs and outputs in the controller design. Input weighting filters are chosen to look like expected disturbance or command inputs. Output weighting filters or penalty functions are chosen with a frequency band to match the desired output. The higher the magnitude of a penalty function for a commanded input the harder the controller will try to obtain that commanded input relative to the other inputs.

The block diagram form of the transfer function G, shown in Figure 7.1, for this problem with the required weighting filters is shown in Figure 7.2.

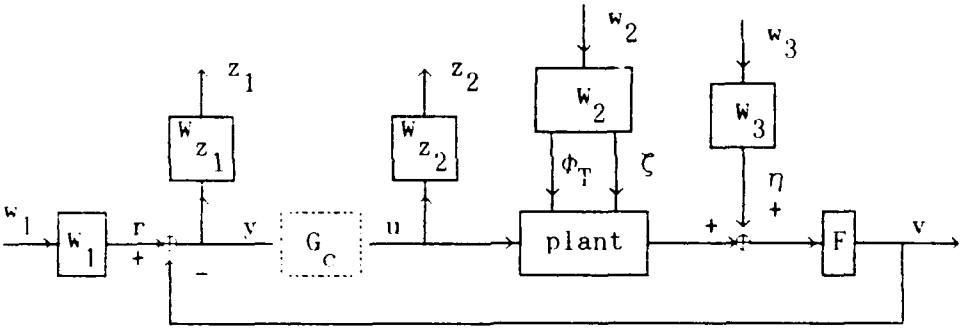

Figure 7.2
Block Diagram Showing Weighting Filters Used In
Construction of H_2 and H_∞ Controllers

The compensator in Figure 7.2 is considered open. The weighting filters are shown in Equations (7.3) through (7.7).

$$W_1 = \left[\begin{array}{c|c} A_{W_1} & B_{W_1} \\ \hline C_{W_1} & D_{W_1} \end{array}\right] \tag{7.3}$$

$$W_2 = \left[\begin{array}{c|c} A_{w_2} & B_{w_2} \\ \hline C_{w_2} & D_{w_2} \end{array}\right] \tag{7.4}$$

$$W_3 = \left[\begin{array}{c|c} A_{w_3} & B_{w_3} \\ \hline C_{w_3} & D_{w_3} \end{array}\right] \tag{7.5}$$

$$W_{z_1} = \left[\begin{array}{c|c} A_{w_{z_1}} & B_{w_{z_1}} \\ \hline C_{w_{z_1}} & D_{w_{z_2}} \end{array}\right] \tag{7.6}$$

$$W_{z_2} = \begin{bmatrix} \rho_1 & 0 \\ 0 & \rho_2 \end{bmatrix} \quad \text{no states} \tag{7.7}$$

The state space form of G is shown in Equations (7.8) through (7.16).

$$\dot{x} = A\,x + B_1\,w + B_2\,u \tag{7.8}$$

$$z = C_1\,x + D_{11}\,w + D_{12}\,u \tag{7.9}$$

$$y = C_2\,x + D_{21}\,w + D_{22}\,u \tag{7.10}$$

$$G = \left[\begin{array}{c|cc} A & B_1 & B_2 \\ \hline C_1 & D_{11} & D_{12} \\ C_2 & D_{21} & D_{22} \end{array}\right] \tag{7.11}$$

$$\begin{bmatrix} z \\ y \end{bmatrix} = G \begin{bmatrix} w \\ u \end{bmatrix} \tag{7.12}$$

where

$$A_1 = \begin{bmatrix} A_p & 0 & \begin{bmatrix} B_{p12} & B_{p2} \end{bmatrix} C_{w_2} & 0 & 0 \\ 0 & A_{w_1} & 0 & 0 & 0 \\ 0 & 0 & A_{w_2} & 0 & 0 \\ 0 & 0 & 0 & A_{w_3} & 0 \\ -B_{w_{z_1}} F C_p & B_{w_{z_1}} C_{w_1} & -B_{w_{z_1}} F \begin{bmatrix} D_{p12} & D_{p2} \end{bmatrix} C_{w_2} & -B_{w_{z_1}} F C_{w_{z_3}} & A_{w_{z_1}} \end{bmatrix} \tag{7.13}$$

$$\begin{bmatrix} B_1 & B_2 \end{bmatrix} = \left[\begin{array}{ccc:c} 0 & \begin{bmatrix} B_{p12} & B_{p2} \end{bmatrix} D_{w_2} & 0 & B_{p11} \\ B_{w_1} & 0 & 0 & 0 \\ 0 & B_{w_2} & 0 & 0 \\ 0 & 0 & B_{w_3} & 0 \\ B_{w_{z_1}} D_{w_1} & -B_{w_{z_1}} F \begin{bmatrix} D_{p12} & D_{p2} \end{bmatrix} D_{w_2} & -B_{w_{z_1}} F D_{w_3} & -B_{w_{z_1}} F D_{p11} \end{array}\right] \tag{7.14}$$

$$\begin{bmatrix} C_1 \\ C_2 \end{bmatrix} = \begin{bmatrix} -D_{w_{z_1}} F C_p & D_{w_{z_1}} C_{w_1} & -D_{w_{z_1}} F \begin{bmatrix} D_{p12} & D_{p2} \end{bmatrix} C_{w_2} & -D_{w_{z_1}} F C_{w_3} & C_{w_{z_1}} \\ 0 & 0 & 0 & 0 & 0 \\ -F C_p & C_{w_1} & -F \begin{bmatrix} D_{p12} & D_{p2} \end{bmatrix} C_{w_2} & -F C_{w_3} & 0 \end{bmatrix} \tag{7.15}$$

$$\begin{bmatrix} D_{11} & D_{12} \\ D_{21} & D_{22} \end{bmatrix} = \left[\begin{array}{cccc:c} D_{w_{z_1}} D_{w_1} & -D_{w_{z_1}} F \begin{bmatrix} D_{p12} & D_{p2} \end{bmatrix} D_{w_2} & -D_{w_{z_1}} F D_{w_3} & \vdots & -D_{w_{z_1}} F D_{p11} \\ 0 & 0 & 0 & \vdots & D_{w_{z_2}} \\ \hdashline D_{w_1} & -F \begin{bmatrix} D_{p12} & D_{p2} \end{bmatrix} D_{w_2} & -F D_{w_3} & \vdots & -F D_{p11} \end{array}\right] \quad (7.16)$$

The derivation of these matrices is similar to the derivation of the missile state space transfer function found in Appendix A.

The Bode magnitude plots of the weighting filters chosen are shown in Figures 7.3 through 7.7. The magnitudes of these filters were then scaled to produce the desired affect. Once the filters were chosen, automated H_2 and H_∞ design routines were employed to get the controllers. The information to write the H_2 and H_∞ design routines can be found in [5].

Finally, the controllers were multiplied by a -H matrix to convert y_g outputs of the guidance block into the (r-v) inputs expected by the controller and to convert the controller from one designed for positive feedback to one that uses negative feedback, as shown in Figure 7.8. The values chosen for H are shown in Equation (7.17).

$$H = \begin{bmatrix} -1 & 0 & 0 & 0 & 0 & 1 \\ 0 & -1 & 0 & 0 & 0 & 0.51 \\ 0 & 0 & -1 & 0 & 0 & 0 \\ 0 & -1 & 2 & -1 & 0 & 0 \\ 0 & 0 & 1 & 0 & 0 & 0 \end{bmatrix} \begin{matrix} \left(A_{ncom} - A_n\right) \\ \left(\dot{\theta}_{mcom} - \dot{\theta}_m\right) \\ \left(0 - \phi\right) \\ \left(\dot{\theta}_{scom} - \dot{\theta}_s\right) \\ \left(\theta_{scom} - \theta_s\right) \end{matrix} \quad (7.17)$$

The resulting compensator is run through the analysis described in Chapter 6 and then the scaling on the filters is adjusted to get the desired

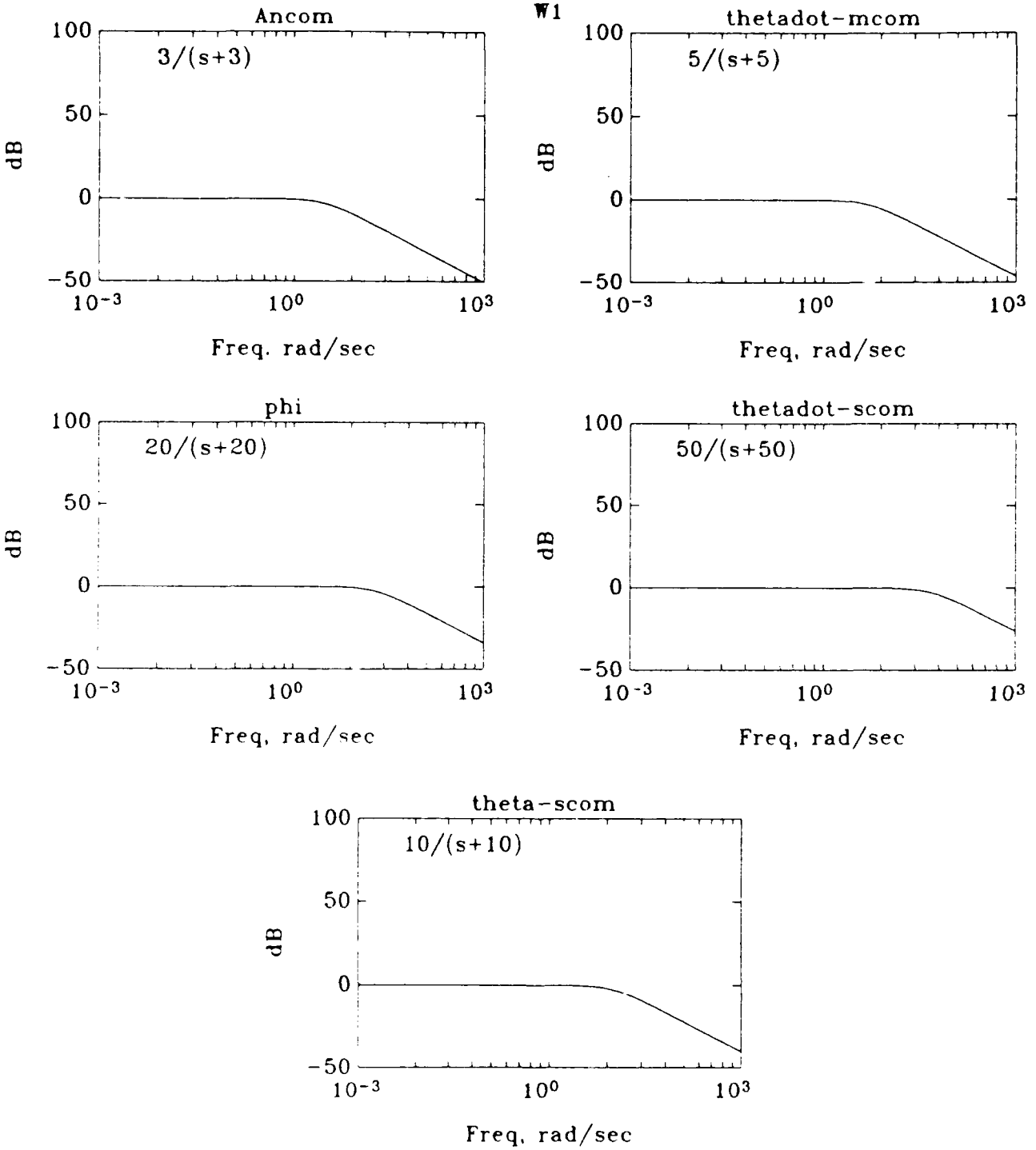

Figure 7.3 W_1 Filter Selection

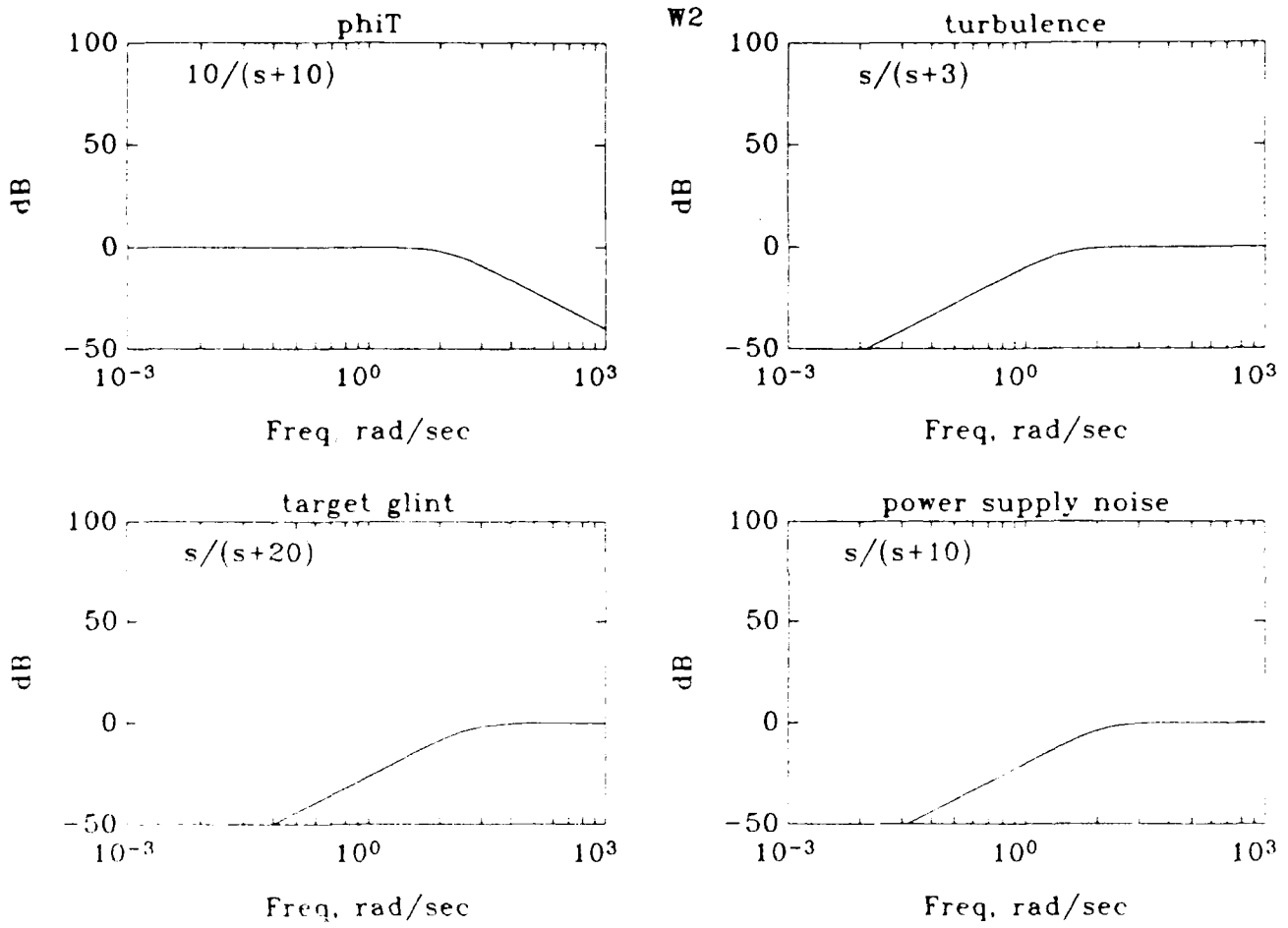

Figure 7.4 W_2 Filter Selection

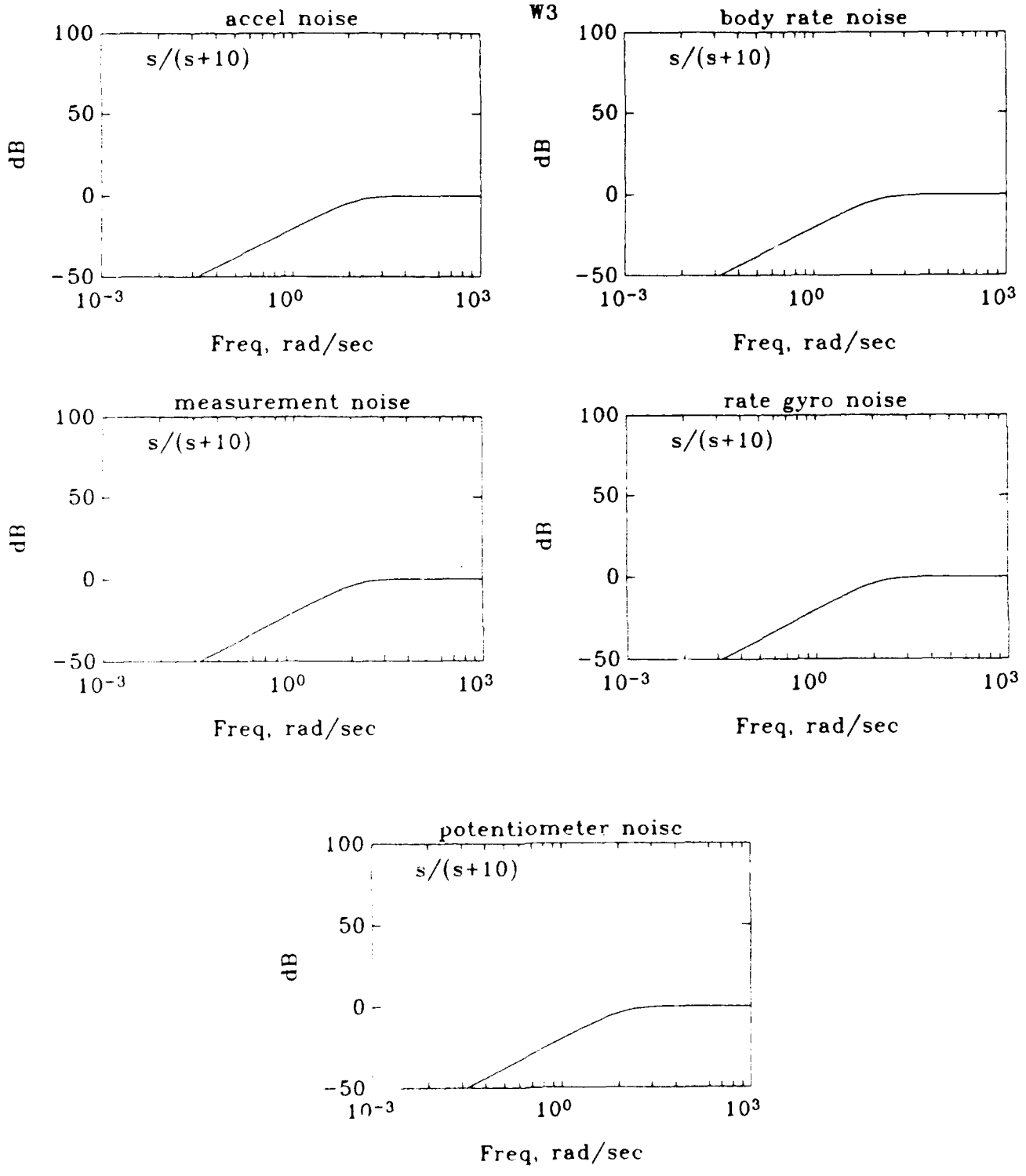

Figure 7.5 W_3 Filter Selection

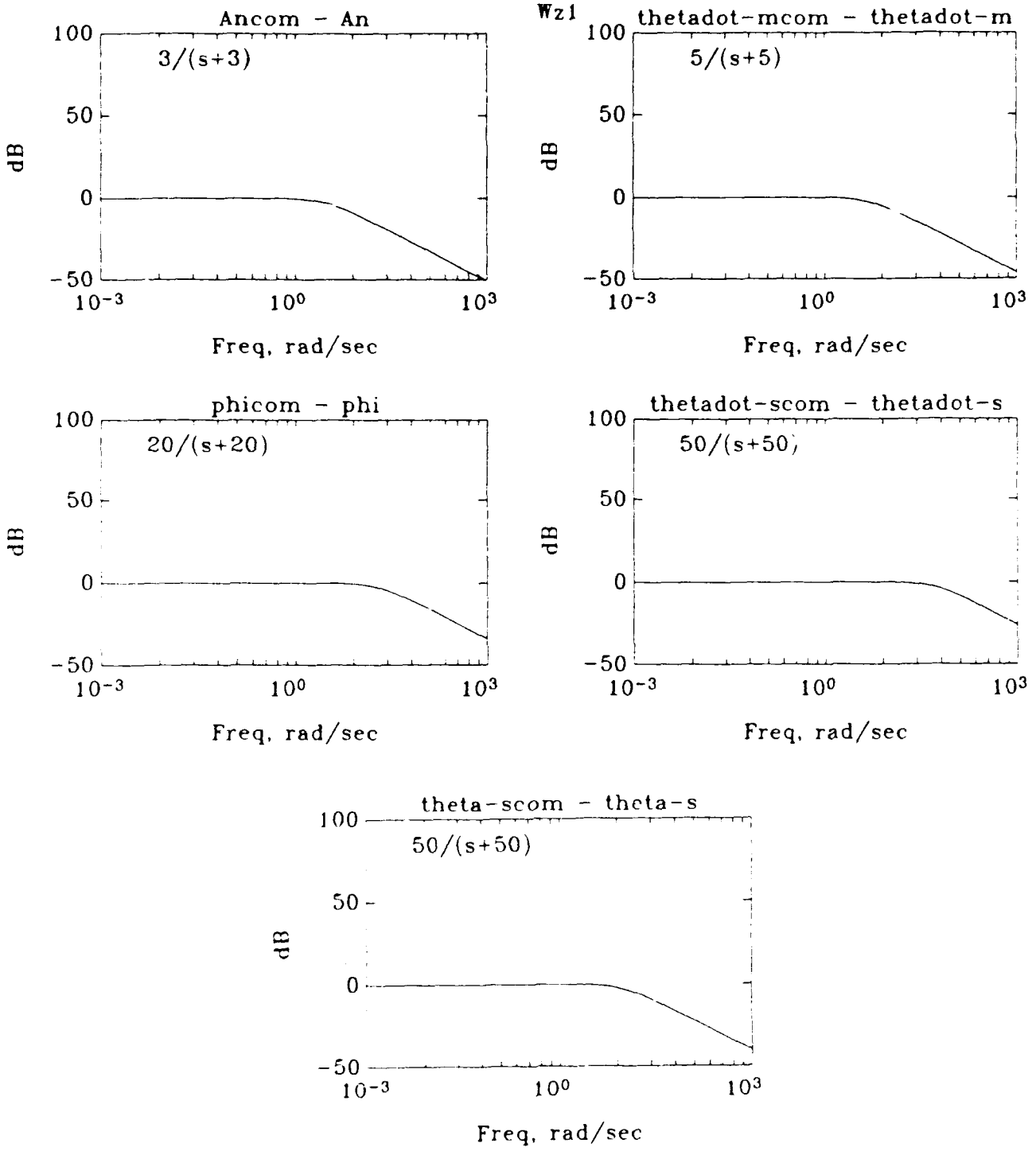

Figure 7.6 W_{z_1} Filter Selection

Wz2

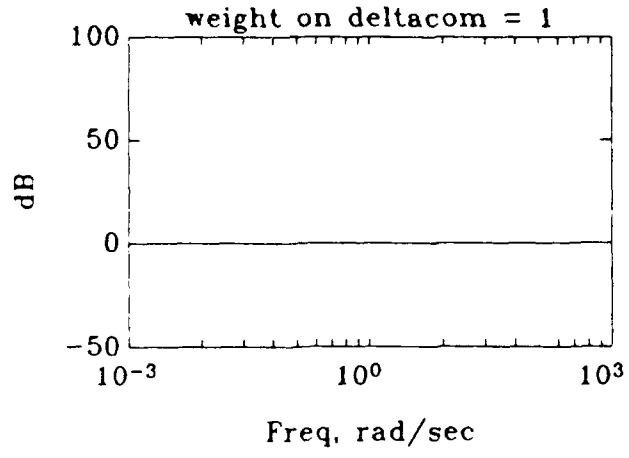

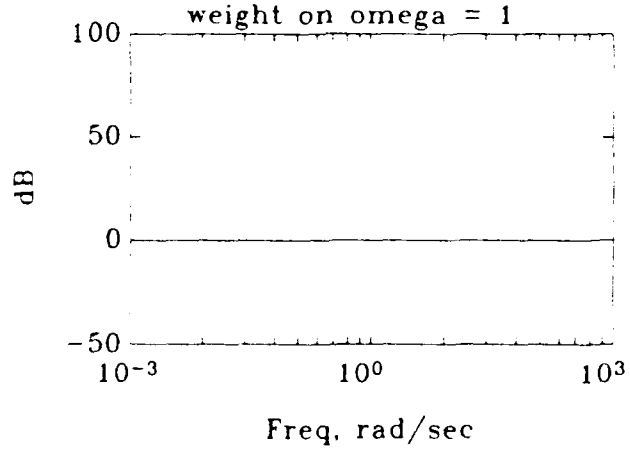

Figure 7.7 W_{z_2} Filter Selection

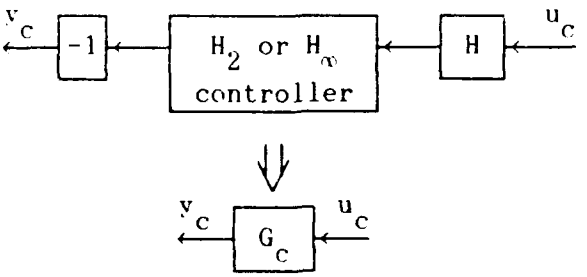

Figure 7.8 H_2 and H_∞ Controller Adaptation

improvements. The process is difficult because there are many filters involved and a change in one can often have unexpected effects on the others. A working controller is achieved.

VIII Simulation Runs

One scenario is selected for the simulation runs to eliminate scenario dependent variations in miss distance and bring out variations due to the missile controller performance. A turning tail chase scenario is selected with the target pulling 8.4 g's at Mach 1.5. It was hoped that the added missile flyout time of a tail chase would better differentiate controller performance. The 8.4 g target turn is chosen because the navigational constant (K_g) of 3.3 used in this study and Capt Riddle's is best suited for highly maneuverable targets. The run matrix chosen is shown in Table 8.1.

8.1 Ideal Flyout

First the simulation is run with no missile dynamics to confirm the efffectiveness of the guidance command block, Run 1, Figure 5.1. Next, the simulation is run again with no missile dynamics but with a 0.9 second lag in carrying out the guidance commands as a point of comparison for the lags caused by the actual missile dynamics, Run 2, Figure 4.2.

8.2 Baseline Runs

A baseline run is made for each controller with the nominal plant, no high frequency unmodelled missile dynamics, and no disturbances (noise), Run 3 through Run 5.

8.3 Plant Variation Effects

The effects of plant variations alone are examined for each controller with Runs 6 through 8. Again the miss distances shown in Table 8.1 are improved with the plant variations compared to the nominal plant as was explained in Chapter 5.

Table 8.1 Simulation Run Selection

Run Number	Controller	Features	Time Step (seconds)	Miss Distance (meters)
1	guide	no lag	0.02	1.56
2	guide	0.9 sec lag		35.04
3	conv.	Baseline	0.02	49.00
4	H_2	pnom nodyn nodis		47.35
5	H_∞			102.30
6	conv.	Plant Variations	0.02	40.90
7	H_2	pvar nodyn nodis		36.67
8	H_∞			72.49
9	conv.	Unmodelled Dynamics	0.001	48.81
10	H_2	pnom undyn nodis		47.56
11	H_∞			185.50
12,13 14	conv.	Noise	0.001	48.89, 48.89 48.89
15,16 17	H_2	pnom nodyn noise		46.84, 47.26 46.84
18,19 20	H_∞			110.40,111.40 110.40
21,22	conv.	Combined Effects	0.001	40.85, 40.61
23,24	H_2	pvar undyn noise		37.45, 35.79
25,26	H_∞			48.02.646.30

8.1 High Frequency Unmodelled Dynamics Effects

The effects of high frequency unmodelled dynamics alone were examined for each controller in Runs 9 through 11. The step size of 0.001 second was used to make sure the simulation captured these effects. As predicted by the μ-analysis in Chapter 6, the missile with the "psuedo H_∞" controller can

hardly be called stable, Figure 8.1. The μ-analysis also predicted the missile with the conventional controller would be unstable with unmodelled dynamics. The commanded inputs achieved in this engagement may not have been high enough or of the right frequency to bring out the predicted instability. Each time the fin of the missile is jerked quickly the missile rings from the high frequency unmodelled dynamics shown in Figure 8.2 taken from Run 9 and Figure 8.3 taken from Run 10.

8.5 Noise Effects

The effects of noise added to the baseline runs are examined with Runs 12 through 20. The noise simulations are run more than once to see how much the simulation results change each time due to the randomness of the noise inputs. Again a 0.001 second time step is chosen to ensure high frequency noise effects can be seen.

The miss distances with the conventional and H_2 controller change vary little from their baseline values with added noise. Miss distance values with the H_∞ controller increase somewhat over its baseline values. The noise attenuation ability of the controllers is shown in Figures 8.4 through 8.6. The missile with the H_2 controller has the least noise in commanded turn rate tracking followed closely by the missile with the conventional controller. The missile with the H_∞ controller has about three times the variations in commanded turn rate as the other two. Actual turn rate variations are about equal for the three controllers in high frequencies but in low frequency deviations, the conventional controller clearly does better followed by the H_2 and the H_∞ controllers.

8.6 Combined Effects

Finally the combined effects of plant variations, high frequency

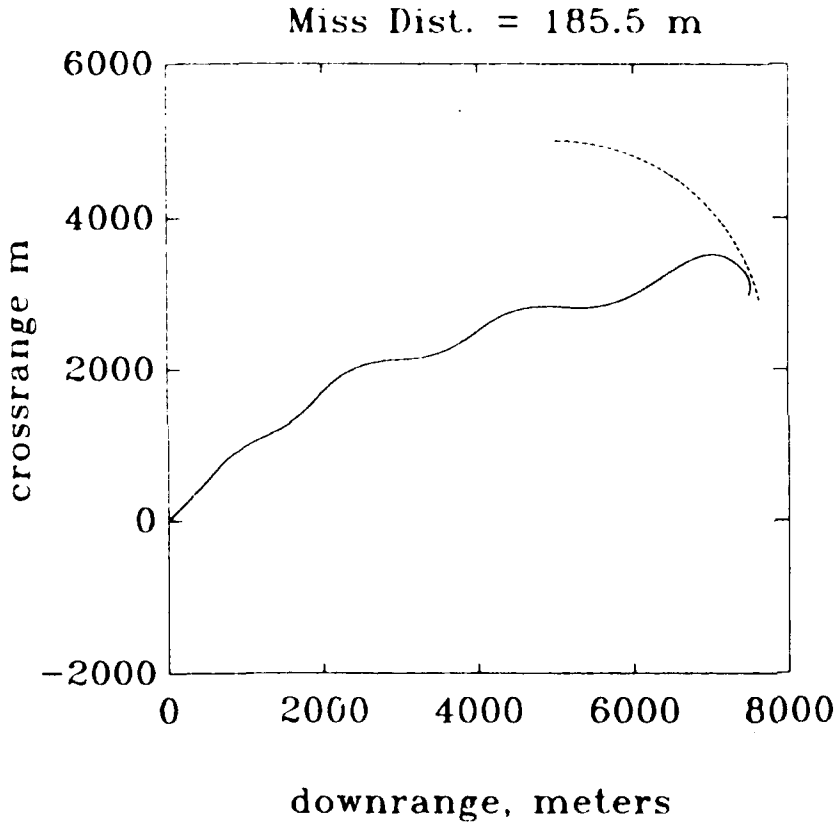

Run number 11
Time Step (sec) = 1.0000e-03
Flyout Time (sec) = 7.798
Target velocity (m/s) = 470
Target turn rate (deg/s) = -9.964
Navigation Constant = 3.3
Comptype = Riddle hi
Environment: pnom undyn nodis

Figure 8.1 Run 11, Unmodelled Dynamics Effects on Missile with H_∞ Controller

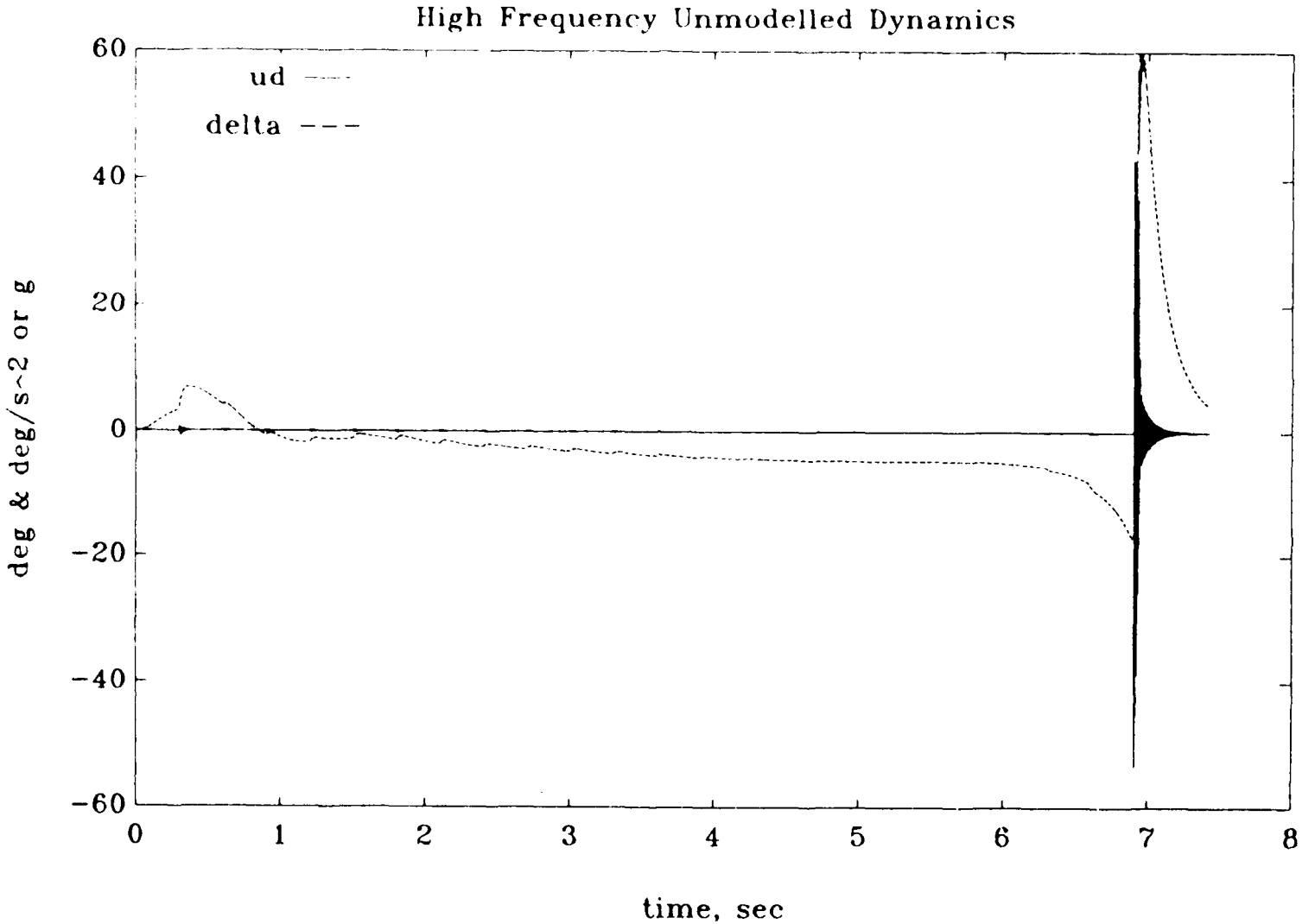

Figure 8.2 Run 9, Generating High Frequency Unmodelled Dynamics, Conventional Controller, Nominal Missile

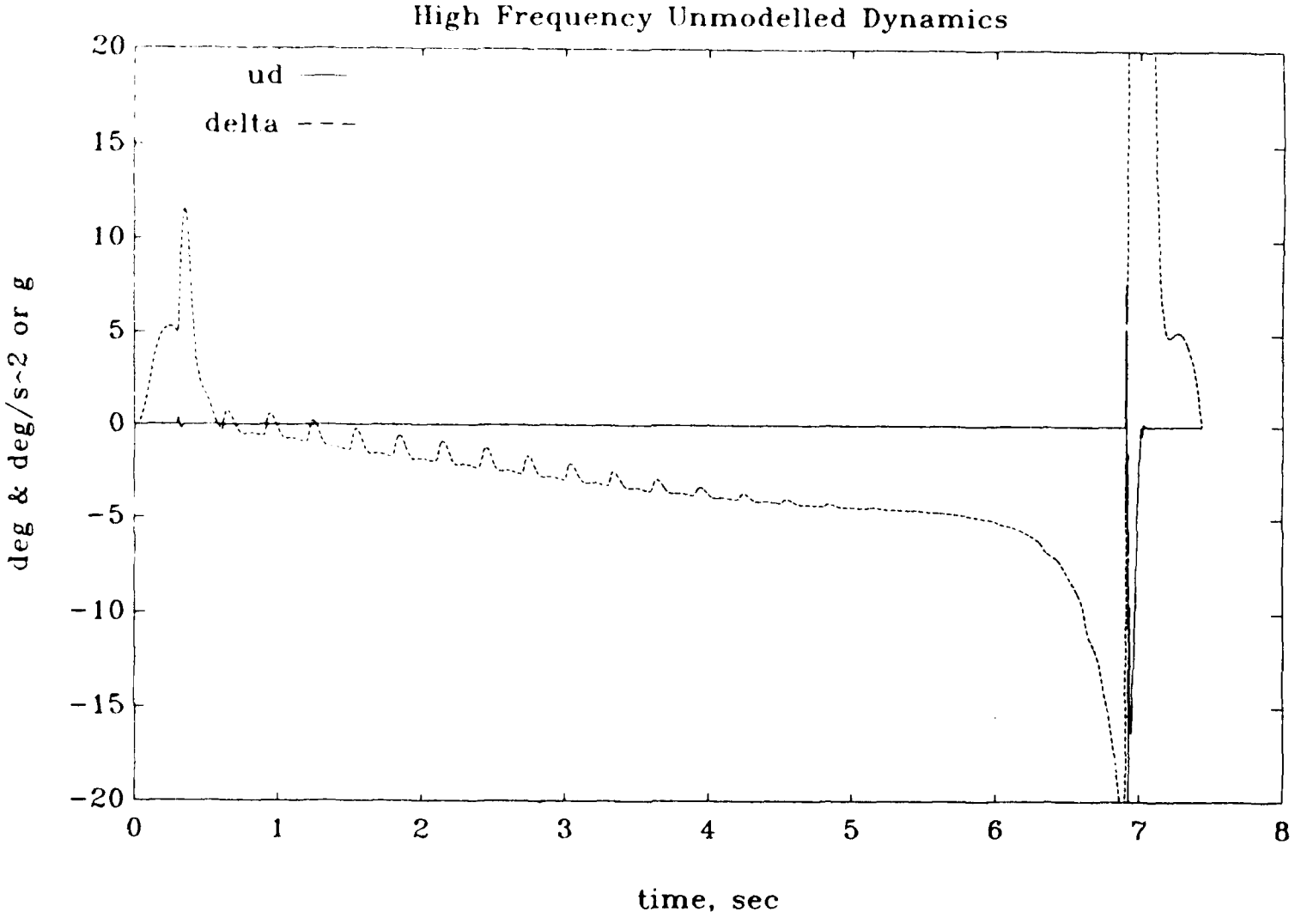

Figure 8.3 Run 10, Generating High Frequency Unmodelled Dynamics, H_2 Controller, Nominal Missile

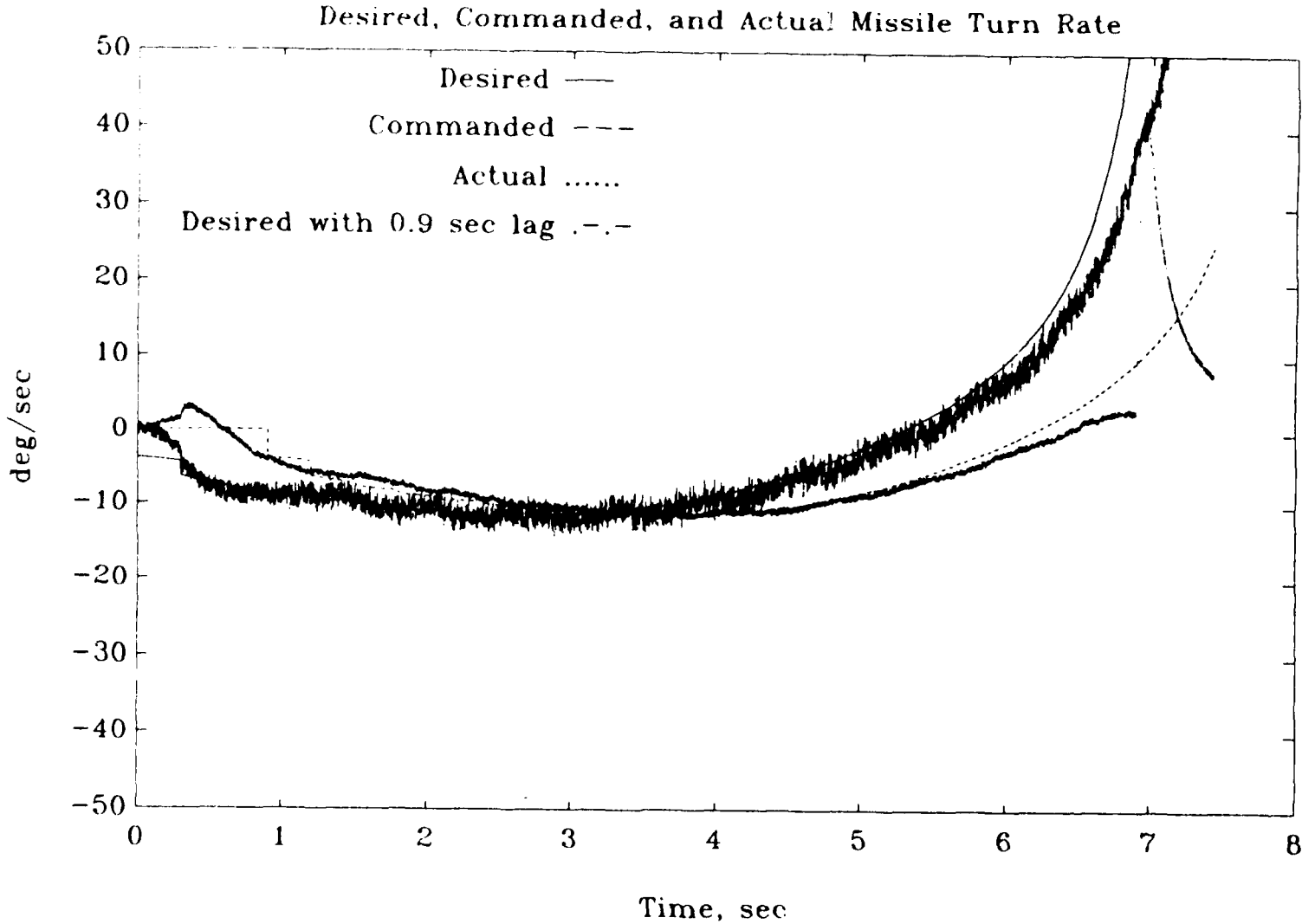

Figure 8.4 Run 14, Turn Rate Responses,
Conventional Controller, Nominal Missile with Added Noise

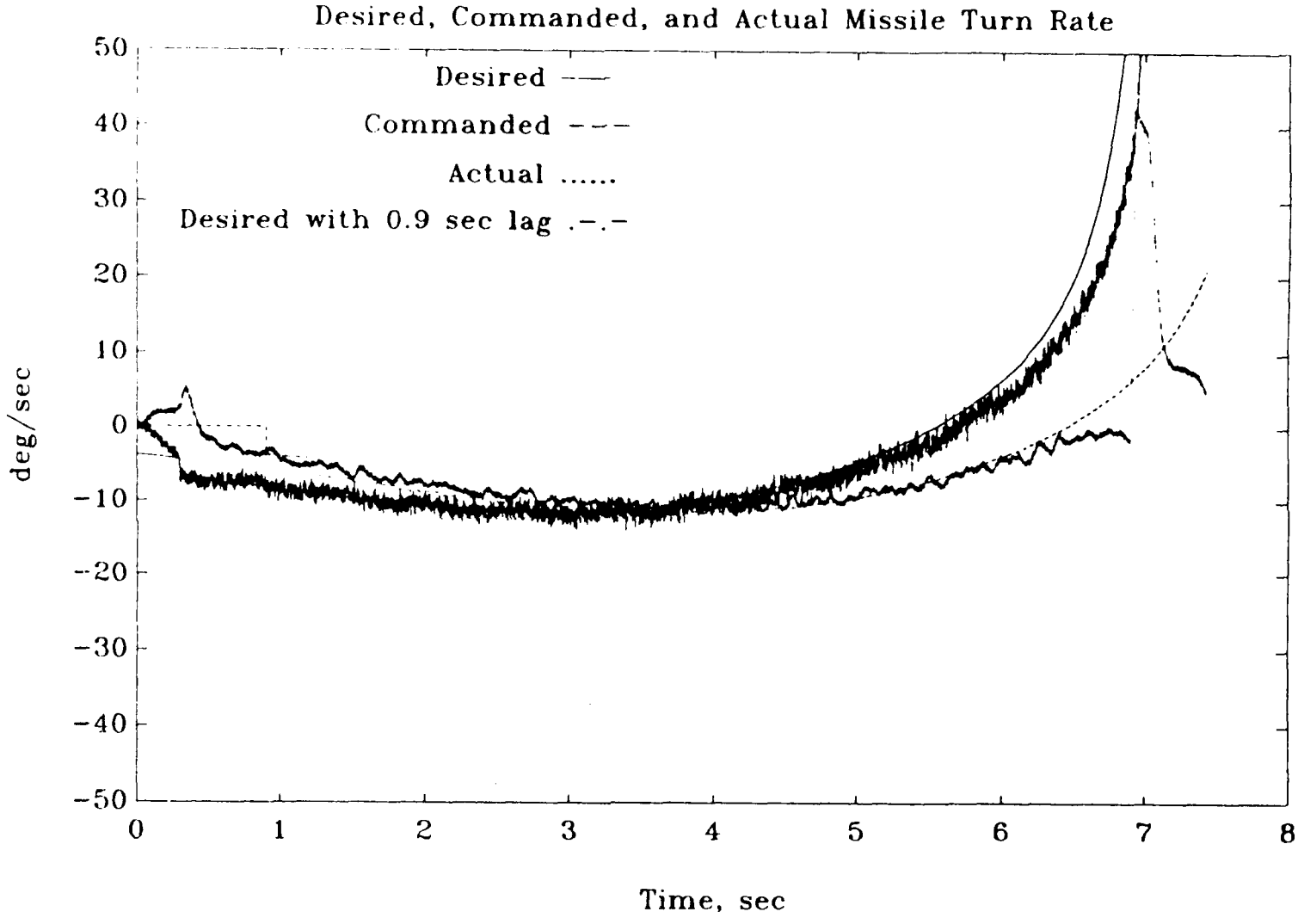

Figure 8.5 Run 17, Turn Rate Responses,
H_2 Controller, Nominal Missile with Added Noise

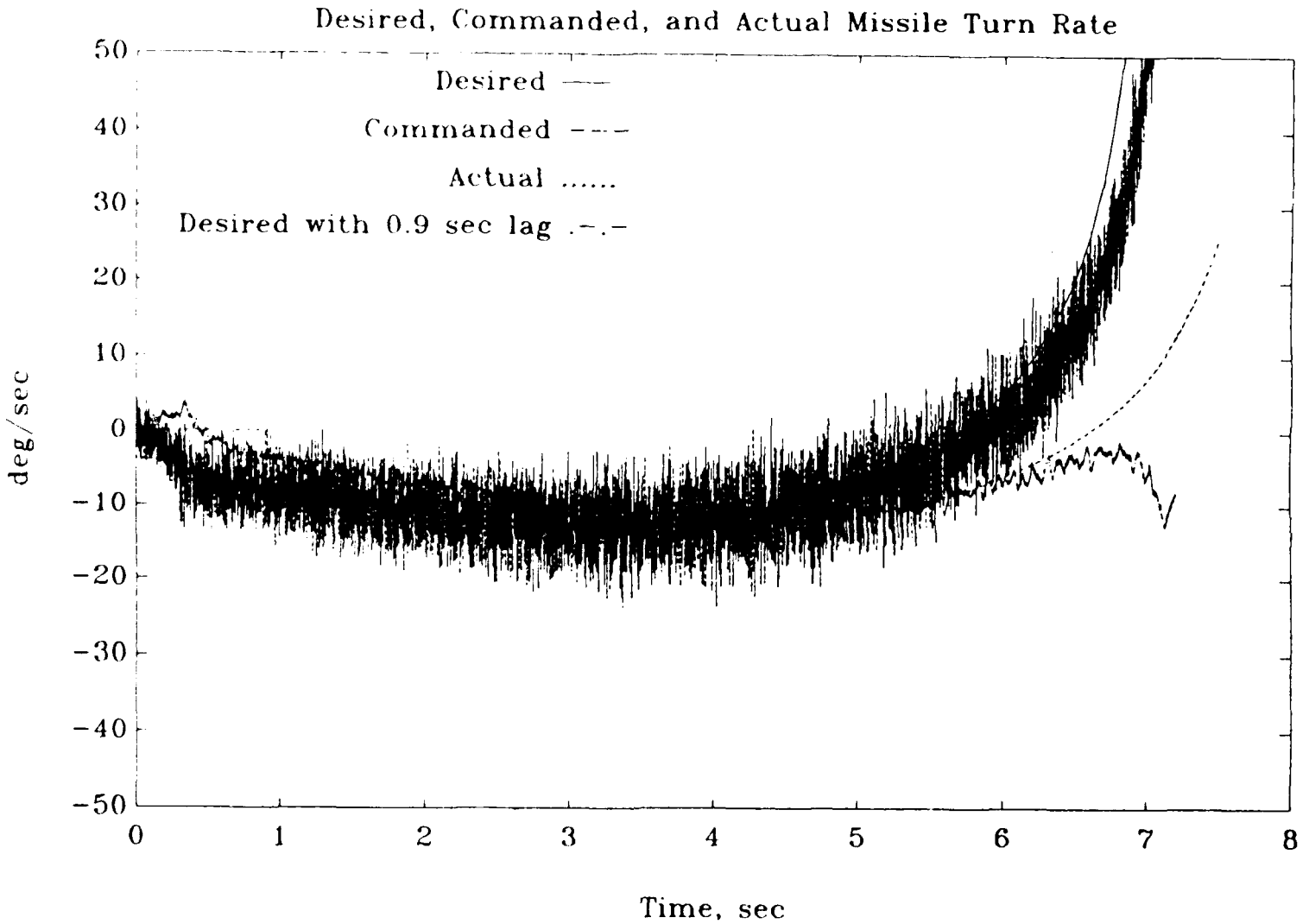

Figure 8.6 Run 20, Turn Rate Responses,
H_{∞} Controller, Nominal Missile with Added Noise

unmodelled dynamics, and noise inputs are examined for each simulation with Runs 21 through 26. The miss distances with the conventional and H_2 controllers are similar to their baseline runs with plant variations. Again the missile with the H_∞ controller goes unstable though it still manages to get near the target in Run 25 but not Run 26.

Comparing Figures 8.7 and 8.8 it can be seen that commanded turn rate has less variations with the H_2 controller than with the conventional controller. It can also be seen that the conventional controller has less low frequency turn rate deviations and slightly more high frequecy deviations than with the H_2 controller. Both match the 0.9 second lag approximation fairly well.

Adding noise brought out more of the high frequency unmodelled dynmics with all the controllers. This effect can be seen in Figure 8.9 with the conventional controller and Figure 8.10 with the H_2 controller.

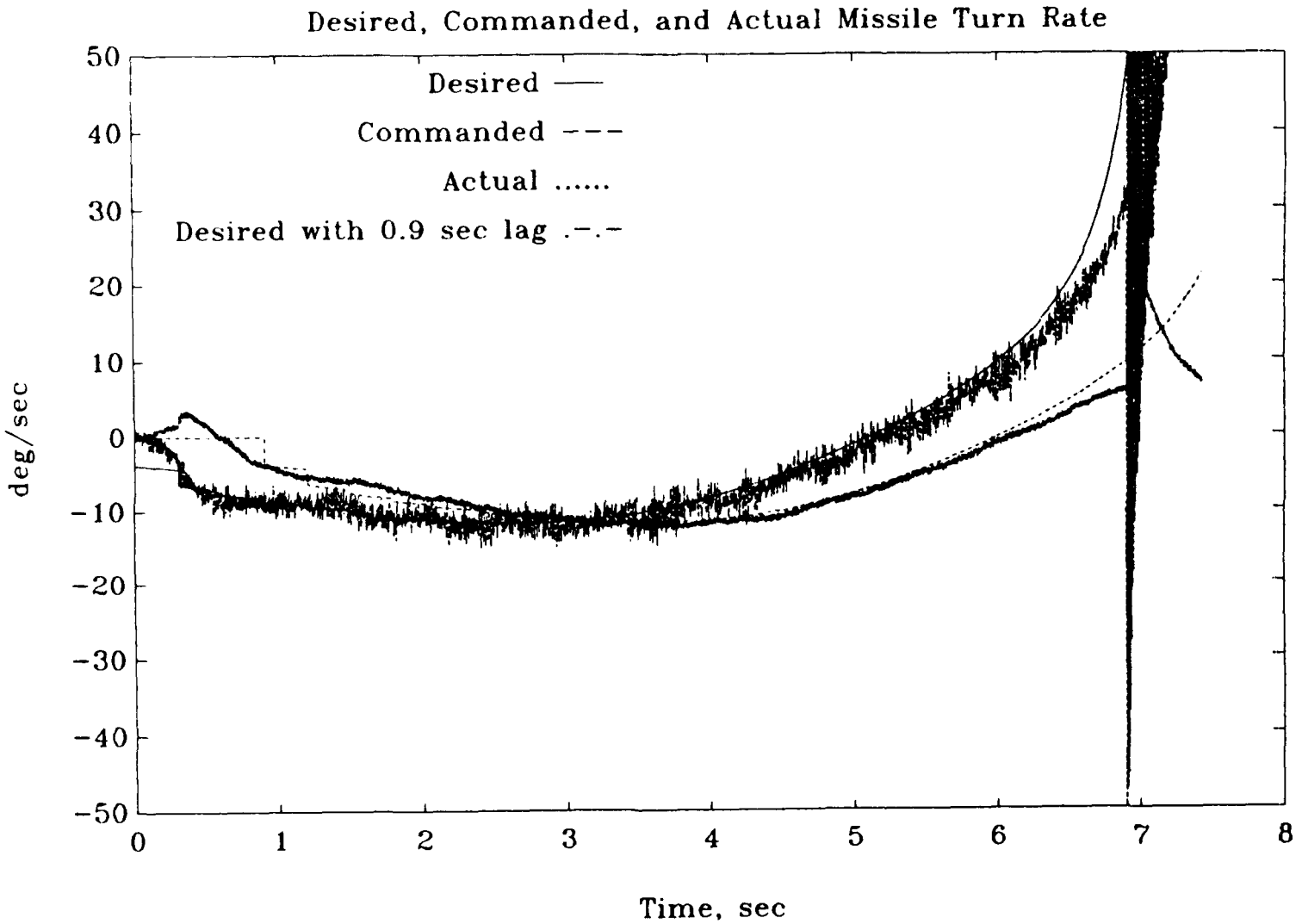

Figure 8.7 Run 22, Turn Rate Responses,
Conventional Controller, Combined Effects

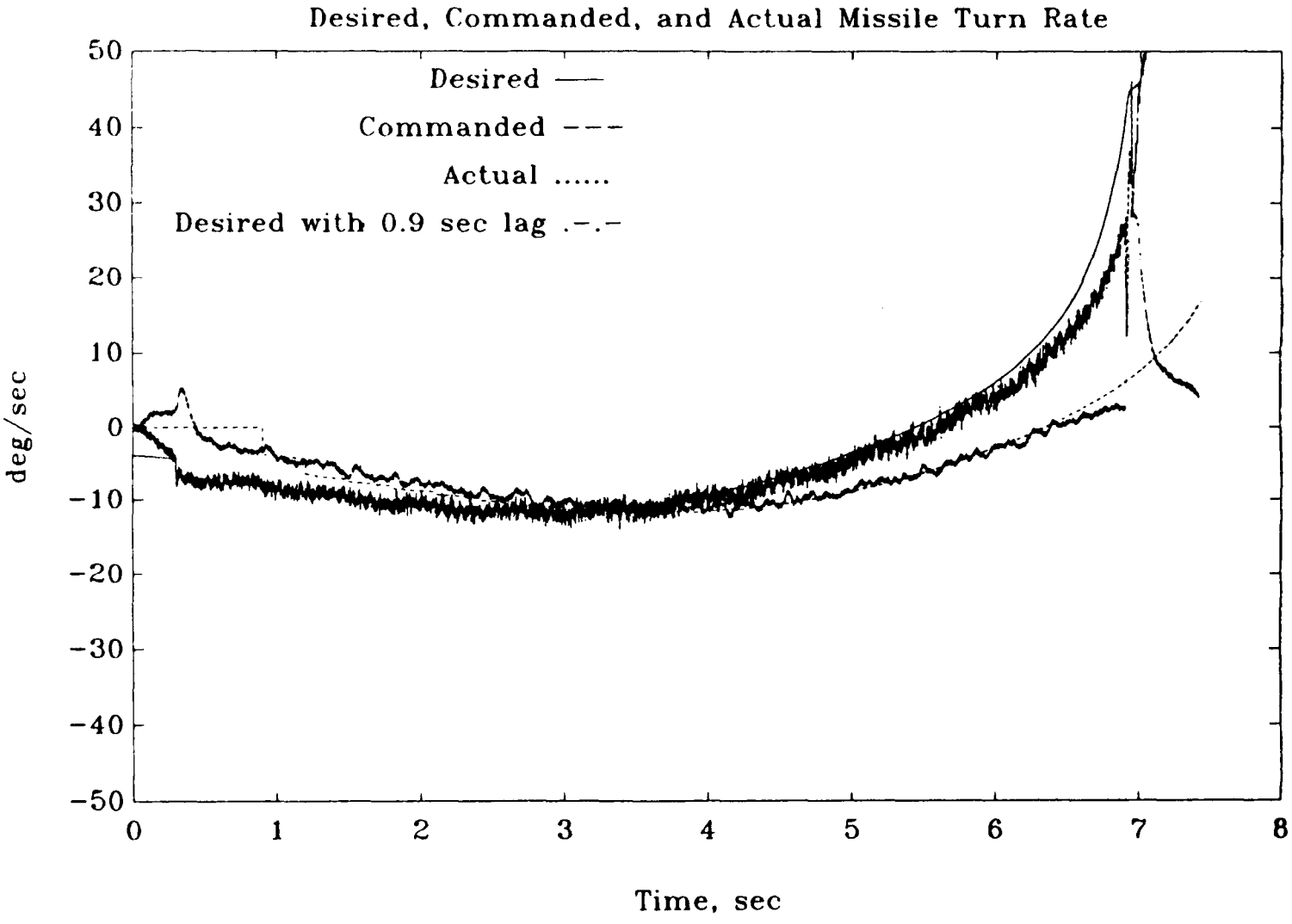

Figure 8.8 Run 24, Turn Rate Responses,
H_2 Controller, Combined Effects

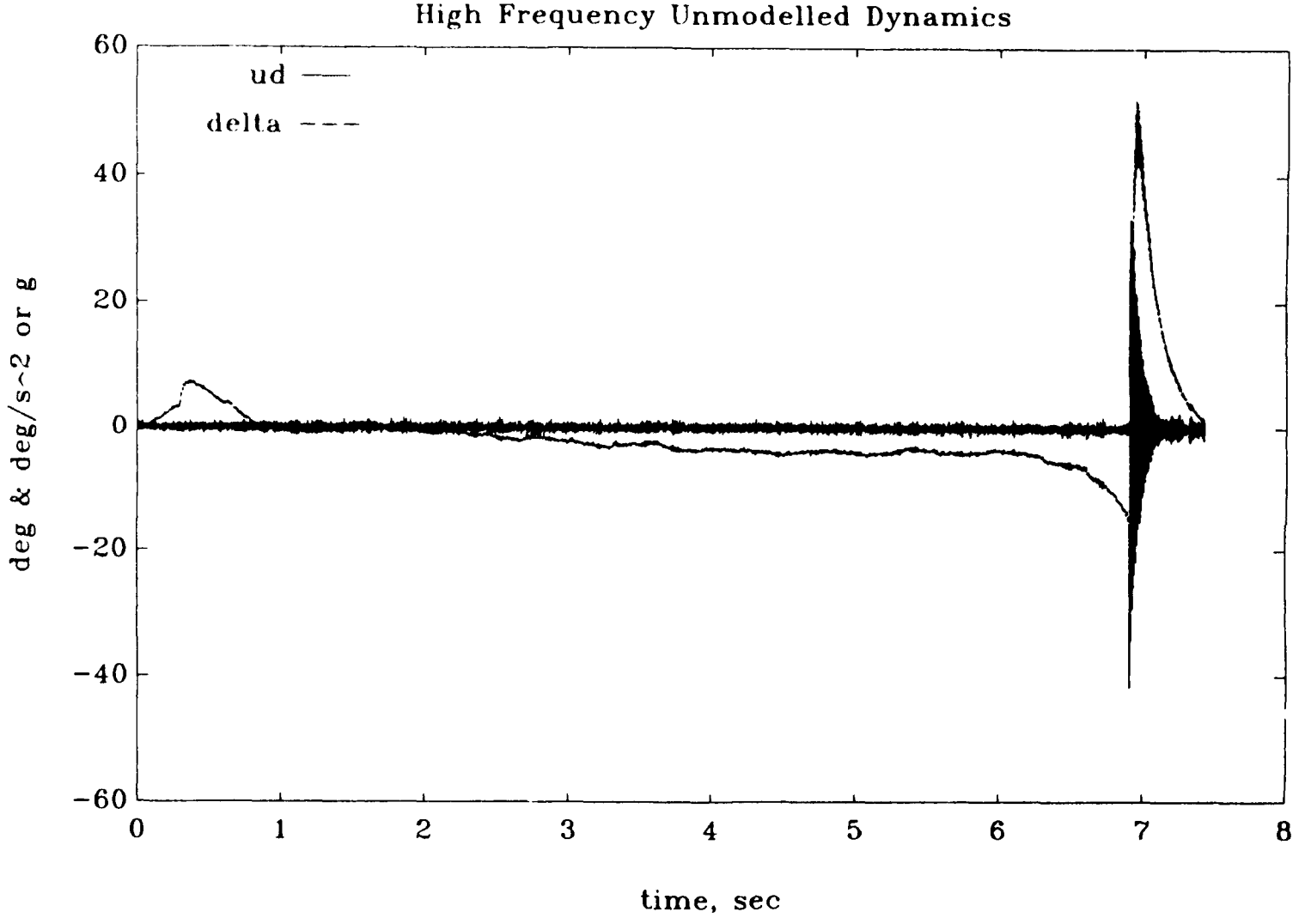

Figure 8.9 Run 21, Generating High Frequency Unmodelled Dynamics
Conventional Controller, Combined Effects

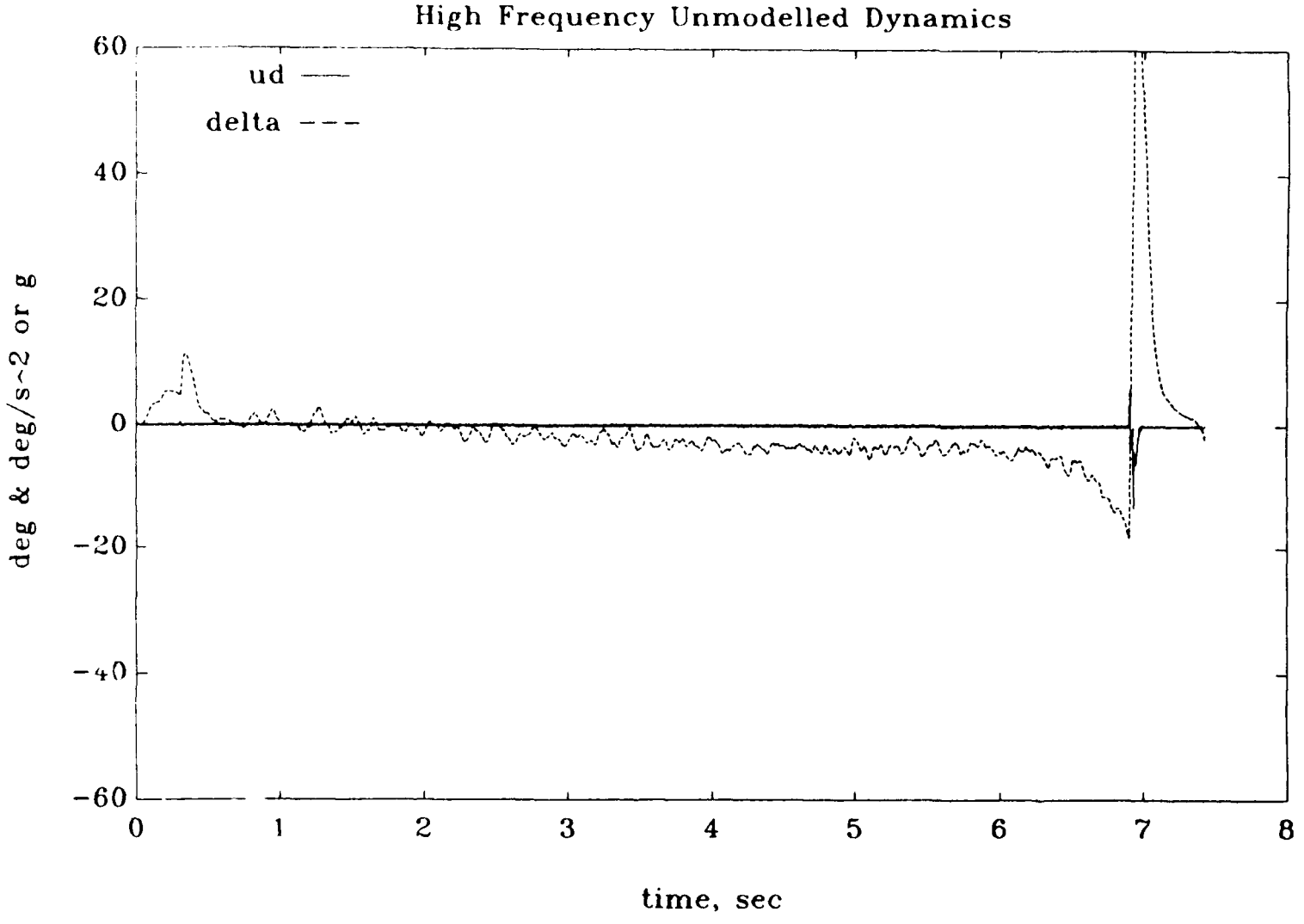

Figure 8.10 Run 23, Generating High Frequency Unmodelled Dynamics, H_2 Controller, Combined Effects

IX Conclusions And Recommendations

9.1 Conclusions

Care must be taken when judging missile controllers based on target miss distances obtained from missile flyout simulations even though low miss distance is the desired real world end result. This is due to the fact that the chosen engagement scenario and navigational constant also drive miss distance values. Reducing command execution lag time caused by the missile dynamics has the greatest impact on reducing miss distances. This lag is the combination of the seeker tracking lag and lag in pointing the missile velocity vector. A plot of desired, commanded, actual, and desired with lag missile turn rates obtained during the missile flyout simulation proved very useful in evaluating controller performance. The controller can compensate for the missile dynamics, but there is a physical limit to what the missile seeker combination can do as is well shown by Nesline, William and Nesline in reference [6].

The results of the controller analyses correlated well with the simulation runs. The H_∞ controller did not perform as it should have and must have been incorrectly formulated by Capt Riddle. The H_2 controller passed the robustness tests, but other analyses showed its noise attenuation and time response could be improved. A redesign of these controllers was initiated, but time limitations prohibited the completion of an improved controller design. Correlating the choice of weighting filters in the controller design with a given controller performance result was more difficult than anticipated.

9.2 Recommendations

This study was a follow on to Capt Riddle's 1989 thesis work. The model and simulation used is therefore in its second generation. Because of this, the documentation is much improved and the computer code, despite its added features, is more readable. There are still more benefits to be gained by continuing this study. It is suggested that the H_2 and H_∞ controllers be redesigned based on the information gained from the controller analyses. An iterative design technique using μ-analysis could ensure the full potential of the controllers would be reached. Simulation runs would then determine whether or not reduced miss distances could be acheived with this missile. μ-synthesis is another option for designing the controllers [7].

Another suggested area for follow-on work is to improve the controller analysis by using μ-analysis for noise attenuation and performance as well as robustness. The performance, noise attenuation, and robustness analyses could then be combined into one μ-analysis. The μ-analysis computer code [4] used in this study was unable to handle performance and noise analysis, which is why time responses and singular value plots of nominal transfer functions were used instead. The μ robustnes, performance, and noise anaylsis block diagrams are shown in Figures 9.1 through 9.3 respectively. The combined performance, noise attenuation, and robustness μ analysis is shown in Figure 9.4.

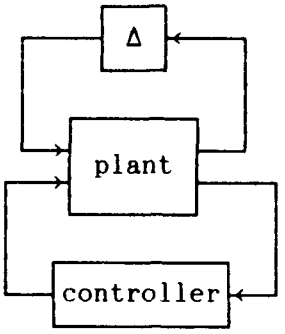

Figure 9.1 μ Robustness Analysis

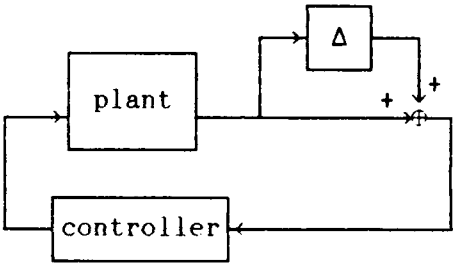

Figure 9.2 μ Performance Analysis

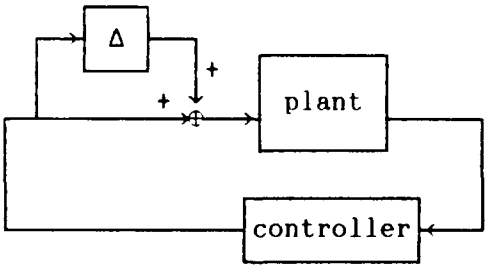

Figure 9.3 μ Noise Analysis

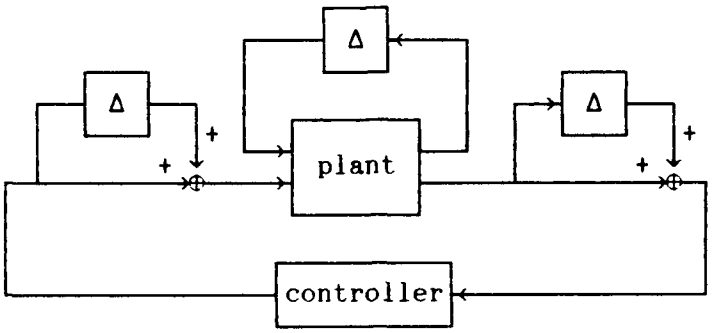

Figure 9.4 μ Combined Performance, Noise, And Robustness Analysis

Appendix A: Missile Transfer Functions to State Space

Converting the missile transfer functions to state space in Chapter 2, forming the transfer function for the missile simulation in Chapter 3, and forming the transfer functions for the controller analysis in Chapter 6 all make use of the following equations. "Transfer function to state space operation" is shown with Equations (A.1) through (A.4).

$$A = \begin{bmatrix} -\text{den}(2:N) \\ I(N-2,N-1) \end{bmatrix} \tag{A.1}$$

$$B = I(N-1,1) \tag{A.2}$$

$$C = \text{num}(:,2:N) - \text{num}(:,1)\ \text{den}(2:N) \tag{A.3}$$

$$D = \text{num}(:,1) \tag{A.4}$$

where

num = matrix of the numerator coefficients of the transfer function

den = vector of the transfer fuction's denominator coefficients

I(m,n) = identity matrix with dimensions m rows by n columns

N = power of transfer function's characteristic equation (denominator) plus one

: = through or all

Transfer function multiplication or series operation is shown in Figure A.1 and Equations (A.5) through (A.7). These equations may not yield a transfer function with minimal states.

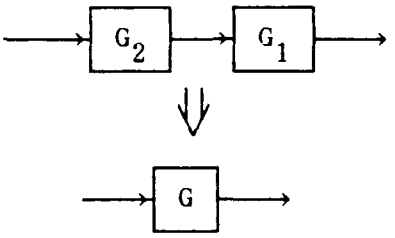

Figure A.1 Series Operation

$$G = G_1 G_2 \tag{A.5}$$

$$G = \left[\begin{array}{cc:c} A_1 & B_1C_2 & B_1D_2 \\ 0 & A_2 & B_2 \\ \hdashline C_1 & D_1C_2 & D_1D_2 \end{array}\right] \tag{A.6}$$

$$G = \left[\begin{array}{cc:c} A_2 & 0 & B_2 \\ B_1C_2 & A_1 & B_1D_2 \\ \hdashline D_1C_2 & C_1 & D_1D_2 \end{array}\right] \tag{A.7}$$

Transfer function addition or parallel operation is shown in Equations (A.8) through (A.9) and in Figure A.2. Again a transfer function with minimal states may not be produced with these equations.

$$G = G_1 + G_2 \tag{A.8}$$

$$G = \left[\begin{array}{cc:c} A_1 & 0 & B_1 \\ 0 & A_2 & B_2 \\ \hdashline C_1 & C_2 & D_1+D_2 \end{array}\right] \qquad (A.9)$$

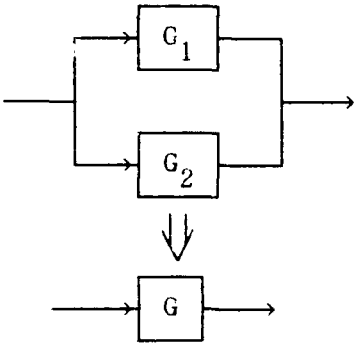

Figure A.2 Parallel Operation

Since the transfer functions used all started as single input single output equations, the transpose relationship in Equation (A.10) can also be used.

$$G = \left[\begin{array}{c:c} A & B \\ \hdashline C & D \end{array}\right] = \left[\begin{array}{c:c} A & B \\ \hdashline C & D \end{array}\right]^T = \left[\begin{array}{c:c} A^T & B^T \\ \hdashline C^T & D \end{array}\right] \qquad (A.10)$$

Equations (A.11) through (A.17) briefly go through the formation of the missile state space transfer function formation from Figure 2.11 to Equation (2.20).

$$\delta_{com} \rightarrow \boxed{\frac{77}{s+77}} \rightarrow \delta \quad = \quad \left[\begin{array}{c:c} -77 & 77 \\ \hdashline 1 & 0 \end{array}\right] \qquad (A.11)$$

$$\dot{\delta} \rightarrow \boxed{\frac{-2.74s-3.2589}{s^2+1.02s-.91}} \theta_m \rightarrow = \frac{-2.74s+\{-.51\times.91-(-1.02\times-2.74)\}}{s^2+1.02s-.91}$$

$$\Downarrow \qquad\qquad \Downarrow$$

$$\left[\begin{array}{cc|c} -1.02 & .91 & 1 \\ 1 & 0 & 0 \\ \hline -2.74 & -3.2589 & 0 \end{array}\right] = \left[\begin{array}{cc|c} -1.02 & .91 & 0 \\ 1 & 0 & 1 \\ \hline -.51 & -2.74 & 0 \end{array}\right]$$

series with fin servo

$$\left[\begin{array}{cc|c} -77 & 77 & \\ \hline 1 & 0 & \end{array}\right] \left[\begin{array}{cc|c} -1.02 & .91 & 0 \\ 1 & 0 & 1 \\ \hline -.51 & -2.74 & 0 \end{array}\right]$$

$$\Downarrow$$

$$\left[\begin{array}{ccc|c} -77 & -.51 & -2.74 & 0 \\ 0 & -1.02 & .91 & 0 \\ 0 & 1 & 0 & 1 \\ \hline 77 & 0 & 0 & 0 \end{array}\right]$$

$$\Downarrow$$

$$\left[\begin{array}{ccc|c} -77 & 0 & 0 & 77 \\ -.51 & -1.02 & 1 & 0 \\ -2.74 & .91 & 0 & 0 \\ \hline 0 & 0 & 1 & 0 \end{array}\right]$$

$$\Downarrow$$

$$\delta_{com} \rightarrow \left[\begin{array}{ccc|c} -77 & 0 & 0 & 77 \\ -2.74 & 0 & .91 & 0 \\ -.51 & 1 & -1.02 & 0 \\ \hline 0 & 1 & 0 & 0 \end{array}\right] \dot{\theta}_m \rightarrow \qquad (4.12)$$

$$\dot{\theta}_m \rightarrow \boxed{\frac{1}{s}} \theta_m \rightarrow = \left[\begin{array}{c|c} 0 & 1 \\ \hline 1 & 0 \end{array}\right]$$

series with the integrator

$$\left[\begin{array}{c|c} 0 & 1 \\ \hline 1 & 0 \end{array}\right] \left[\begin{array}{ccc|c} -77 & 0 & 0 & 77 \\ -2.74 & 0 & .91 & 0 \\ -.51 & 1 & -1.02 & 0 \\ \hline 0 & 1 & 0 & 0 \end{array}\right]$$

$$\Downarrow$$

$$\delta_{com} \rightarrow \left[\begin{array}{cccc|c} 0 & 0 & 1 & 0 & 0 \\ 0 & -77 & 0 & 0 & 77 \\ 0 & -2.74 & 0 & .91 & 0 \\ 0 & -.51 & 1 & -1.02 & 0 \\ \hline 1 & 0 & 0 & 0 & 0 \end{array}\right] \rightarrow \dot{\theta}_m \qquad \text{(A.13)}$$

$$\delta \rightarrow \boxed{\frac{-.51s-2.74}{s^2+1.02s-.91}} \rightarrow \alpha \quad = \quad \left[\begin{array}{cc|c} -1.02 & .91 & 1 \\ 1 & 0 & 0 \\ \hline -.51 & -2.74 & 0 \end{array}\right]$$

series with fin servo

$$\left[\begin{array}{c|c} -77 & 1 \\ \hline 77 & 0 \end{array}\right] \left[\begin{array}{cc|c} -1.02 & .91 & 1 \\ 1 & 0 & 0 \\ \hline -.51 & -2.74 & 0 \end{array}\right]$$

$$\Downarrow$$

$$\left[\begin{array}{ccc|c} -77 & -.51 & -2.74 & 0 \\ 0 & -1.02 & .91 & 1 \\ 0 & 1 & 0 & 0 \\ \hline 77 & 0 & 0 & 0 \end{array}\right]$$

$$\Downarrow$$

$$\left[\begin{array}{ccc|c} -77 & 0 & 0 & 77 \\ -.51 & -1.02 & 1 & 0 \\ -2.74 & .91 & 0 & 0 \\ \hline 0 & 1 & 0 & 0 \end{array}\right]$$

$$\Downarrow$$

$$\delta_{com} \rightarrow \left[\begin{array}{ccc|c} -77 & 0 & 0 & 77 \\ -2.74 & 0 & .91 & 0 \\ -.51 & 1 & -1.02 & 0 \\ \hline 0 & 0 & 1 & 0 \end{array}\right] \rightarrow \alpha \qquad \text{(A.14)}$$

$$\phi_T - \theta_m - \theta_s \rightarrow \boxed{\frac{20.7}{s+5.26}} \rightarrow \phi = \left[\begin{array}{c|c} -5.26 & 20.7 \\ \hline 1 & 0 \end{array}\right]$$

$$\Downarrow$$

$$\begin{array}{c} \qquad\quad \theta_m \qquad \phi \qquad\quad \theta_s \qquad \phi_T \\ \phi_T \rightarrow \left[\begin{array}{ccc|c} -20.7 & -5.26 & -20.7 & 20.7 \\ \hline 0 & 1 & 0 & 0 \end{array}\right] \rightarrow \phi \end{array} \qquad \text{(A.15)}$$

$$\omega \rightarrow \boxed{\frac{94}{s+104}} \rightarrow \dot{\theta}_s = \left[\begin{array}{c|c} -104 & 94 \\ \hline 1 & 0 \end{array}\right]$$

series with intregrator

$$\left[\begin{array}{c|c} 0 & 1 \\ \hline 1 & 0 \end{array}\right] \left[\begin{array}{c|c} -104 & 94 \\ \hline 1 & 0 \end{array}\right]$$

$$\Downarrow$$

$$\omega \rightarrow \left[\begin{array}{ccc|c} 0 & 1 & 0 & \\ 0 & -104 & 94 & \\ \hline 1 & 0 & 0 & \end{array}\right] \rightarrow \theta_s \qquad \text{(A.16)}$$

$$\delta \rightarrow \boxed{6.4} \rightarrow \boxed{\frac{s+10}{s+400}} \rightarrow \boxed{\frac{s+10}{s+400}} \rightarrow \boxed{\frac{s+10}{s+400}} \rightarrow ud$$

$$\Downarrow$$

$$\delta \rightarrow \boxed{6.4} \rightarrow \left[\begin{array}{c|c} -400 & -390 \\ \hline 1 & 1 \end{array}\right] \rightarrow \left[\begin{array}{c|c} -400 & -390 \\ \hline 1 & 1 \end{array}\right] \rightarrow \left[\begin{array}{c|c} -400 & -390 \\ \hline 1 & 1 \end{array}\right] \rightarrow ud$$

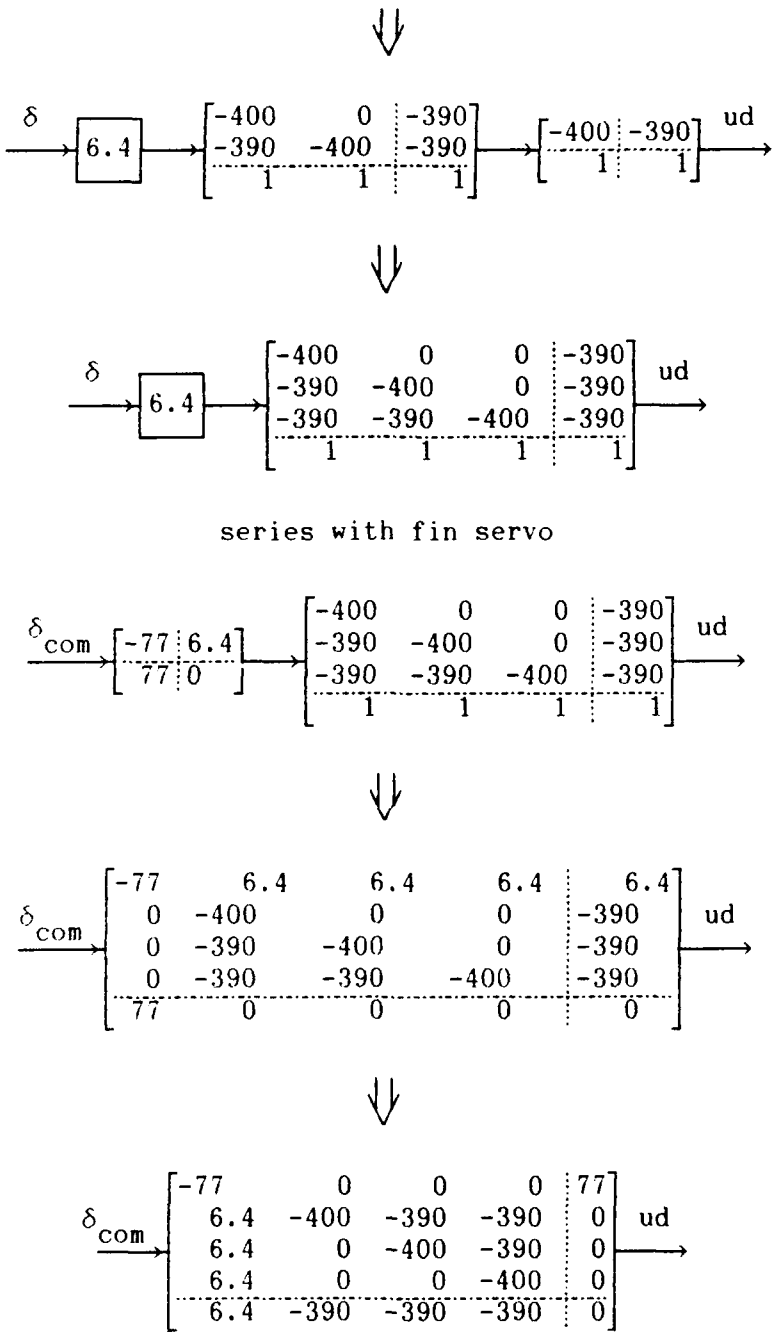

(A.17)

Equations (A.11) through (A.17) are combined to form the plant state space transfer function seen in Equation (2.20).

Appendix B: Description of Code Created For Study

Pro-Matlab, a control design program, was used for this study. Programming can be done within Pro-Matlab using m files. Capt Riddle's code was used as a starting point since it performed some of the same functions needed for this study. The code was entirely rewritten in an attempt to make it easy to understand, to identify errors, and to modify it. It is heavily commented. Much of this document was taken directly from the commented code. The computer code consists of five "m" files, four used in controller design and evaluation shown in Figure B.1 and the fifth used to study the missile's navigational command block. Though the code is readable and self explanitory, some of its features will be described here.

Missile.m is a function which contains all the missile state space information described in Chapter 2. It also has the equations needed to compute the transfer functions used in the controller analysis. Mrform.m is called by missile.m to form the M matrix for μ analysis.

The weighting filters are chosen by the designer in build.m. Build.m calls missile.m to get plant state space information. Using the transfer function G from Chapter 7 and the chosen weighting filters, the automated H_2 and H_∞ design functions, h2opt2.m and hinf3.m, are called to form the controllers. If requested, Bode plots of the filters as seen in Chapter 7 are also provided.

Analyze.m calls missile.m to get needed transfer functions and then produces the requested plots. The plots, which can be seen in Chapter 6, include $\dot{y}$ time response and singular value plots, noise attenuatuation

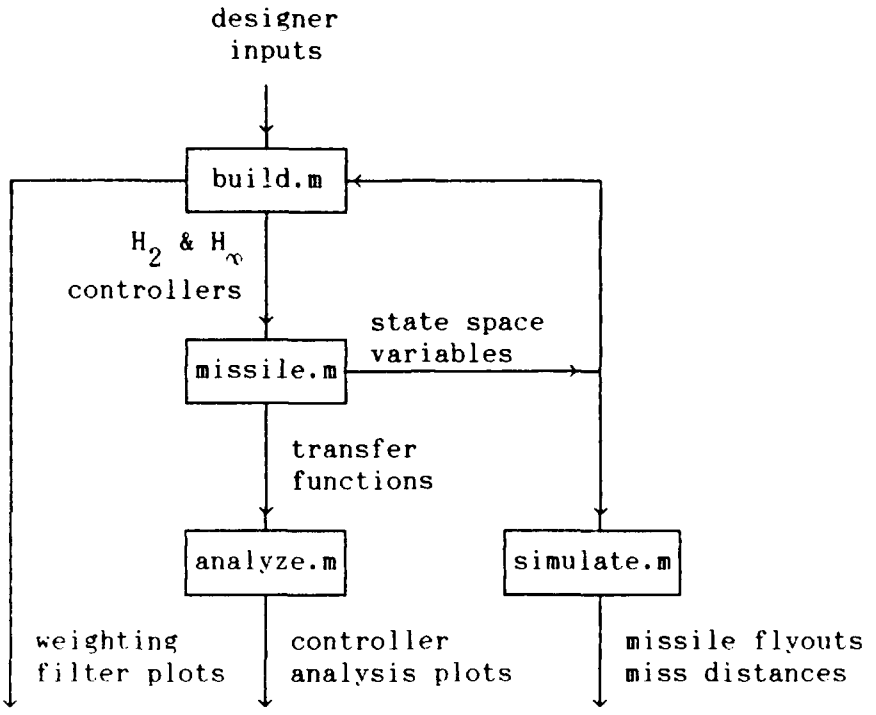

Figure B.1 Computer Codes Used In Controller Design And Evaluation

singular value plots, and μ analysis plots. Mureal.m is called to produce the μ analysis plots. Analyze3.m is similar to analyze.m except it performs the analysis for three controllers at once for comparison.

Simulate.m calls missile.m to get missile state space information. It uses Equation (3.7) to calculate the missile simulation transfer function and then performs the simulation as shown in Figure 3.1. If the user doesn't input simulation initial conditions, defaults will be used. The 0.001 second time step simulations could take up to four hours Vax CPU time to run so they were run in batch mode. Simulate.m also has options to provide many plots in addition to missile flyout for use in diagnosing errors and confirming reasonable simulations.

Since the navigational command block plays an important role in resulting missile miss distances, guide.m was written to study the effects of changes in navigational constants and differences in execution lag time independent of the missile dynamics. Guide.m is basically simulate.m with all missile dynamics stripped out. A missile g limiter can be used to keep the flyouts realistic.

Bibliography

1. Riddle, Randall L., Design of A Robust Controller For An Unstable Nonminimum Phase Guided Missile. MS Thesis. AFIT/GAE/ENY/89D-29. School of Engineering Air Force Institute of Technology (AU), Wright Patterson AFB OH, December 1989. AD-A216 417

2. Breuer, D. Wallace, The Fundamentals of Weapons Engineering. Volume I, Section 2.11, School of Engineering, Air Force Institute of Technology (AU), Wright Patterson AFB OH, Prepared under Contract F33601-81-C0185, Second Printing, February 1984.

3. Reichert, R. T., Robust Autopilot Design Using μ-Synthesis. 1989 American Control Conference, 2368-23735, American Control Conference, Pittsburgh PA, June 1989.

4. Manning, Mary K., and Banda, Siva S., Some Useful Algorithms For Robustness Analysis Studies. WRDC-TM-89-164. Flight Control Division, Flight Dynamics Laboratory, Wright Research and Development Center, Wright Patterson AFB OH, March 1989.

5. Doyle, John; Glover, K.; Khargonekar, P.; and Francis, B., State-space Solution to Standard H_2 and H_∞ Control Problems. 831-846, IEEE Transactions on Automatic Control, Vol 34, No. 8, August 1989.

6. Nesline, F. William, and Nesline, Mark L., How Autopilot Requirements Constrain The Aerodynamic Design of Homing Missiles. 716-730, American Control Conference, Pittsburgh PA, June 1989.

7. Wise, Kevin A., and Mears, Barry C., Missile Autopilot Design Using H_∞ Optimal Control With μ-Synthesis. 2362-2367, American Control Conference, Pittsburgh PA, June 1989.

Vita

Capt Steven R. Kolbow [redacted] He graduated from Northwestern Preparatory School in Watertown Wisconsin, in 1980 and attended Tri-State University in Angola, Indiana, from which he received a Bachelor of Science in Aerospace Engineering in February 1984. Upon graduation he attended Officer Training School in San Antonio, Texas, and received a commission in the USAF in May 1984. He worked as a Tactical Air Combat Analyst in the Technology Assessment Office of the Flight Dynamics Laboratory, Wright Patterson AFB, Ohio from June 1984 through December 1987. From January 1988 until entering the School of Engineering, Air Force Institute of Technology in May 1989, he worked as Manager of the B-1B Windshield Improvement Program in the Vehicle Equipment Division of the Flight Dynamics Laboratory.

[redacted]

REPORT DOCUMENTATION PAGE

Form Approved
OMB No. 0704-0188

1. AGENCY USE ONLY (Leave blank)	2. REPORT DATE	3. REPORT TYPE AND DATES COVERED
	December 1990	Master's Thesis

4. TITLE AND SUBTITLE
ROBUSTNESS OF H_2 AND H_∞ DESIGN TECHNIQUES IN THE DESIGN OF A GUIDED MISSILE CONTROLLER

5. FUNDING NUMBERS

6. AUTHOR(S)
Steven R. Kolbow, Captain, USAF

7. PERFORMING ORGANIZATION NAME(S) AND ADDRESS(ES)
Air Force Institute of Technology, WPAFB OH 45433-6583

8. PERFORMING ORGANIZATION REPORT NUMBER
AFIT/GAE/ENY/90D-13

9. SPONSORING/MONITORING AGENCY NAME(S) AND ADDRESS(ES)
Dr Siva Banda, WRDC/FIGC, WPAFB OH 45433-6523

10. SPONSORING/MONITORING AGENCY REPORT NUMBER

11. SUPPLEMENTARY NOTES

12a. DISTRIBUTION/AVAILABILITY STATEMENT
Approved for public release; distribution unlimited

12b. DISTRIBUTION CODE

13. ABSTRACT (Maximum 200 words)

This work follows Capt Riddle's 1989 thesis which compared conventional, H_2, and H_∞ controlled guided missiles in simulated flyouts against an airborne target. The simulation results did not clearly demonstrate the H_2 and H_∞ controller advantages. In this study the missile model and simulation were refined. In addition to simulation runs, performance, noise attenuation, and μ robustness analyses were conducted. Results showed areas where improvement was needed in the H_2 and H_∞ controllers used in the study. An H_2 and H_∞ controller redesign is recommended using the μ synthesis design technique. Additional simulation runs are also recommended to examine whether the improved controllers reduce miss distances.

14. SUBJECT TERMS
Feedback Controller, H_2 and H_∞ Optimization, μ-Analysis, Proportional Navigation, Simulation, Surface-to-Air Missile

15. NUMBER OF PAGES
115

16. PRICE CODE

17. SECURITY CLASSIFICATION OF REPORT	18. SECURITY CLASSIFICATION OF THIS PAGE	19. SECURITY CLASSIFICATION OF ABSTRACT	20. LIMITATION OF ABSTRACT
Unclassified	Unclassified	Unclassified	UL